

SUBSURFACE MAP AND SEISMIC RISK ANALYSIS OF THE SALT LAKE VALLEY

by

Hugh Radkins, Mary Murphy, and Gerard T. Schuster

March, 1989

Utah Geological and Mineral Survey
Open-File Report 152

This open-file release makes information available to the public which will not appear in another published form but is considered to be of value. It may not necessarily conform to formal UGMS policy, technical review, or editorial standards, and therefore it may be premature for an individual or group to take action based on the contents of this report.

THE PUBLICATION OF THIS REPORT IS MADE POSSIBLE WITH FUNDING FROM
THE MINERAL LEASE SPECIAL PROJECTS PROGRAM

**FINAL REPORT To UGMS:
SUBSURFACE MAP AND SEISMIC RISK ANALYSIS OF
THE SALT LAKE VALLEY**

January 19, 1989

*Hugh Radkins
Mary Murphy
Gerard T. Schuster*

Geology and Geophysics Department
University of Utah
Salt Lake City, Utah 84112
(801) 581-4373

Contract 5-24496

Table of Contents

ABSTRACT	1
INTRODUCTION	2
Salt Lake Valley Basin	2
Data Overview	3
Wave Propagation Simulation	6
MODEL OF SALT LAKE BASIN FROM INTEGRATED GEOPHY- SICAL DATA	7
Seismic Data Model	7
*) Shallow Seismic Data	7
*) Deep Seismic Data	14
Gravity Data Model of Salt Lake Valley	19
Integrated Seismic Well-Log Gravity Model	28
*) Arnow's Quaternary Thickness Map	34
NUMERICAL SIMULATION OF WAVE PROPAGATION	39
P-SV Wave Simulation	39
Three-dimensional Elastic Wave Simulation	65
SUMMARY	76
ACKNOWLEDGEMENTS	78
APPENDIX	79
REFERENCES	81

hcr, mem, and gts

ABSTRACT

This report is divided into two sections: 1). a compilation and integration of existing geophysical data pertaining to the sub-surface structure of Salt Lake Basin, and 2). a suite of synthetic seismograms which attempt to simulate the site amplification in Salt Lake Valley due to low frequency incident P-SV waves.

The central portion of the valley is found to be less well determined than the northern and southern portions due to lack of seismic data. Work at the University of Utah is continuing, with this compilation of data being used to constrain 2 1/2-D gravity inversion along cross sections of the Salt Lake Valley. The purpose of this inversion is to determine in more detail the sub-surface structure in the central portion of the valley.

The 2-D P-SV synthetic seismograms have shown that the deep basin structure is responsible for much of the low frequency site amplification, and that site response in Salt Lake Valley is sensitive to the incidence angle of the source. Most of the low frequency energy collects over the deeper part of the basin, with surface waves as a dominant waveform. Steeply dipping basin walls enhance the formation of surface waves, and convert more energy into the horizontal direction than do shallowly dipping walls.

hcr, mem, and gts

I. INTRODUCTION

The objective of this report is two-fold:

- 1). collect and integrate existing geophysical data pertaining to the structure of Salt Lake Basin. Until now, most geophysical models for the Salt Lake Basin have been constructed without integrating the entire composite of existing data.
- 2). compute synthetic seismograms for sources incident to Salt Lake Basin at a variety of angles. These synthetic seismograms can be used to understand which parts of the basin are most susceptible to low frequency ground motion amplification.

This report is organized into two sections: geophysical data and numerical simulations. The first section presents the shallow and deep seismic data, followed by models derived from gravity data, and well-log data. The second section presents the synthetic seismograms, their interpretation, and their comparison with USGS site response data. In addition, the appendix describes the contouring of the gravity data. This contour map is included in this report.

Salt Lake Valley Basin

Located within the Intermountain Seismic Belt, the Salt Lake Valley is located in an area of high seismic risk (Youngs et al., 1987). Regional historical seismicity includes large magnitude earthquakes ($M_L > 6.5$) in southern Idaho, northern Utah, and eastern Nevada. In addition to the Wasatch fault which bounds the eastern side of the valley, several other active Quaternary faults have been identified in the area (Youngs et al., 1987). These faults include the West Valley fault zone, which may or may not be part of the Wasatch Fault, the Oquirrh Mountain fault zone, which is located west-southwest of the valley, and the Great Salt Lake fault zone, which is located to the northwest of the Salt Lake

Valley. Probabilistic analysis of the ground shaking hazard along the Wasatch Front suggests that the Wasatch fault zone is the greatest single contributor to the mean seismic hazard in the Salt Lake City region. Measurements of slip indicate the Wasatch fault is capable of generating large ($M_L > 6.5$) normal-faulting earthquakes. A recurrence interval of 250 to 280 years is estimated for a single large earthquake occurring anywhere along the entire fault (Machette et al., 1987).

To analyze the earthquake hazards associated with the Salt Lake Basin, a good knowledge of the basin's structure and lithology is required. Unfortunately, previous Salt Lake Basin models have been obtained in a piece-meal manner using just one or a few of the existing geophysical data sets. The main objective of this report is to analyze the existing geophysical data and construct a consistent model of the Salt Lake Basin.

Data Overview

The compiled geophysical data includes: (1) excellent quality CDP seismic sections from Celsius Energy Company, (2) sonic and density log data from USGS files, (3) shallow seismic record sections from recent work by King et al. (1987) of USGS, (4) a gravity contour map generated from USGS records and additional gravity data from Dick Fox, (5) Bashore's (1982) refraction survey in the southern part of the basin, (6) Fox's basement structure based on gravity modeling, (7) Arnow's (1970) Quaternary structure map based on log data (mud-log), (8) Wong's shallow refraction and deep gravity survey, and (9) Kennecott Corporation's gravity modeling and magnetic anomaly map. In addition to compiling these data, we also integrated them and compared them for consistency. The sonic log, density log, CDP seismic data, and Fox's gravity inverted basement depths are in excellent agreement with one another for the

northern part of the basin; the shallow to intermediate structure model of the northern basin is very reliable. Along the CDP seismic profile locations, Arnow's depth to the Quaternary contact varies by up to 50% in this area. Therefore we determine that the accuracy of Arnow's map, based on mud-logging results, to be questionable.

For the southern part of the basin, Bashore's (1982) unreversed refraction model and Fox's gravity model are in rough agreement with one another. Therefore, the shallow to intermediate model of the southern portion of the basin is only of fair reliability.

The main problem area for the determination of structure seems to be within the center of the valley where deep seismic control is not available. Fox's gravity basement model and Arnow's log-based Quaternary depth model of the basin are available, but their reliability in this area is unknown at present. Fox's gravity basement model and Wong's gravity basement model do correlate fairly well. This still leaves much area that is considered unknown. The reliability of these interpretations will be better known when the complete gravity inversion is finished.

The comparisons of this geophysical data for mutual consistency show that the best complete single source for an interpretation of the Salt Lake Valley basement structure is the result of R. C. Fox's (1983) gravity modeling. The best combination of sources for the whole Salt Lake Valley interpretation consists of: Celsius Energy Company's reflection lines in the northern portion of the basin; Bashore's (1982) seismic-gravity models in the southern portion of the basin; and a combination of the other interpretations in the remainder of the basin. Table I lists the data sets collected and interpretations compared in this study.

TABLE I.
TABLE OF COLLECTED AND COMPARED GEOPHYSICAL DATA

Data Type	Map/Figure	Comments	Reference
Seismic	Fig 1	Seismic Data Sites	<i>King 1987</i>
Reflection	Fig 2	Shallow Seismic Profile	<i>King 1987</i>
Reflection	Fig 3	Shallow Seismic Profile	<i>King 1987</i>
Reflection	Fig 4	Shallow Seismic Profile	<i>King 1987</i>
Refraction	Fig 5	Seismograph Sites	<i>Wong 1979</i>
Refraction	Fig 6	Shallow Seismic Models	<i>Wong 1979</i>
Refraction	Fig 7	Refraction Profile Sites	<i>Bashore 1982</i>
Refraction	Fig 8	Velocity Structure Model	<i>Bashore 1982</i>
Gravity	Fig 9	Gravity Profile-Model	<i>Bashore 1982</i>
Seismic-Well	Fig 10	Reflection Line & Well Sites	<i>Hill 1988</i>
Reflection	Fig 11	Seismic Interpretation	<i>Hill 1988</i>
Gravity-Well	Fig 12	Depth to Basement Map	<i>Fox 1983</i>
Grav-Grav	Fig12a	Model Comparison	<i>Fox-Kennecott Corp</i>
Gravity	Fig 13	Model Comparison	<i>Fox-Bashore</i>
Gravity	Fig 14	Gravity Model	<i>Wong 1979</i>
Gravity	Fig 15	Model Comparison	<i>Fox-Wong</i>
Well	Fig 16	Density Well #1	<i>Hill 1988</i>
Well	Fig 17	Sonic Well #2	<i>Hill 1988</i>
Well	Fig 18	Density Well #2	<i>Hill 1988</i>
Well	Fig 19	Sonic Well #3	<i>Hill 1988</i>
Well	Fig 20	Velocity Comparison	<i>Hill 1988</i>
Grav-Seismic	Fig 21	Model Comparison	<i>Fox-Radkins</i>
Grav-Seismic	Fig 22	Model Comparison	<i>Fox-Radkins</i>
Well	Fig 23	Quaternary Deposits Map	<i>Arnow et al. 1970</i>
Seismic-Well	Fig 24	Model Comparison	<i>Radkins-Arnow</i>
Seis-Grav-Well	Fig 25	Model Comparison	<i>Radkins-Fox-Arnow</i>
Gravity	Map 1	Bouguer Anomaly	<i>Celsius-Hulse</i>
Magnetics	Map pocket	Total Intensity	<i>Kennecott Corp</i>
Seismic R10	Map pocket	Line R10 Seismogram	<i>Celsius</i>
Seismic R11	Map pocket	Line R11 Seismogram	<i>Celsius</i>

Wave Propagation Simulation

The 1985 Michoacan earthquake ($M_s = 8.1$) caused tremendous damage to Mexico City, which is located about 300 km from the epicenter. Much of the damage was caused, not by poor building standards, but by amplification of low frequency (0.5 Hz) seismic waves in the lake bed sediments under Mexico City. Salt Lake City is located in an active seismic zone, and is build upon lake bed sediments. Determining the locations of areas with the greatest ground-shaking hazard by numerical simulations will help planners reduce the risk to life and property.

2-D and 3-D finite difference solutions to the elastic wave equations were used to simulate seismic waves propagating through 2-D and 3-D models of Salt Lake Basin. Synthetic displacement seismograms were computed at the surface. Synthetic seismic amplification due to deep basin structure was compared to seismic amplification measured by King (1987) from Nevada Test Site nuclear explosions. Amplification of alluvial sites was measured by computing the spectral ratio of an alluvial site spectra to a bedrock spectra.

The deep basin structure appears to control the low frequency amplification. Seismic energy tends to be trapped in the deeper part of the basin. Surface waves are a dominant wave form, and have the largest amplitudes over the deeper part of the basin. Steeply dipping basin walls enhance the creation of surface waves and convert much vertical energy into horizontal energy. Good correlation of synthetic spectral ratios measured from NTS explosions suggests that numerical simulations will be effective in predicting the locations of areas with the greatest potential ground-shaking hazard.

hcr, mem, and gts

II. MODEL OF SALT LAKE BASIN FROM INTEGRATED GEOPHYSICAL DATA

Seismic Data Model

Two seismic experiments which imaged the deep part of Salt Lake Basin were a refraction profile in the Southern portion of the basin (Bashore, 1982) and Celsius Energy Co.'s reflection survey conducted in the northern part of the basin. Shallow seismic experiments have been conducted in isolated parts of the valley (King et al. 1987; Wong, 1979), but they image less than the first hundred meters.

Shallow Seismic Data. King et al. (1987) collected high resolution, shallow reflection profiles at five sites in Salt Lake City and the Springville-Spanish Fork area (Figure 1). The profiles were collected with linear arrays ranging from 40 to 160 meters in length and single, 100 Hz, vertical velocity geophones. The energy source was a 12 gauge shotgun with a 28g slug. Splitspread array with multiple shot summing provide 12 fold CDP coverage. The deepest reflection resolved by King et al. (1987) is 58 meters in depth. Figures 2, 3, and 4 show the reflection profiles collected and processed by King et al. (1987) that occur in the Salt Lake Valley; and, Table II tabulates the results from the profiles. King and co-workers continue their shallow reflection studies and analysis of the data is in progress. (King et al. 1987)

Site amplification of seismic shear waves was studied by Wong (1979) using seismograms from six sites in the valley (Figure 5). Source energy for the seismograms include two Bingham mine blasts and a single NTS blast. Wong (1979) also uses reversed hammer source refraction data, some water well data, and existing geologic data to construct subsurface geologic models at these six sites (Figure 6). Wong's work suggests a near-surface low-velocity layer

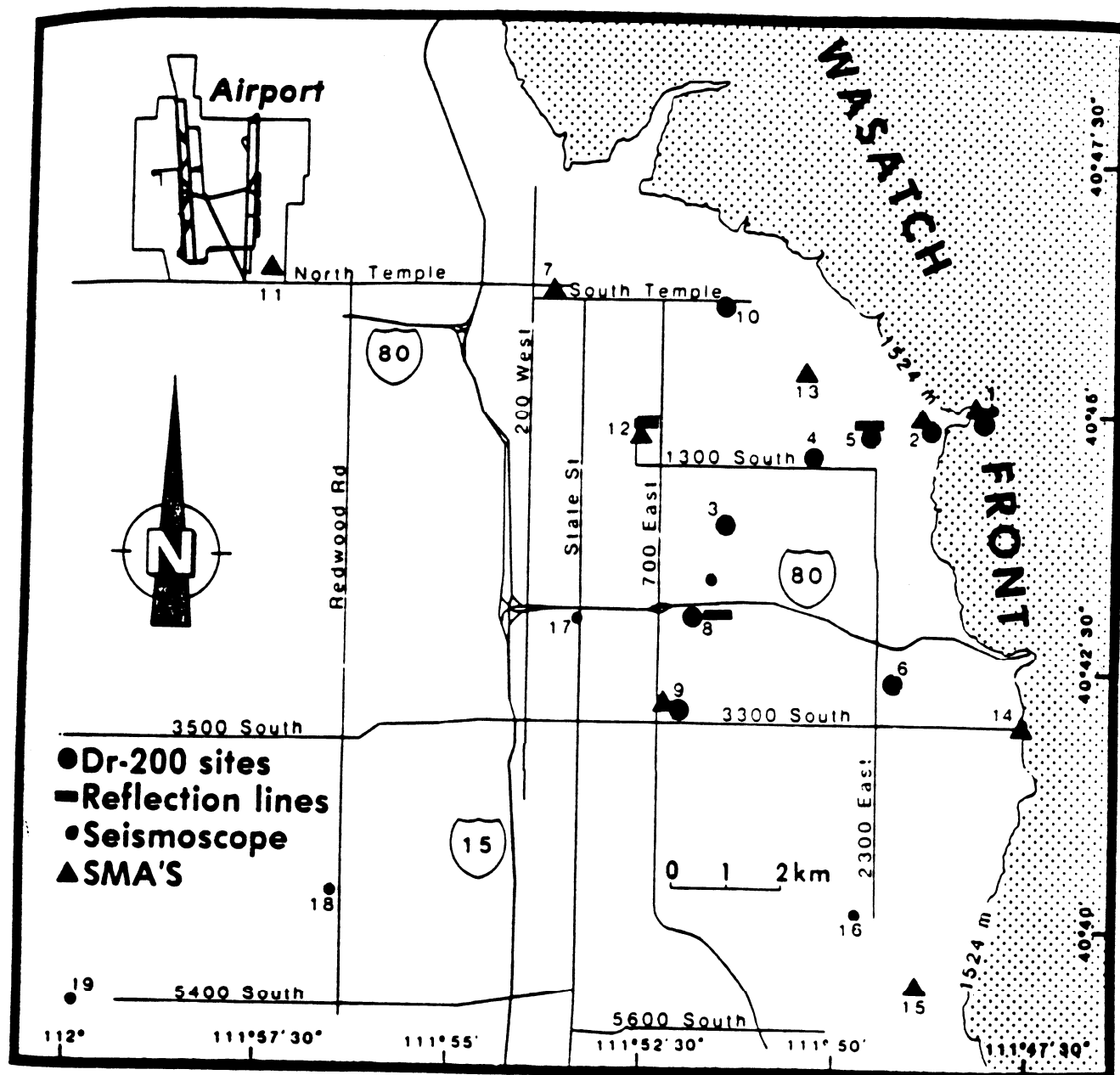


Figure 1. Locations of sites, and their assigned station numbers, in Salt Lake city at which ground-motion recordings of nuclear explosions and shallow seismic reflection profiles were acquired. Seismoscope and SMA instrument sites are also shown (from King 1987).

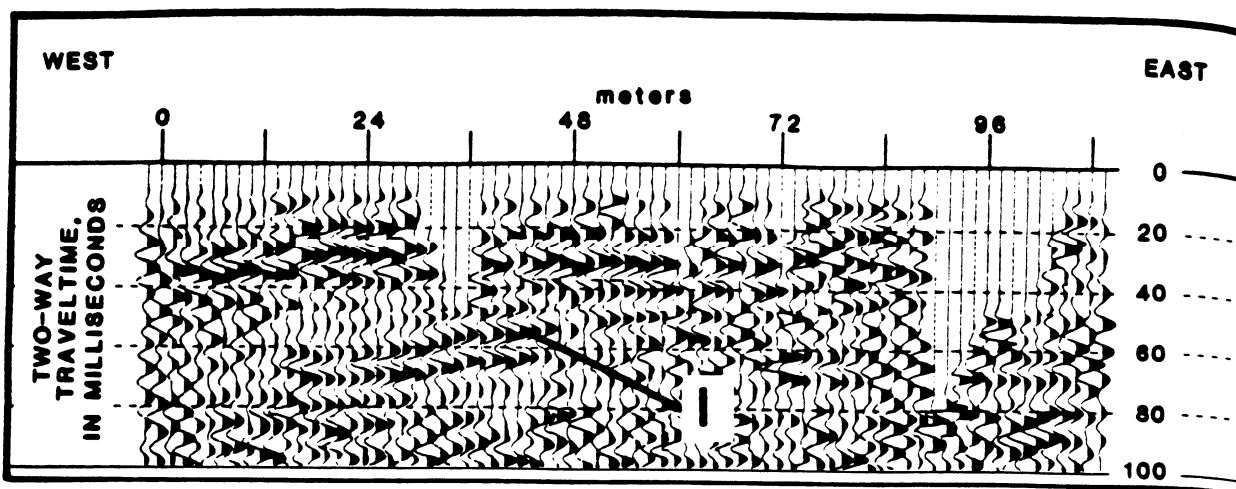


Figure 2. Seismic reflection profile from SLC 5 (Bonneville Golf Course) showing reflection labeled I (from King 1987).

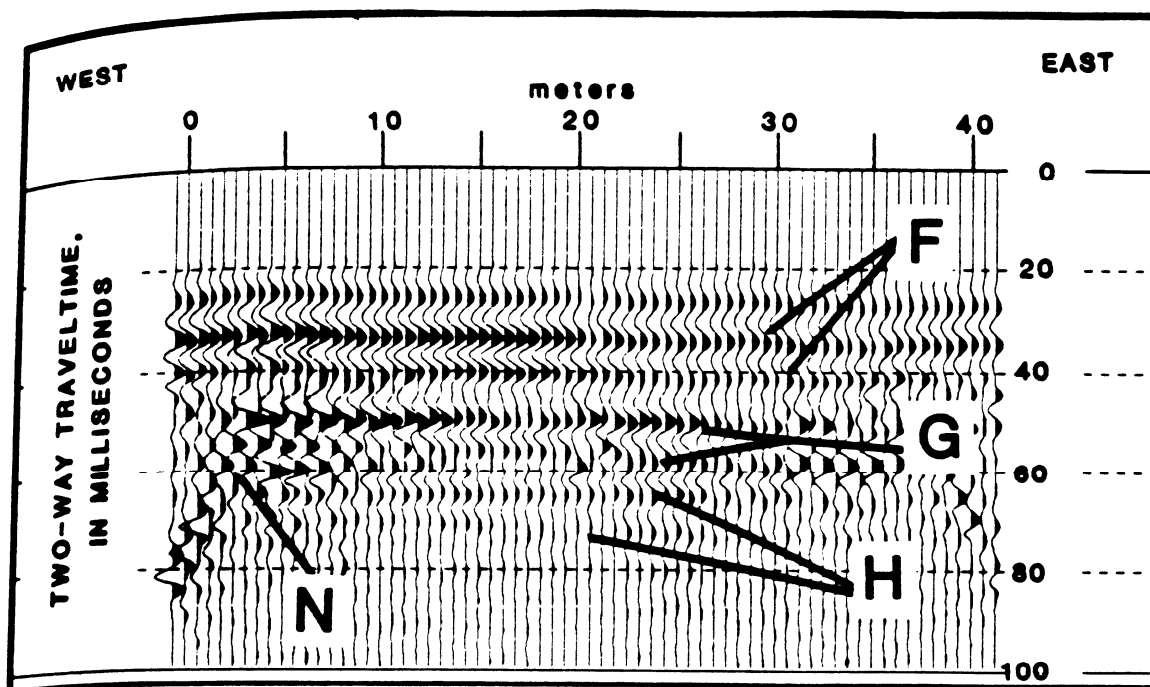


Figure 3. Seismic reflection profile from SLC 12 (Liberty Park) showing reflections labeled F, G, and H. Ground roll dominates in the zone labeled N (from King 1987).

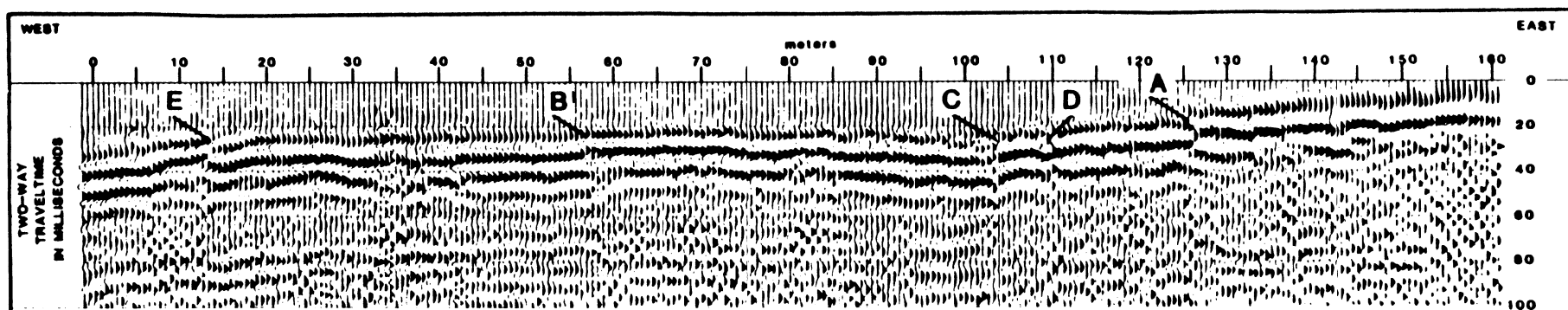


Figure 4. Seismic reflection profile from SLC 8 (Forest Dale Golf Course) showing offset at position A where the profile crosses the East Bench Fault. Region between B and C shows possible backrotation toward the East Bench Fault. Position D and E mark other possible faults (from King 1987).

TABLE II.
SEISMIC REFLECTION AND GROUND RESPONSE DATA
(from King 1987)

	SLC 5	SLC 8	SLC 12	SSF 3	SSF 4
Average spectral ratio factor					
0.2 - 0.7 s	4.5	4.5	8.0	8.5	12.1
0.7 - 1.0 s	2.0	4.2	9.0	5.5	9.0
1.0 - 2.0 s	1.8	4.7	8.5	3.5	12.0
2.0 - 3.3 s	2.0	6.6	6.0	1.6	6.9
No. of reflections on the profile	1	1	3	2	1
Reflection continuity	39	100	100	66	51
	--	--	40	25	--
(in percent of total profile)	--	--	40	--	--
Reflection two-way traveltime	60	30	30	20	80
	--	--	50	45	--
(in milliseconds)	--	--	70	--	--
Stacking Velocity for reflections	600	1000	915	550	1370
	--	--	1475	600	--
(in meters/second)	--	--	1660	--	--
Depth to reflection	18	15	14	8	55
	--	--	37	14	--
(in meters)	--	--	58	--	--

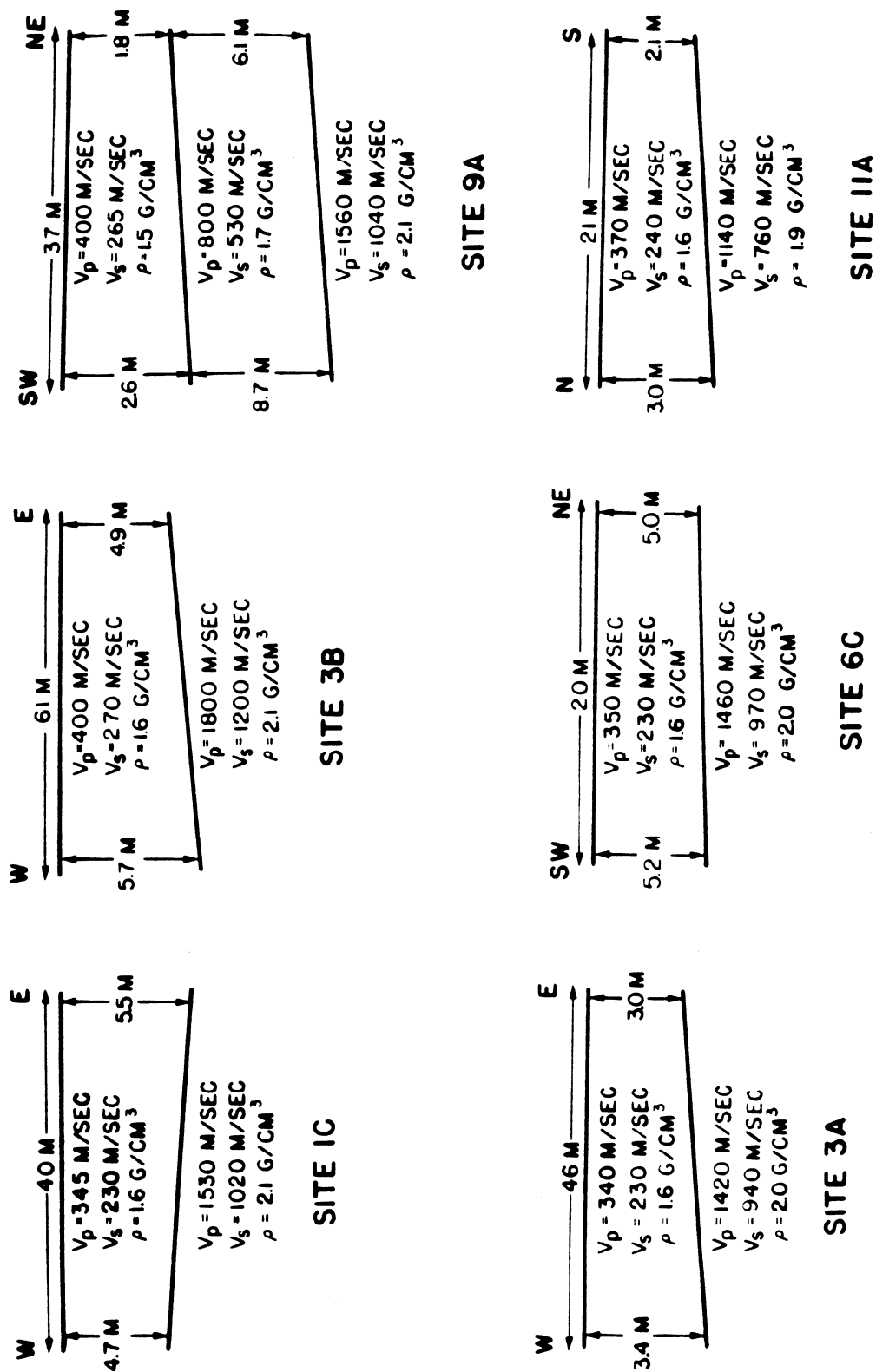


Figure 6. Subsurface modeled from refraction seismograms (from Wong 1979).

combined with a near-surface water table induce shear wave amplification. Wong (1979) also finds that the alluvium-bedrock interface causes low-frequency (< 5 Hz) shear wave amplification. However, Wong's (1979) seismic work only shows depths to less than ten meters.

Deep Seismic Data. Deep seismic data for the Salt Lake Valley consist of Bashore's (1982) seismic refraction profile in the southern portion of the basin and Celsius Energy Co.'s seismic reflection survey in the northern portion of the basin.

Seismic refraction data was collected along two profiles from large blasts in the Bingham mine in the Oquirrh mountains (Bashore, 1982). One profile runs approximately north from the pit to the Great Salt Lake; the other profile runs from the pit, across the valley, up Little Cottonwood Canyon to Alta (Figure 7). Bashore uses the north trending profile for control and does extensive modeling on the east-west profile. This modeling consisted of ray tracing to honor the seismic data, (Figure 8), and 2-D forward gravity modeling to honor the observed gravity data (Figure 9). It should be noted that this refraction survey was not reversed; dips and velocities indicated by the seismic lines could be in error.

Deep seismic reflection data in the basin consist of three profiles in the northern portion of the valley. Celsius Energy Co. collected two parallel good quality lines R-10 and R-11 and one north-south tie line of less use line R-13, lines R-10 and R-11 are included in the map pocket. Figure 10 shows the approximate location of R-11 in the valley. Three main reflectors are detected by these reflection profiles which locate the boundaries of the major layers in the valley: Reflector 1 (R1), divides the unconsolidated Quaternary deposits and the semiconsolidated Tertiary deposits, Reflector 2 (R2) divides the semiconsolidated

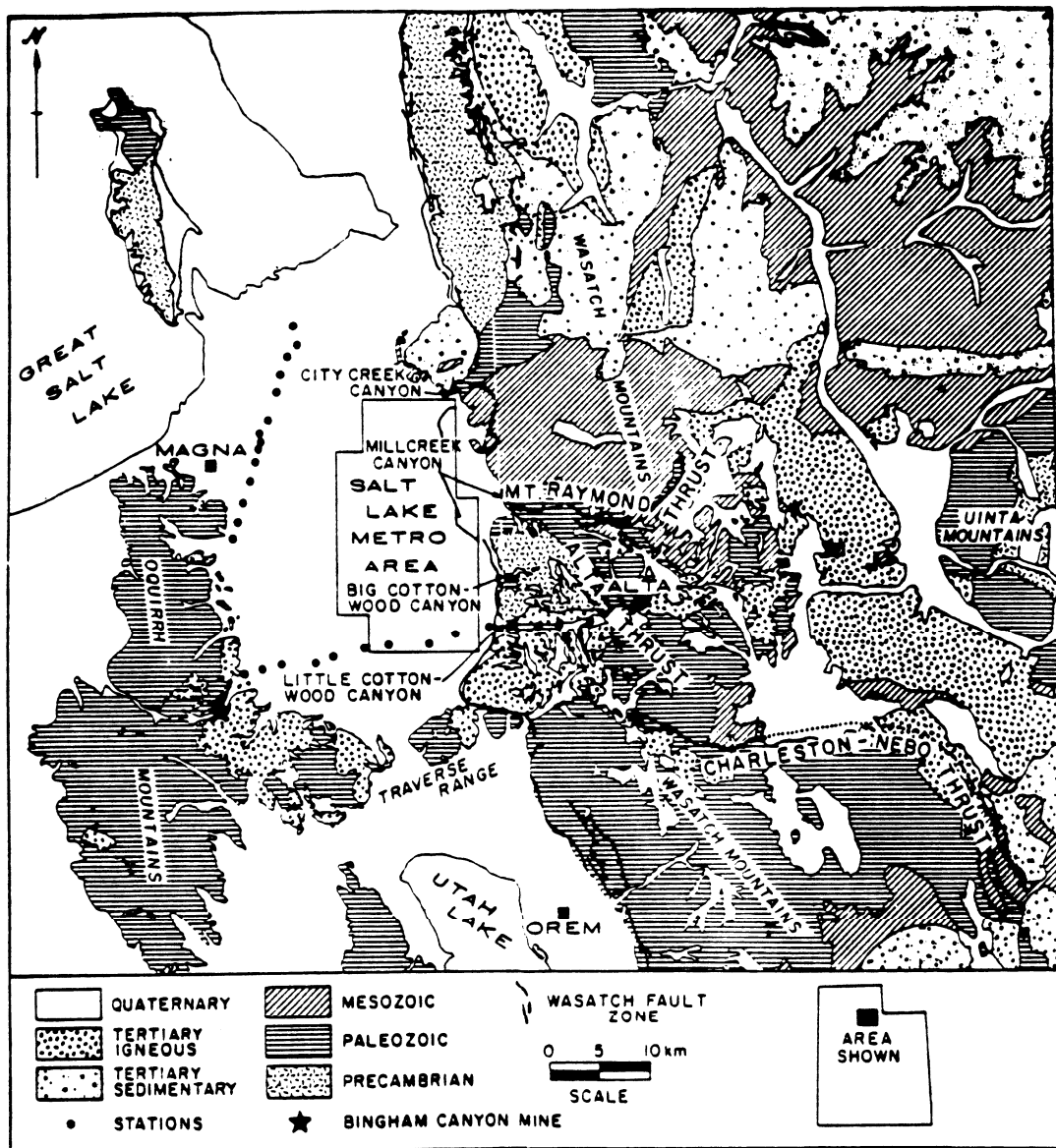


Figure 7. Generalized geology map of study area with station locations of seismic profiles (from Bashore 1982)

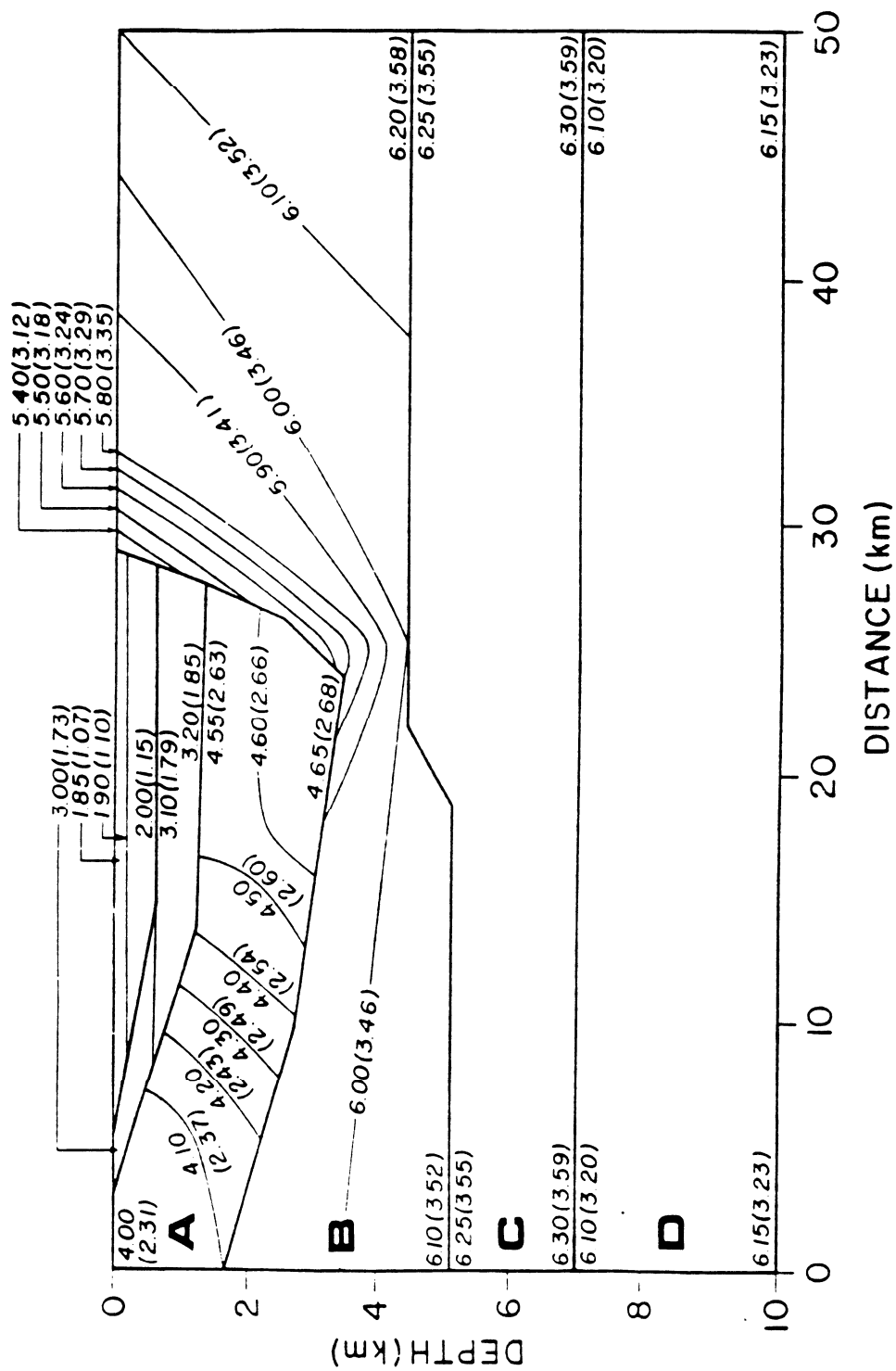


Figure 8. The upper crustal velocity structure of the Bingham-East profile with velocity contour intervals of 0.10 km/sec: P-wave (S-wave) (from Bashore 1982).

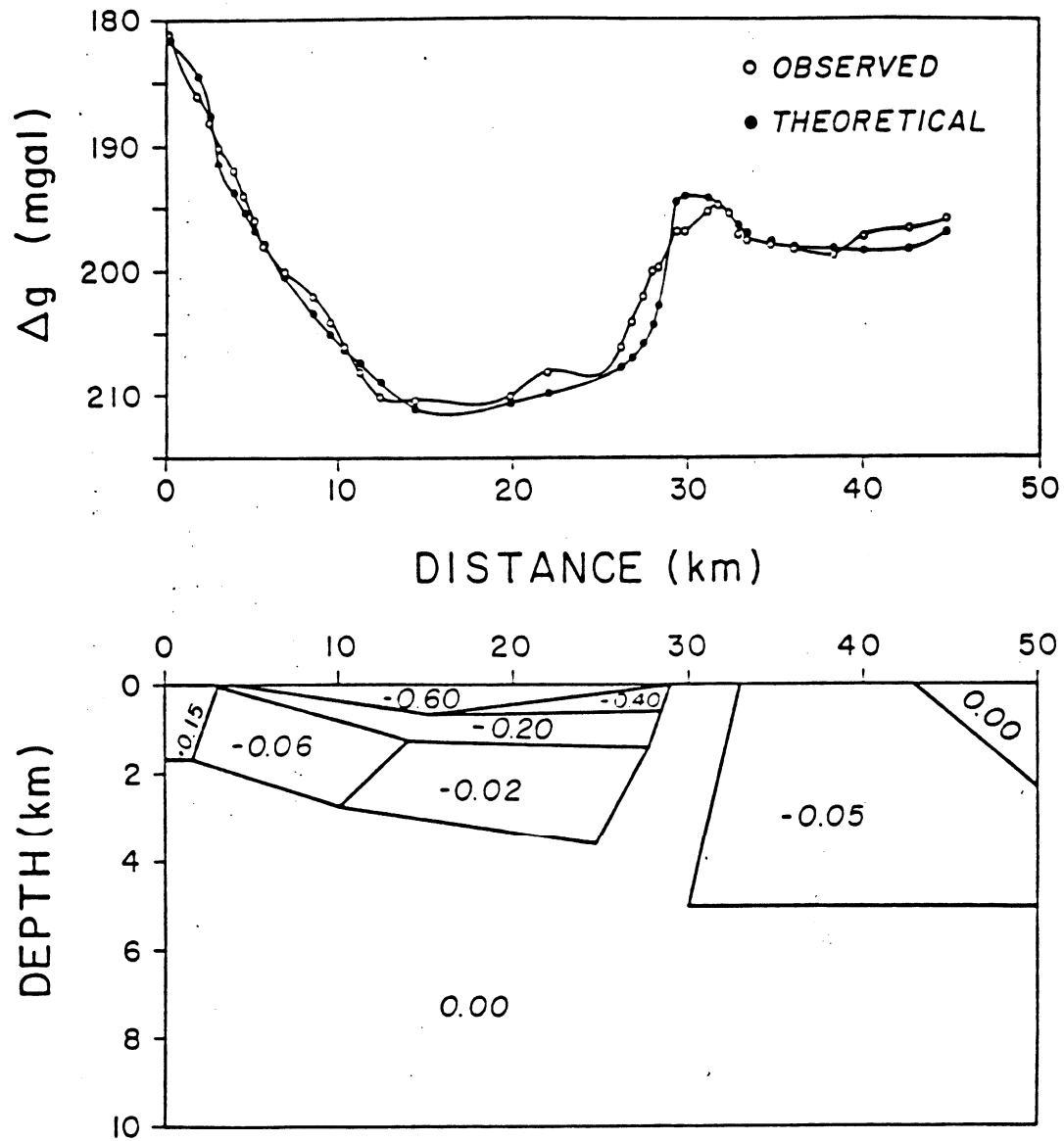


Figure 9. Observed complete Bouguer gravity anomaly of the Bingham-East profile and theoretical gravity anomaly of the given density model (from Bashore 1982).

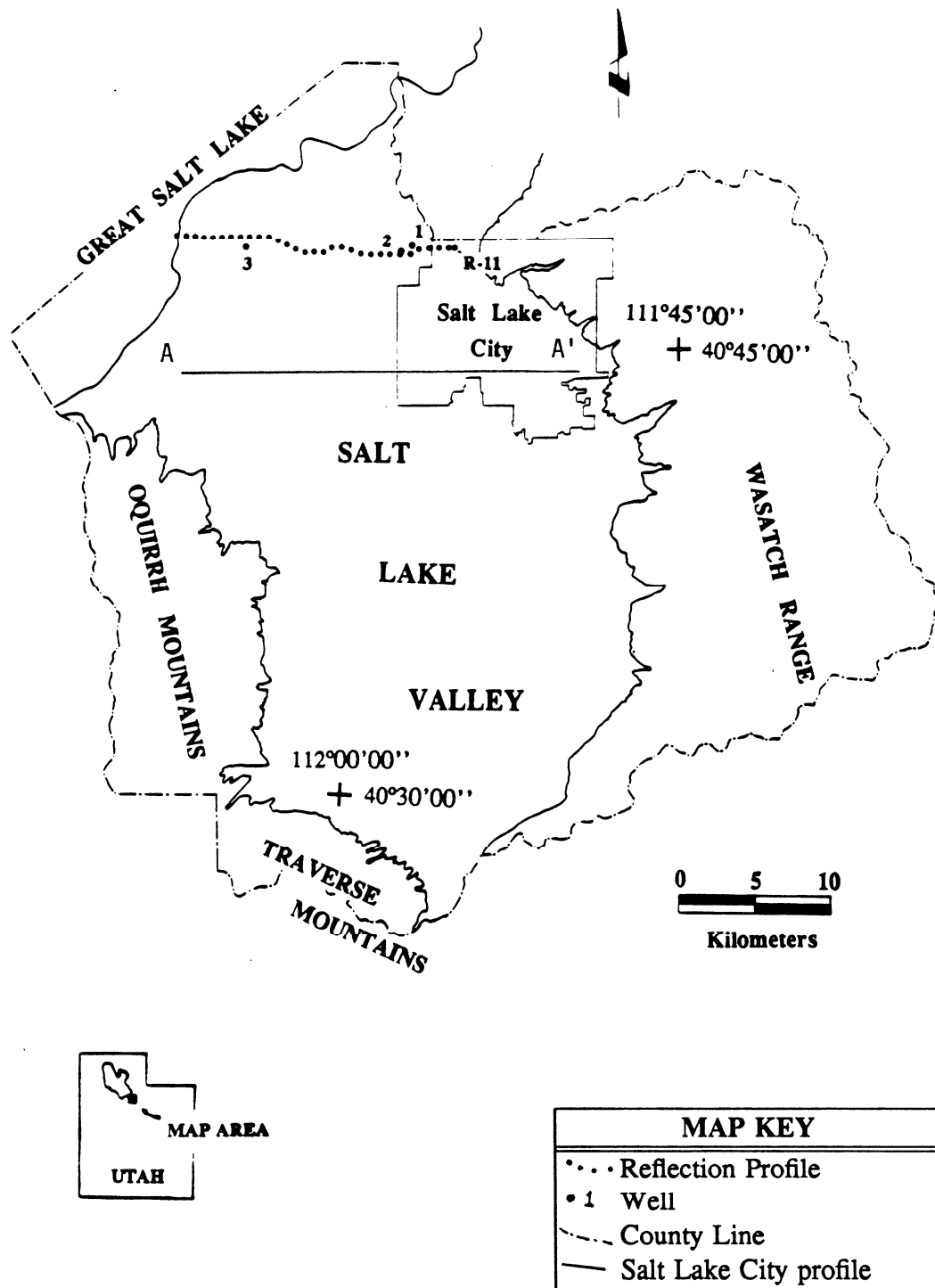


Figure 10. Map of study area with locations of reflection profile R-11, Salt Lake City profile A-A', and wells (from Hill 1988).

deposits and consolidated rocks of several ages, and Reflector 3 (R3) locates the top of basement (Arnow and Mattick, 1968; Mattick, 1970; Hill, 1988).

An interpretation of reflection line R-11 using seismic interval velocities for the depths to R1 and R2 and a constant 5.0 km/sec sonic velocity for the depth to R3 is shown in Figure 11 (Hill, 1988). This interpretation is consistent with sonic and density logs given in figures 16 to 20.

These CDP reflection lines are high quality and locate important reflectors quite well. Depths to the reflectors correlate with depths to well log gradients when travel times are picked from the seismic sections and velocities are picked from the sonic logs. This lends much support to the quality of the reflection data. These well logs are referenced later in this report.

The refraction data provide good control in the southern part of the basin even though the details of the model are less reliable than that of the reflection data. The shallow studies are not as helpful in the large picture of the valley but are important in the analysis of site amplification.

Gravity Data Model Of Salt Lake Valley

Map 1 is a color contour map of the Salt Lake Basin Bouguer gravity anomaly. See the appendix for a more detailed description of the gravity data set and for information on the map plot. Fox (1983) performed 2 1/2-D forward gravity modeling on the Salt Lake Valley gravity data set supplemented with aeromagnetic data to generate a depth to bedrock contour map (Figure 12). The aeromagnetic data was used to locate projections of the Alta stock in the valley to resolve a gravity low in the south east portion of the valley. Workers at Kennecott performed gravity modeling in the early 1960's in the southwest portion of the basin and Fox's gravity modeling is compared to this modeling in Figure 12a. Fox's profiles are picked from his contour map whereas the Kennecott

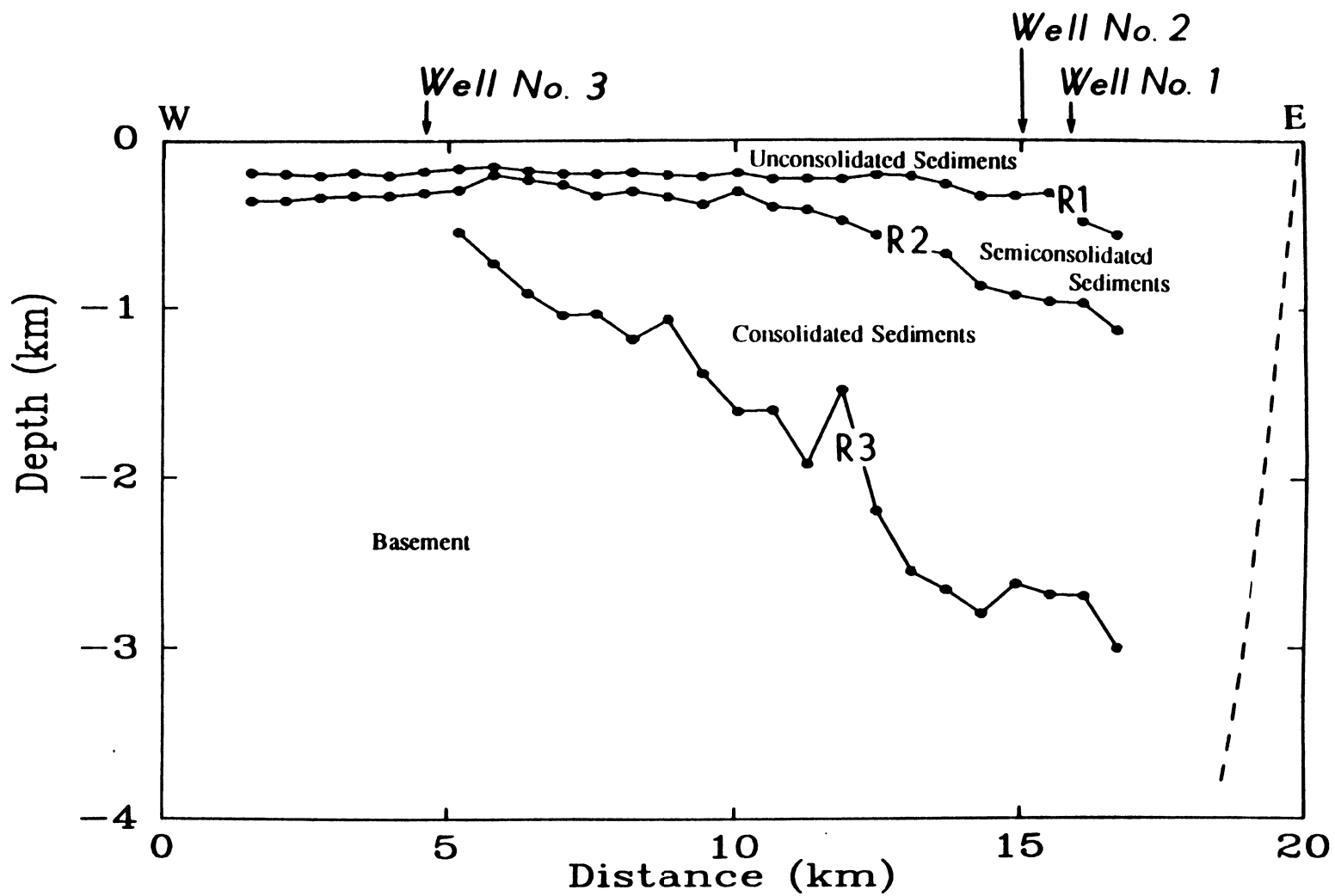
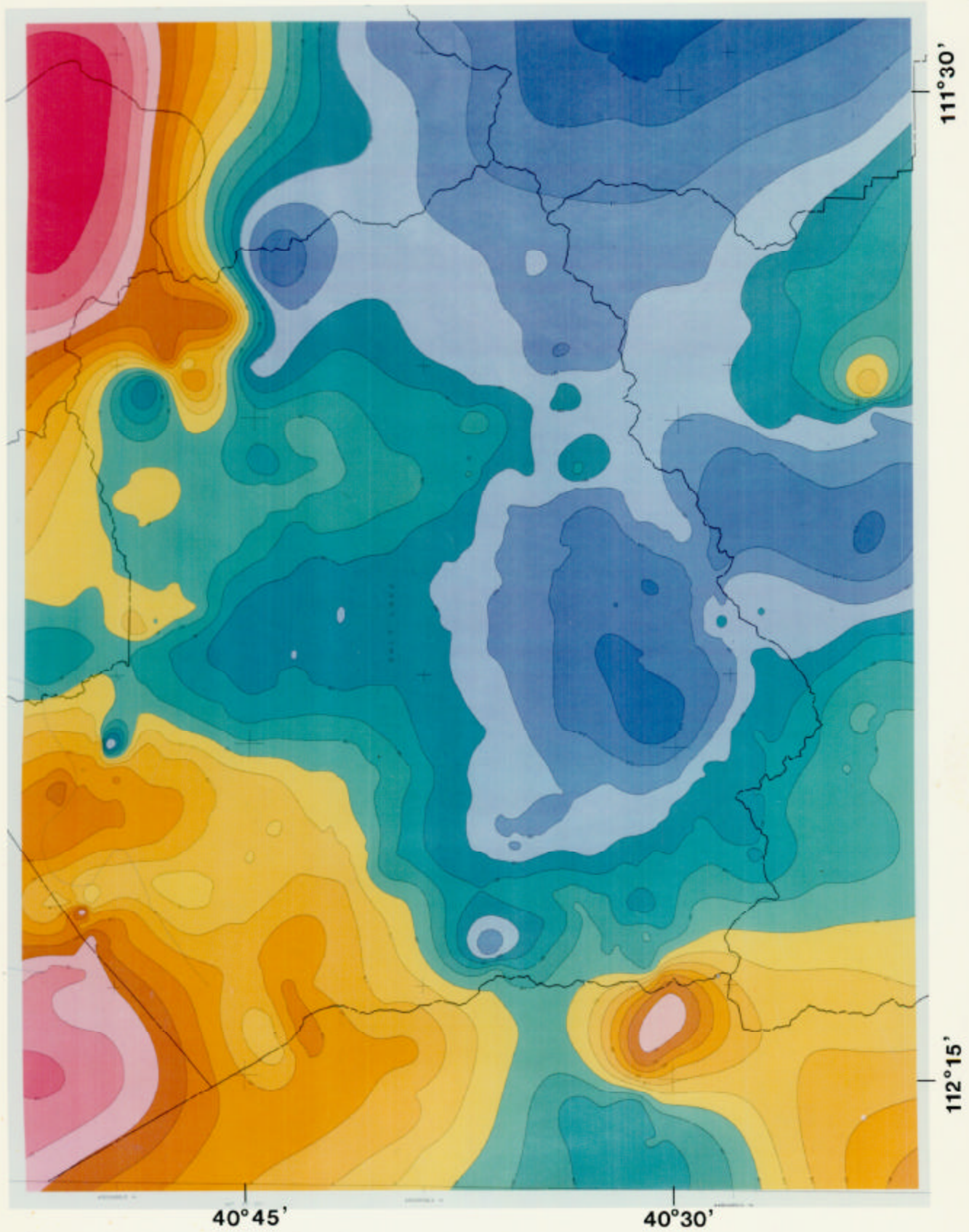


Figure 11. Interpretation of reflection line R-11 (from Hill 1988).

Map 1. Bouguer gravity anomaly for the Salt Lake Basin. Red represents high values and blue represents low values. The highest value or darkest red is bounded by the -135 mgal contour line and is located in the northeast corner of the map. The lowest value or darkest blue is bounded by the -220 mgal contour line and is located in the southeast corner of the map. The contour interval is 5 mgal.

Figure 1



' JORDAN VALLEY BEDROCK MAP '

23

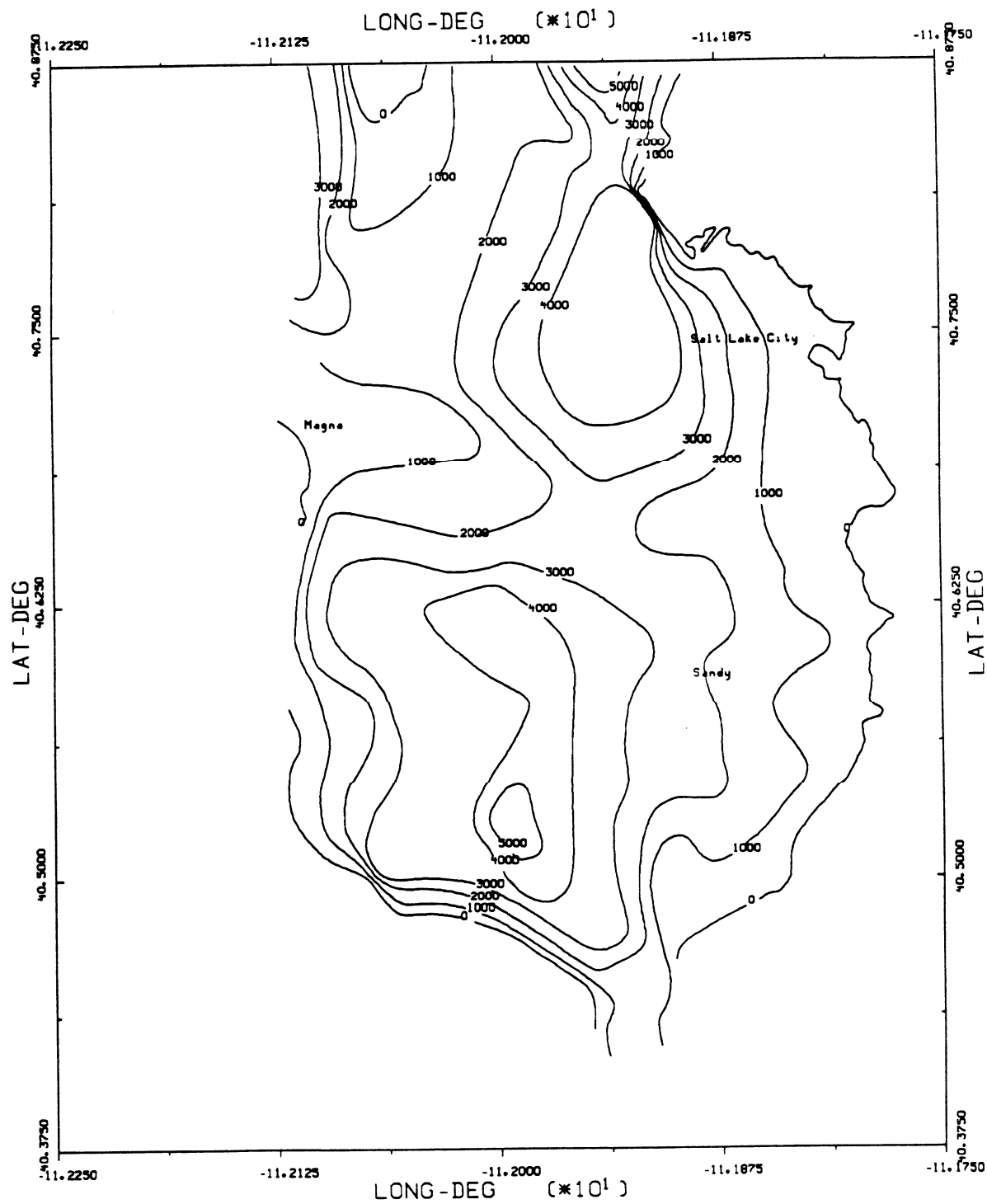


Figure 12. Jordan Valley Bedrock contour map (redigitized from Fox 1983).

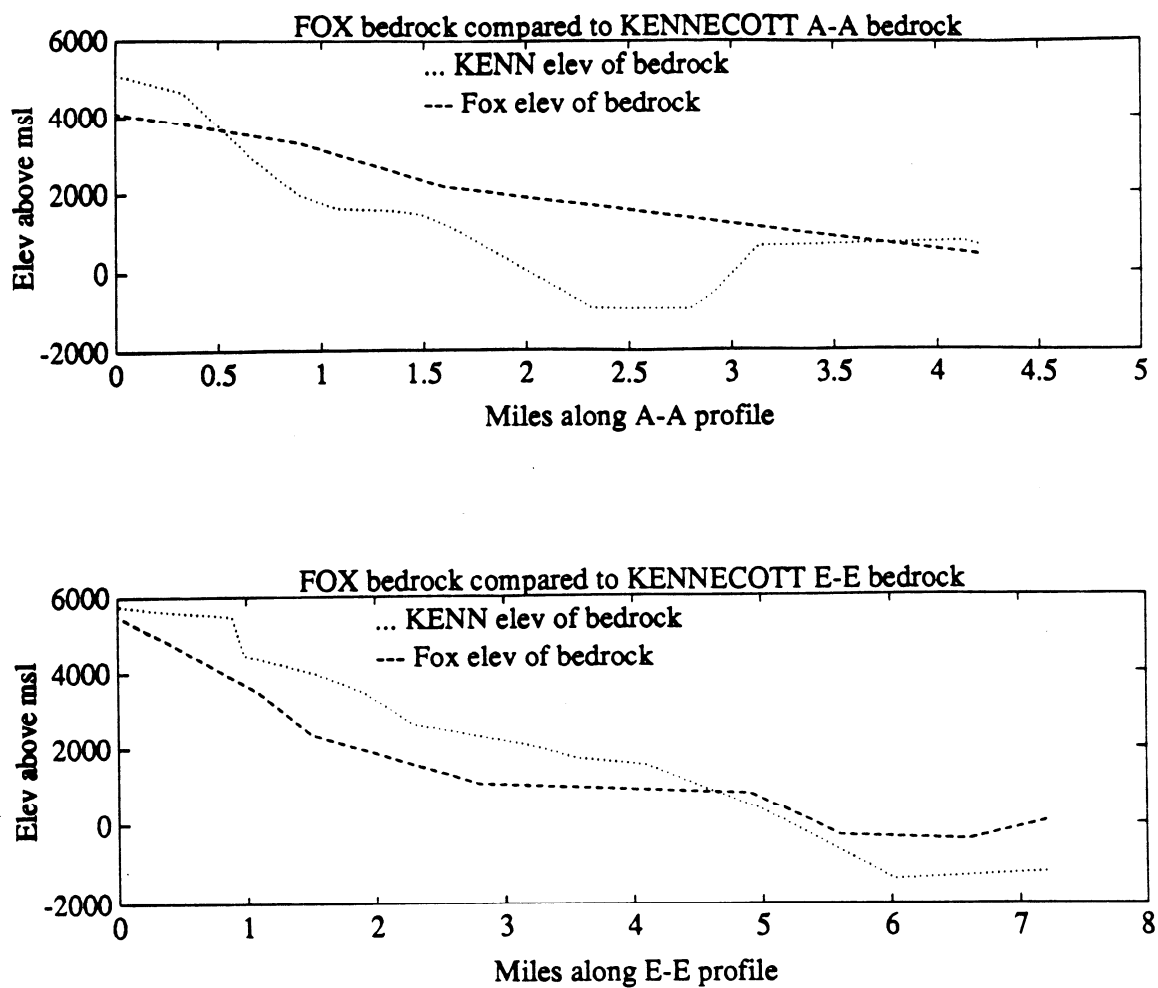


Figure 12a. Fox's (1983) basement depths compared to Kennecott's basement depths.

profiles are taken from the forward modeling profiles themselves. This may be the reason for the less than perfect correlation between the interpretations.

Bashore's (1982) gravity model (Figure 9) does show the Alta stock, but it does not extend into the valley as does Fox's model. However, Bashore's (1982) velocity model (Figure 8) brings stock material under the valley. Figure 13 shows the bedrock location of Fox (1983) superimposed on Bashore's (1982) gravity model. Since a gravity solution is nonunique, it is not surprising Fox's (1983) two layer case does not match Bashore's (1982) more complicated model. It does however show some similarity in dip magnitude and location.

Wong (1979) also generated gravity models for a profile in the Salt Lake Valley. This profile is located along the A-A' line of figure 5. Wong (1979) uses only two layers in the slice across the valley, where Fox uses two layers and in places less dense intrusives and more dense precambrian rocks (Figure 14).

To compare Fox's (1983) depth to bedrock interpretation with Wong's (1979) depth to bedrock interpretation, Fox's depths are converted from feet below valley floor to km above mean sea level (msl). This is done assuming the valley floor is a constant 4500 feet above msl. This conversion is quite valid in the center of the profile but introduces errors of up to 0.2 km near the ends of the profile as the valley laps onto the mountains. However, the error introduced will tend to lessen the difference between the two interpretations as Fox's depths are generally less than Wong's depths.

Figure 15 shows the comparison between Wong's (1979) and Fox's (1983) interpretations. It should be noted Wong's density contrast between alluvium and bedrock is 0.4 gcm^{-3} and Fox's density contrast is 0.45 gcm^{-3} . The comparison shows Fox's depths differing from Wong's depths away from the valley center.

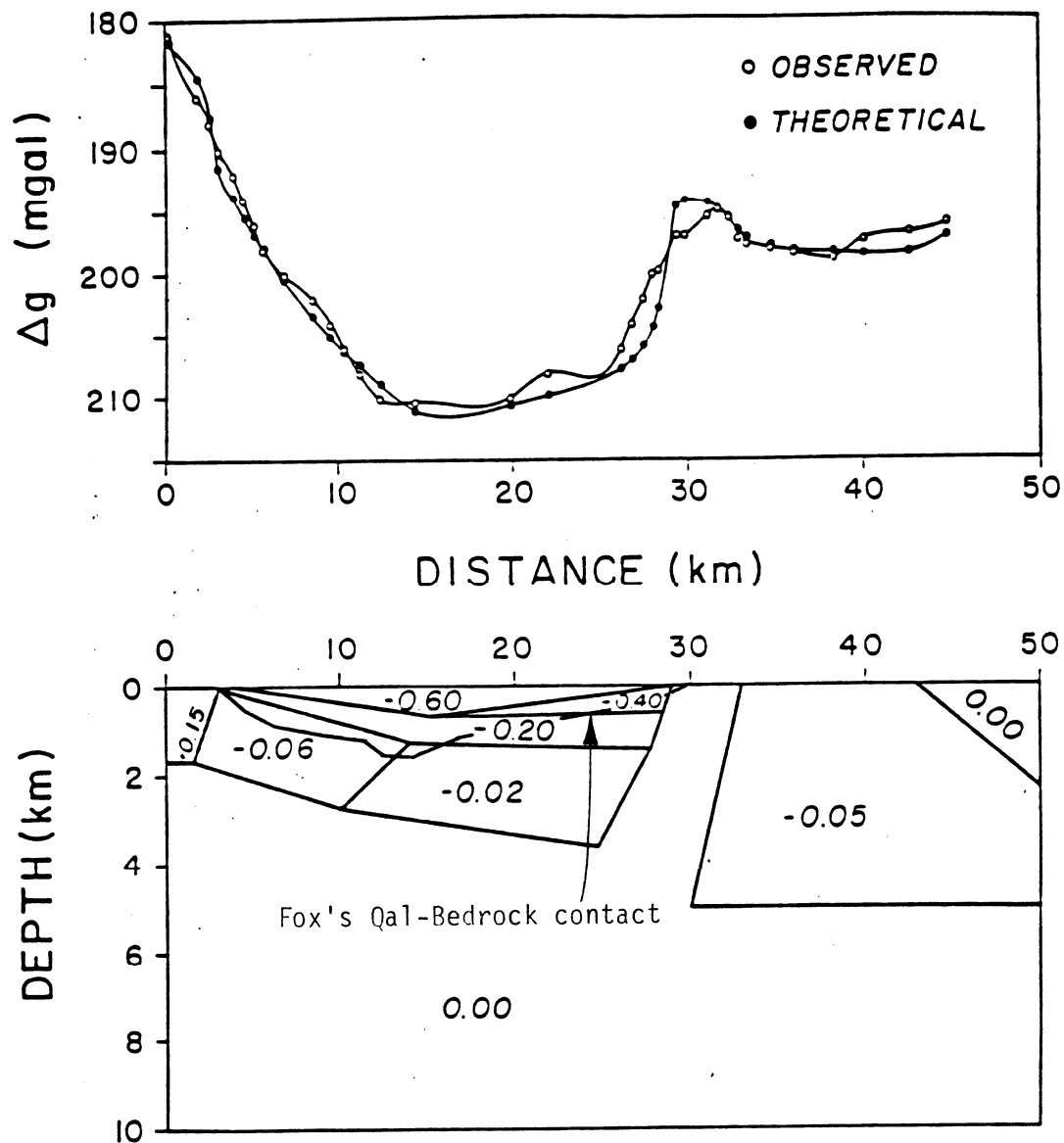


Figure 13. Observed complete Bouguer gravity anomaly of the Bingham-East profile and theoretical gravity anomaly of the given density model with Fox's (1983) Qal-Bedrock contact added (adapted from Bashore 1982).

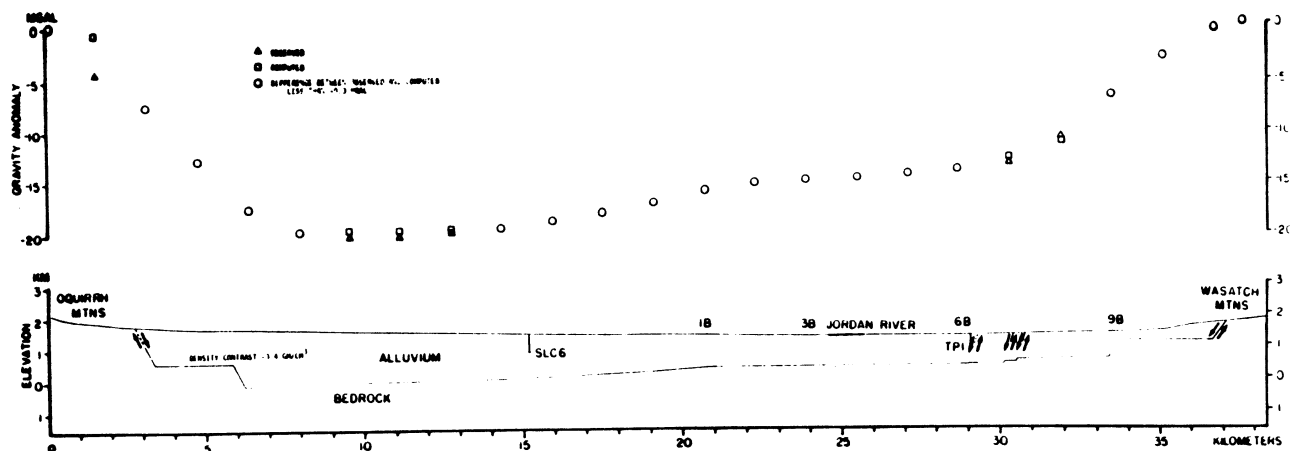


Figure 14. Cross section across Jordan Valley showing depth to bedrock as modeled from gravity data (from Wong 1979).

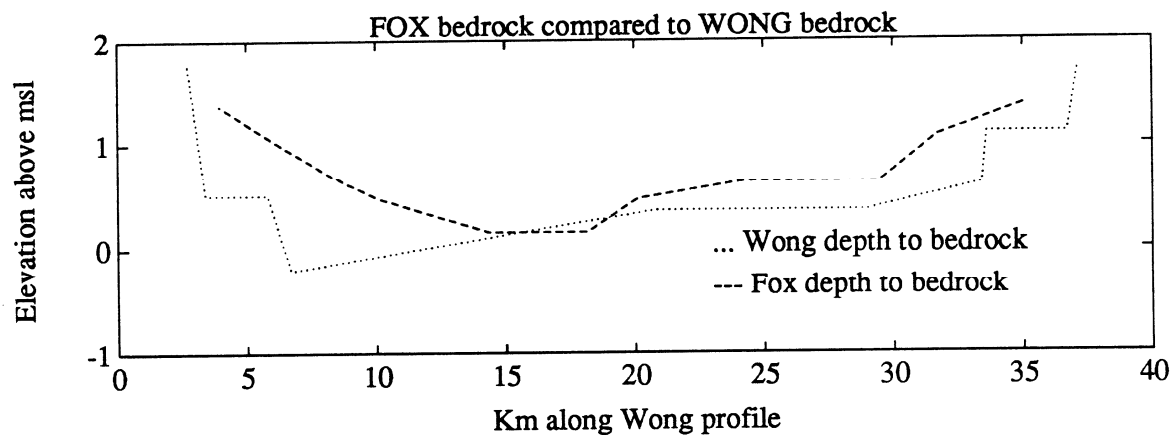


Figure 15. Wong's (1979) gravity model compared to Fox's (1983) gravity model.

However, the two interpretations do show similarity in their trends, and may correlate better if Fox's depths were from a profile instead of from a contour map. Even though there are some similarities between the two interpretations, the differences are large enough to effect the seismic wave focusing in the valley; therefore these differences should be resolved.

Integrated Seismic Well-Log Gravity Model

Hill (1988) digitized the sonic and density logs located in the vicinity of Celsius Energy Co.'s reflection survey (Figures 16, 17, 18, and 19). Figure 10 shows the location of the three wells in relation to R-11. Figure 20 shows a comparison of the well #2 sonic log to the rms velocities derived from the CDP reflection data which indicates a departure from the actual velocity below R2.

Using the sonic log (Figure 17) for well number 2, interval velocities of the three major layers in the valley were picked. The velocities are 1.89, 2.46, and 5.21 km/s for the unconsolidated, semi-consolidated, and consolidated layers respectively. It should be noted that some interpretations suggest that the semi-consolidated/consolidated interface is the alluvium-bedrock contact (Fox, Personal Communication). This may be a question of semantics and will not be addressed. With these velocities and first breaks picked from seismic reflection lines R-10 and R-11, depths to the three reflectors were determined along the entire length of the two profiles. A coarse cross-section from Fox's model along R-10 and R-11 is used to compare these two independent interpretations (Figures 21 and 22.)

Along R-10 Fox's interpretation does not correlate well with the seismic interpretation. However, smoother digitization of the gravity and seismic models may bring Fox's Qal-Bedrock contact more in line with the R2 interface. Also, Fox's pC horst block may possibly be moved to coincide with the 'high'

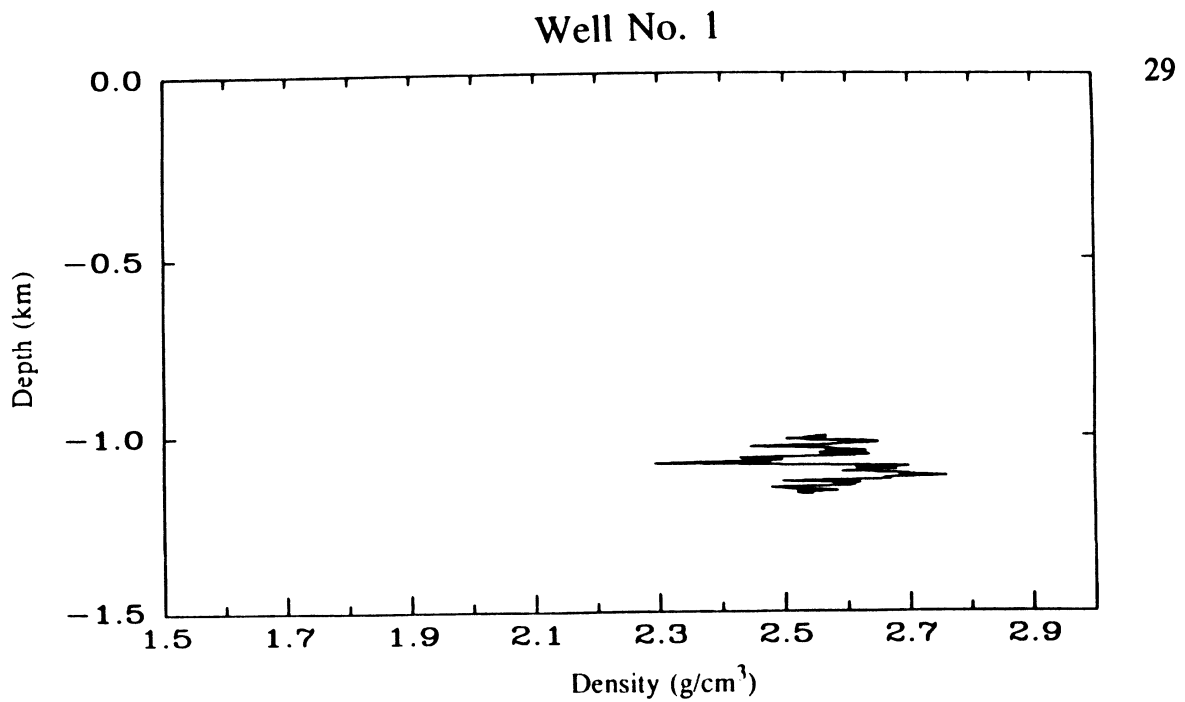


Figure 16. Formation density log for Well no. 1. The log only samples the consolidated sediment layer (from Hill 1988).

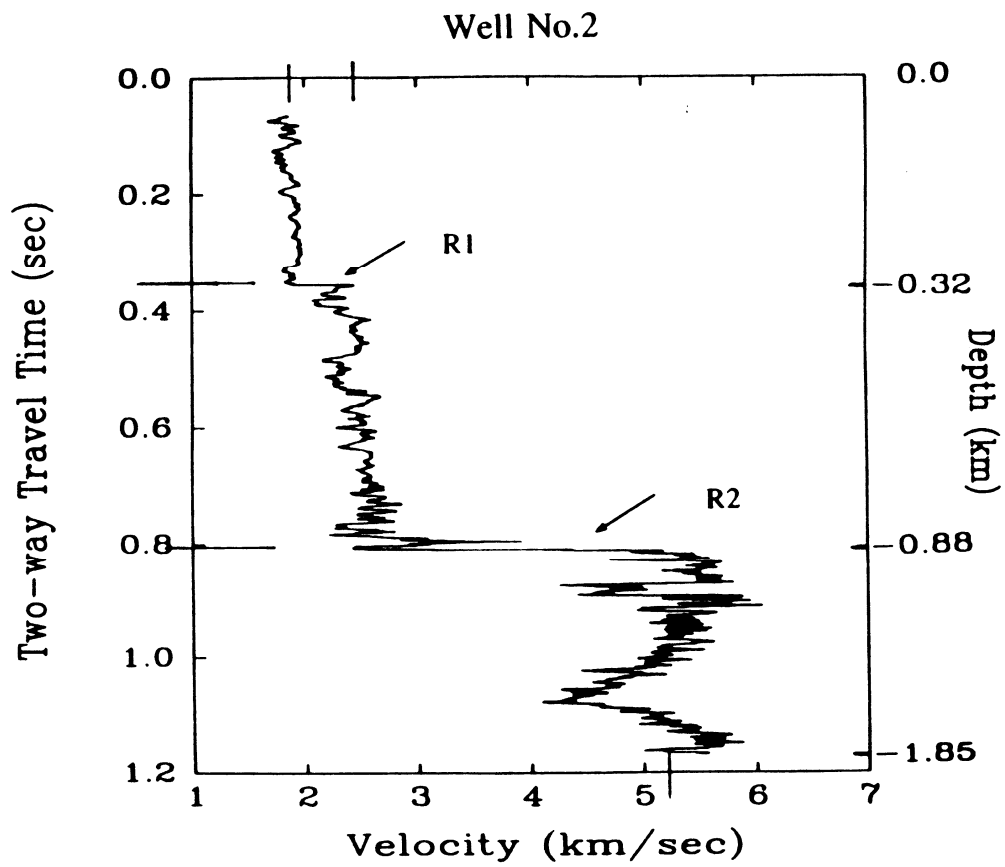


Figure 17. Sonic log for Well no. 2 showing R1 and R2 velocity gradients (from Hill 1988).

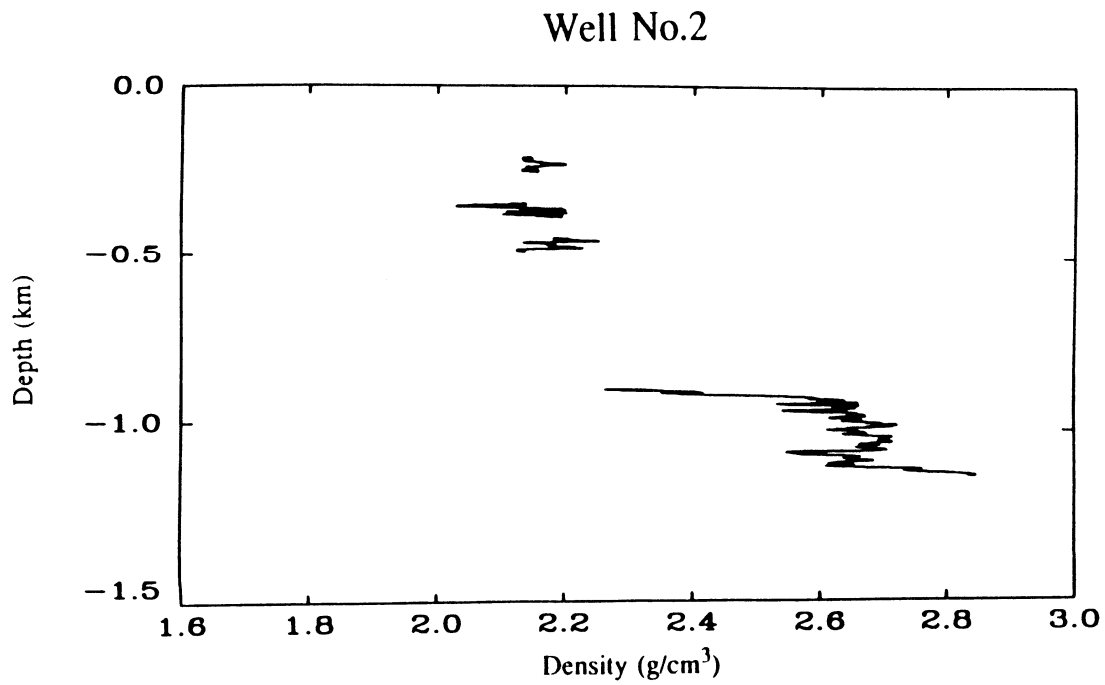


Figure 18. Formation density log for Well no.2 (from Hill 1988).

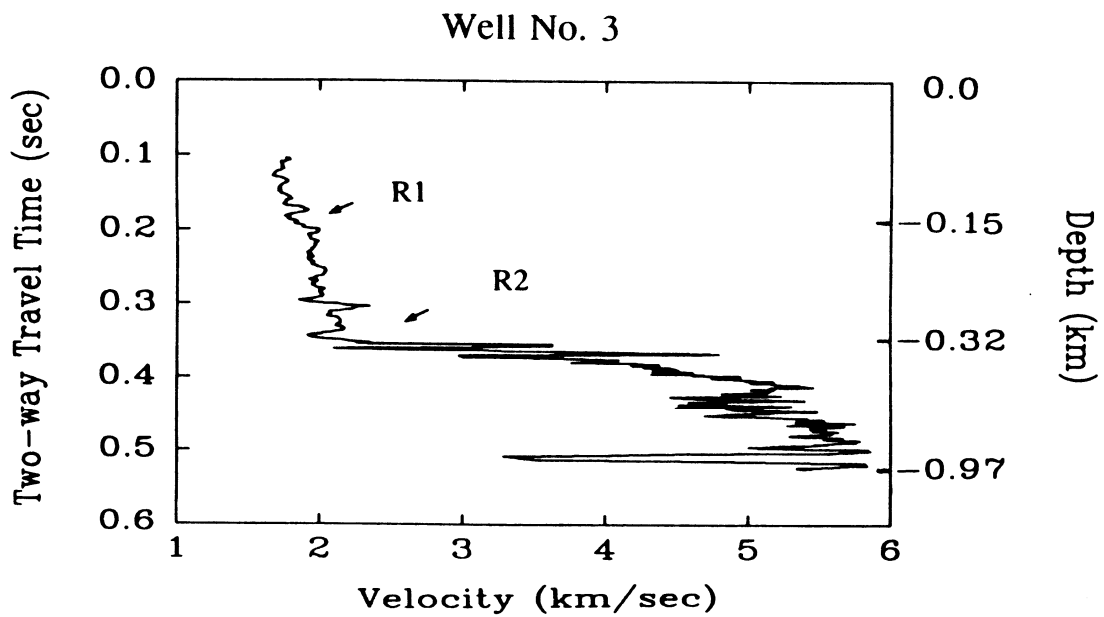


Figure 19. Sonic log for Well no. 3 showing R1 and R2 (from Hill 1988).

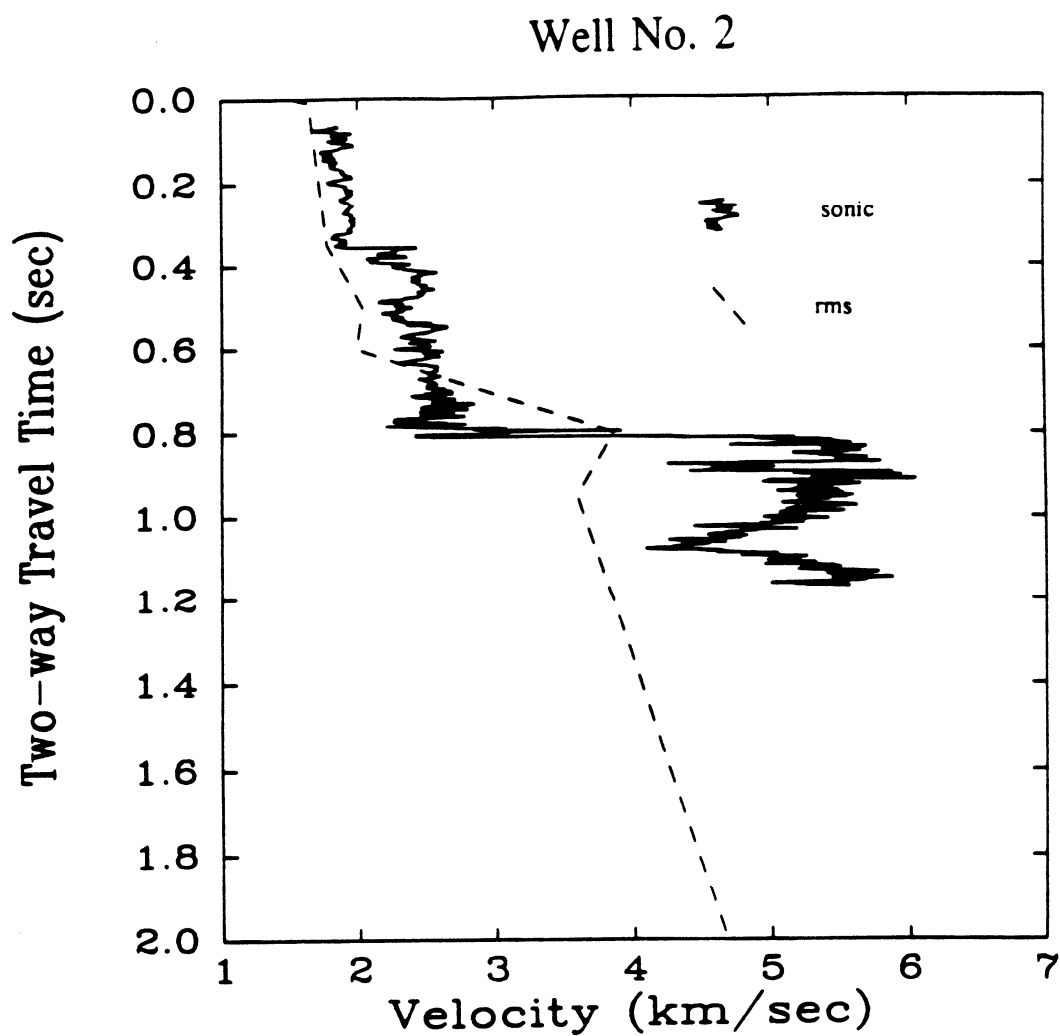


Figure 20. Plot demonstrating inaccuracy of seismic velocities with increasing travel times. Sonic log for Well no. 2 shown with rms velocities for the reflection data at the location of the well (from Hill 1988).

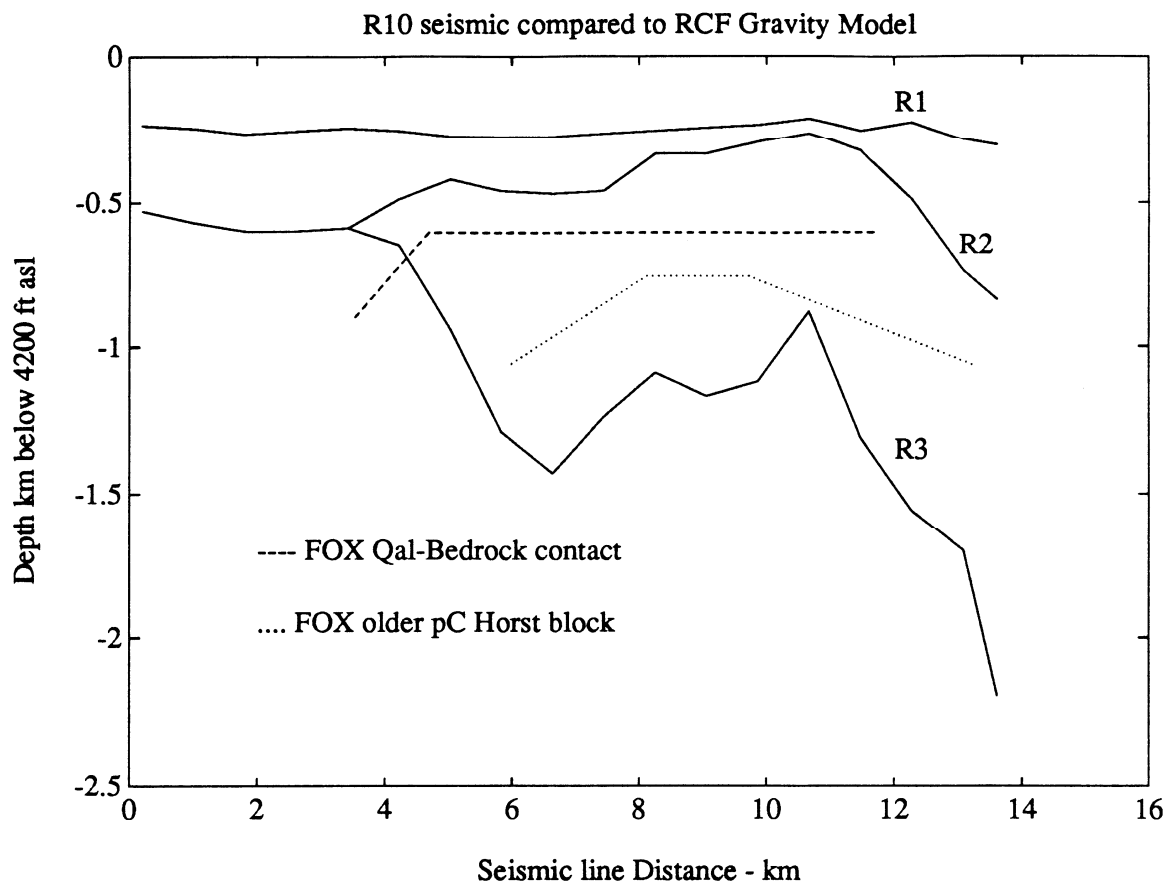


Figure 21. Seismic line R-10 compared to Fox's (1983) gravity model.

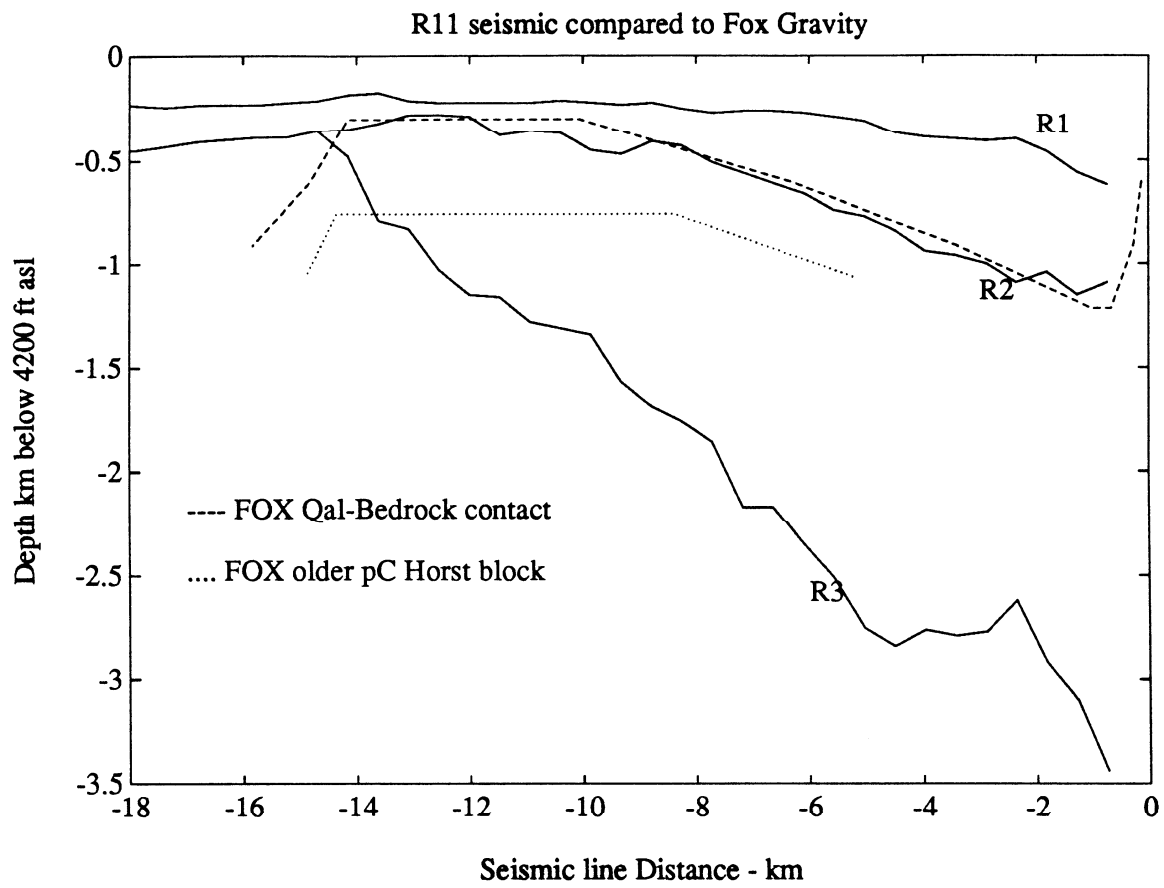


Figure 22. Seismic line R-11 compared to Fox's (1983) gravity model.

interpreted from the seismic data with only slight density change.

Along line R-11 Fox's Qal-Bedrock contact coincides quite well with the interpreted depth of R2, but the pC horst block does not match the R3 reflector. The horst block likely can be moved with little change in density to match R3. It should be noted that Fox did not use the seismic data during his Jordan Valley gravity interpretation but he did use well information.

Arnow's Quaternary Thickness Map. Figure 23 shows the Jordan Valley Quaternary Deposits digitized from a Quaternary thickness map (Arnow et al. 1970). The individual contour lines were digitized and are plotted as feet above mean sea level. The altitude of the valley floor varies by less than a few tens of feet along line R-11 so this conversion seems justified. Figure 24 compares the R-11 interpretation with a profile along the R-11 line taken from the Arnow et al. (1970) map.

This comparison shows some correlation in the western portion of the valley between the two interpretations. However, in the eastern half of the valley the interpreted depth to R2 departs from the Arnow et al. depth by nearly 50%. The correlation deteriorates as the interpreted depths get deeper; this may be a result of less information in the deeper areas being available to Arnow. The coarse digitization of the thickness map may also be responsible for the differences.

Since Arnow's thickness map is interpreted from the driller's logs of water wells, the well density in the deeper portions of the basin that penetrate the layers of interest may be too small for good contour control. This well density has not been studied. Also, the velocities used in the seismic interpretation should be examined for credibility. However, the velocities used are directly from the sonic log (Figure 16), and the well location nearly coincides with line

JORDAN VALLEY QUAT DEPOSITS

35

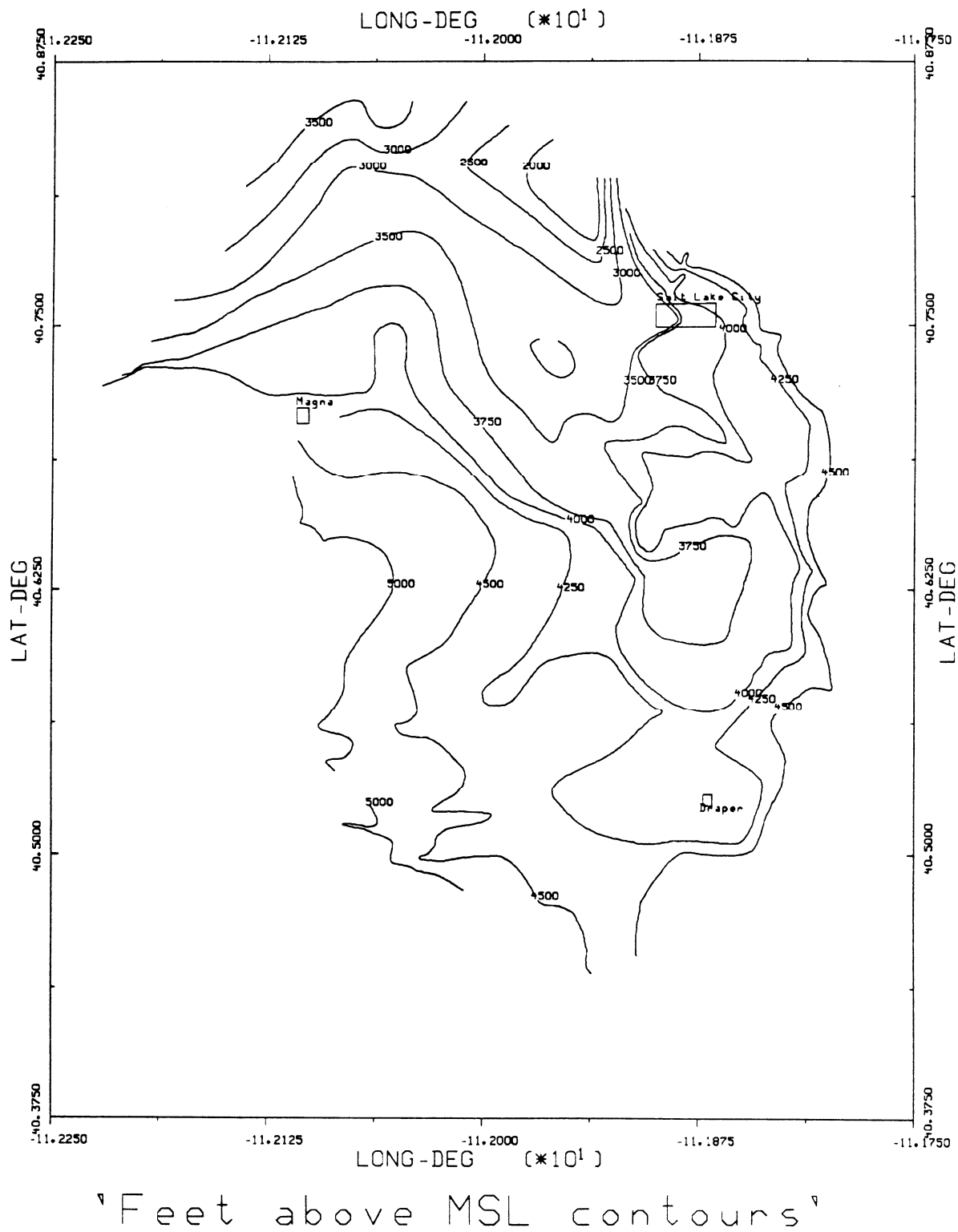


Figure 23. Jordan Valley Quaternary Deposits contour map (redigitized from Arnou et al 1970).

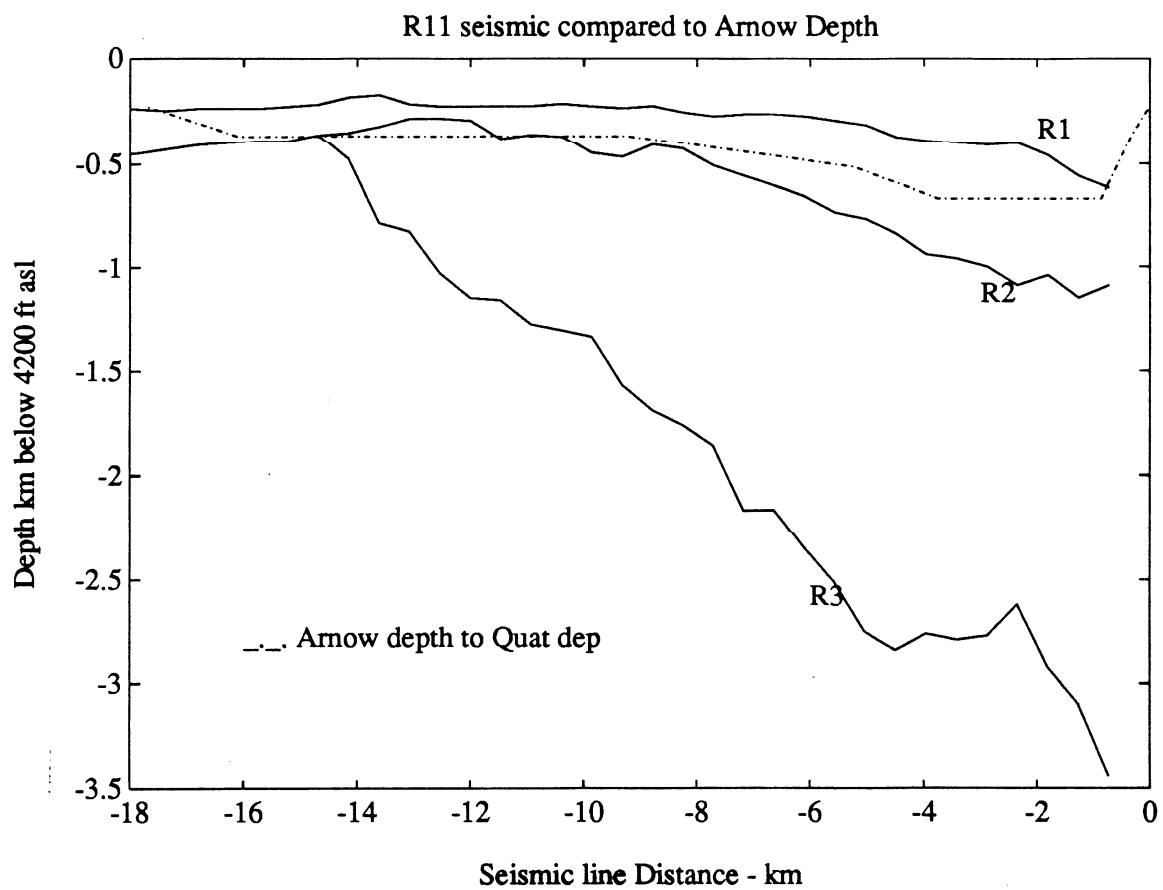


Figure 24. Seismic line R-11 compared to Arnow et al's Quaternary model.

R-11 and is located in the area of discrepancy (Figure 10). Certainly the seismic interpretations are more reliable indicators of the primary reflectors than are various driller's mud logs, and therefore, the depths contoured by Arnow et al. (1970) are in question.

Fox's interpretation through forward gravity modeling may be in error, but its excellent correlation with the seismic interpretation in the northern part of the valley can not be ignored (Figure 25). This conflict of Arnow et al.'s (1970) Quaternary deposits depth with Fox's interpretation and the seismic interpretation is not trivial for this study since the location of R2 is critical to the focusing of seismic energy (Hill, 1988).

USGS workers have compiled data in the Sugar House quadrangle to generate a contour map of loosely packed sediment thicknesses and depth to bedrock. This map is constructed with information presented by Arnow et al. (1970) and Mattick (1970) and is available from the USGS as MAP 1-766-M.

The shallow seismic studies are important to site amplification but, the layers they resolve will play little in the focusing of incoming low frequency seismic energy in the valley as a whole. Since the location of R2 is critical to the seismic focusing studies, its location should be determined by either forward gravity modeling or gravity inversion throughout the valley using all available seismic and well data for control. This work is still in progress at the University of Utah.

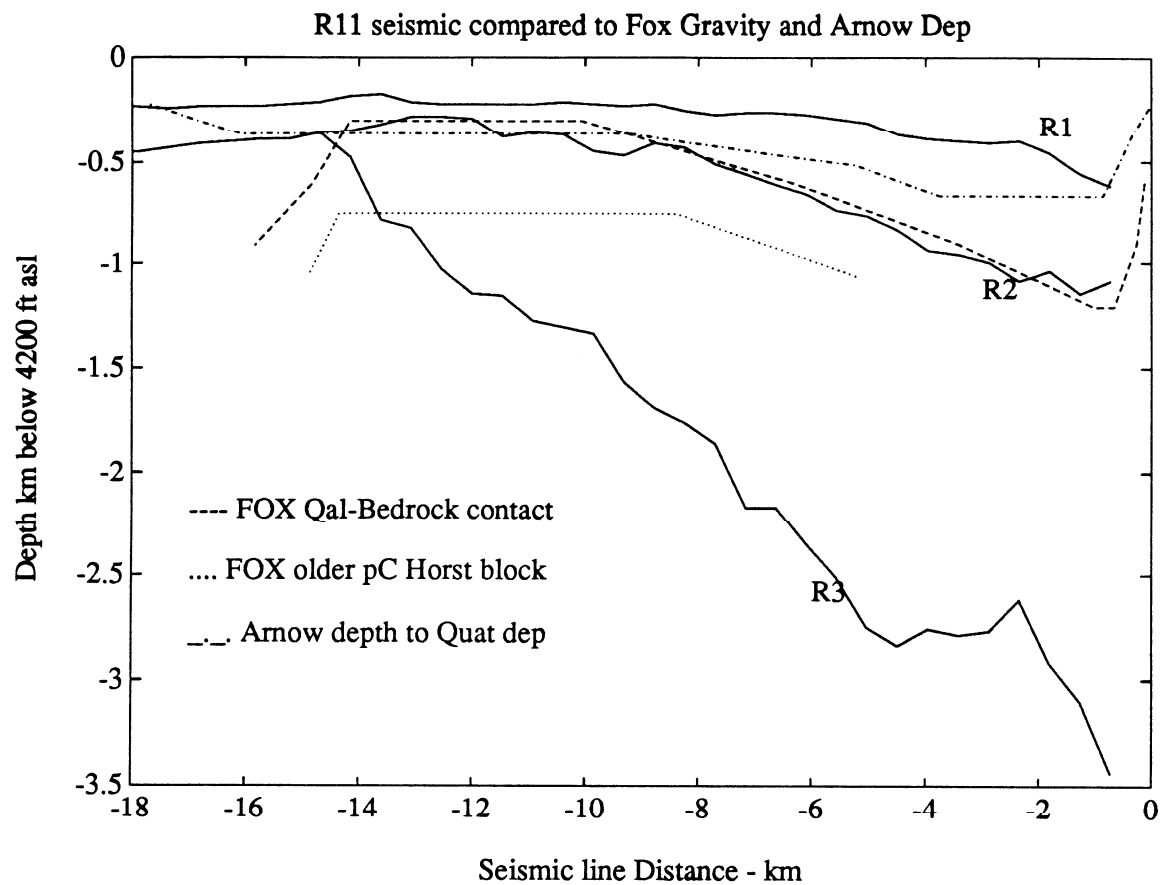


Figure 25. Seismic line R-11 with Fox's (1983) gravity model and Arnow et al's (1970) Quaternary model shown.

hcr, mem, and gts

III. NUMERICAL SIMULATION OF WAVE PROPAGATION

Wave propagation in Salt Lake Basin models is computer simulated to estimate the resonance and focusing patterns in the valley. The first section presents 2-D P-SV modeling of the wave equation by a second-order finite difference method, and the second section gives 3-D elastic results from a fourth-order finite difference method. There are several limitations inherent in finite difference modeling. These limitations include that (1) the material is assumed to be perfectly elastic, which means that non-linear effects cannot be modeled, (2) frequency dependent attenuation cannot be modeled, however, this effect is most likely negligible since the bandwidth examined is very narrow, and (3) knowledge of the basin's structure is not complete.

P-SV Wave Simulation

A second-order finite difference method is used to simulate P-SV wave propagation through 2-D models of the R-11 and Salt Lake City A-A' profiles (Figure 26). Two-component displacement synthetic seismograms are calculated at the surface of the model. The particle motion on the horizontal component is east-west, and both the horizontal and vertical component seismograms are true amplitude, normalized to the maximum amplitude of either seismogram. Poisson's ratio is assumed to be 0.25 throughout the model, and attenuation is assumed to be zero.

The first set of synthetic seismograms of the R-11 profile determines which reflector or combination of reflectors controls the low frequency wave amplification in the basin. The source is a vertically incident plane wave with vertical particle motion, propagating upward from the bottom of the model. The source is a low frequency Ricker wavelet with a dominant frequency of 0.9 Hz. Synthetic horizontal and vertical displacement seismograms were calculated at

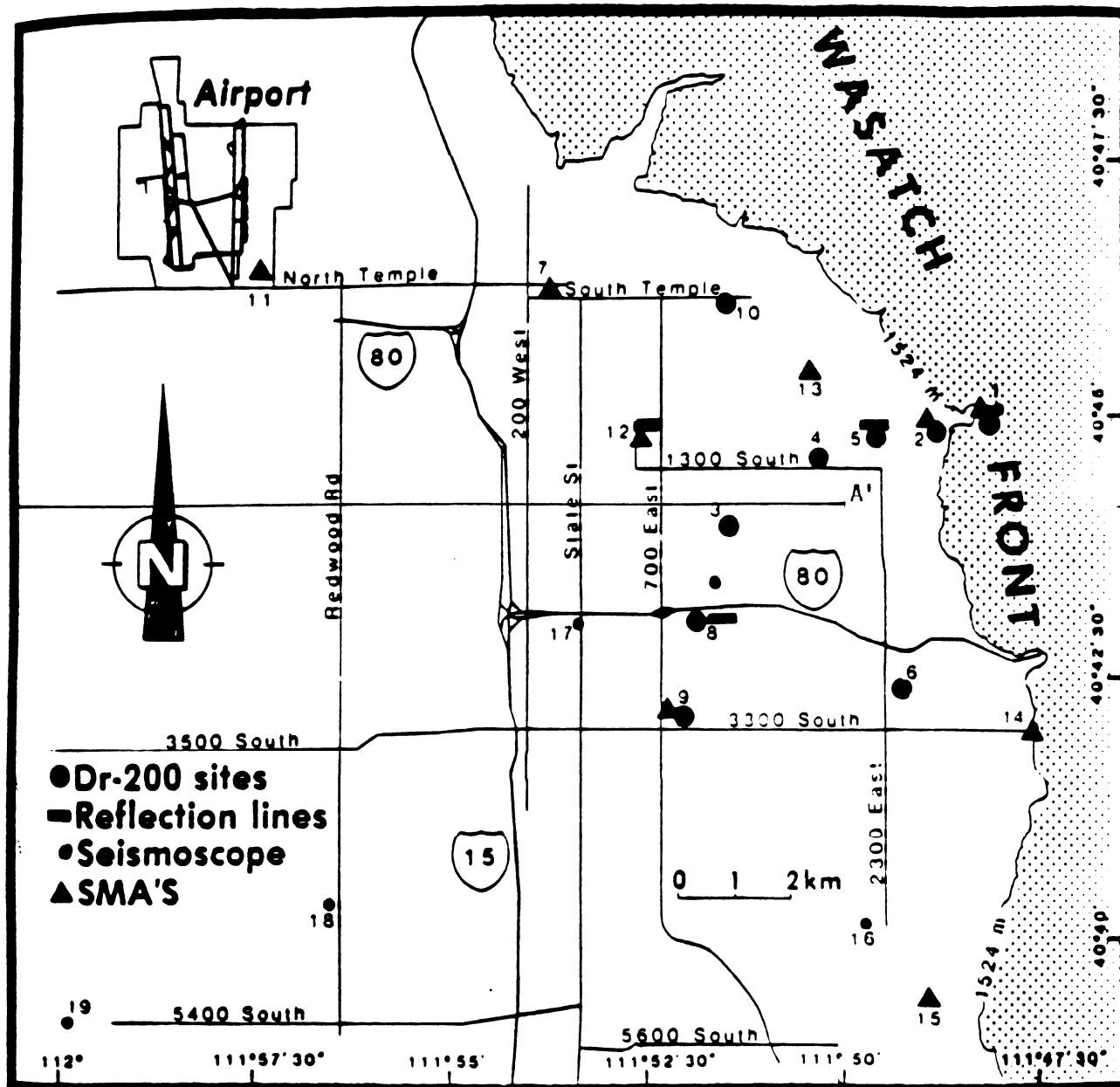


Figure 26. Locations of sites and their assigned station numbers in Salt Lake City at which ground motion recordings of nuclear explosions (closed circles) and shallow seismic reflection profiles (rectangles) were acquired. Eastern location of Salt Lake City profile A-A' is also shown (from King 1987).

the basin surface for models consisting of R2 (Figures 27, 28), R1 and R2 (Figures 29, 30), and R1, R2 and R3 (Figures 31, 32).

Results from this first set of simulations are:

- 1) The R2 reflector controls the general characteristics of the seismograms. Adding the R1 reflector increases the complexity and the duration of the shaking. The R3 reflector has little influence on the seismograms.
- 2) Rayleigh waves, which are surface waves, are the dominant wave form on all the P-SV seismograms. Rayleigh waves are generated off the fault in the east and propagate westward when the source is a vertically incident plane wave. The eastward dipping edge of the basin greatly diminishes the amplitude of the westward traveling Rayleigh waves.
- 3) The asymmetrical wedge shape of the R-11 profile tends to convert vertical seismic wave energy into horizontal wave energy. The maximum displacement is always the direct arrival on the vertical component at 23.2 km, although adding the lower velocity layer R1 increases the horizontal displacements with respect to the vertical displacements. The maximum displacement on the horizontal component always occurs at the surface expression of the fault for these models.

The next set of synthetic seismograms uses a line source instead of a plane wave source through the R-11 profile with all three reflectors. The line source has a peak frequency of 0.95 Hz, and has radial displacements. This type of source approximates a local earthquake rather than a teleseism. Benz and Smith (1988) have examined the effect of different sources on wave propagation through Bashore's model of a southern Salt Lake Valley cross-section.

The line source located at 25 km east and 14.8 km depth simulates an

R-11 Profile

Reflector 2 Model

Semiconsolidated - Consolidated Sediment Contact

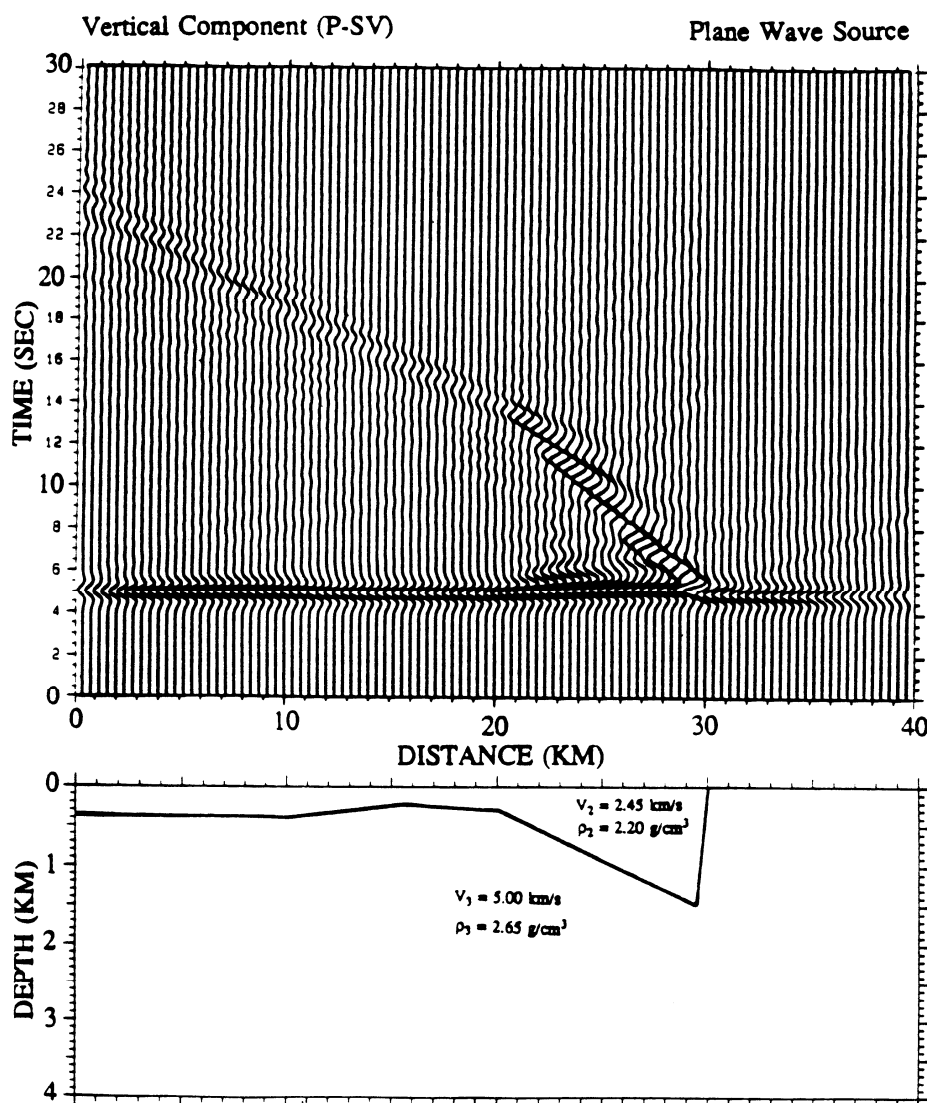


Figure 27. Vertical component synthetic seismogram for model of R-11 consisting of only reflector 2. The source is a vertically incident plane wave with a peak frequency of 0.95 Hz.

R-11 Profile

Reflector 2 Model

Semiconsolidated - Consolidated Sediment Contact

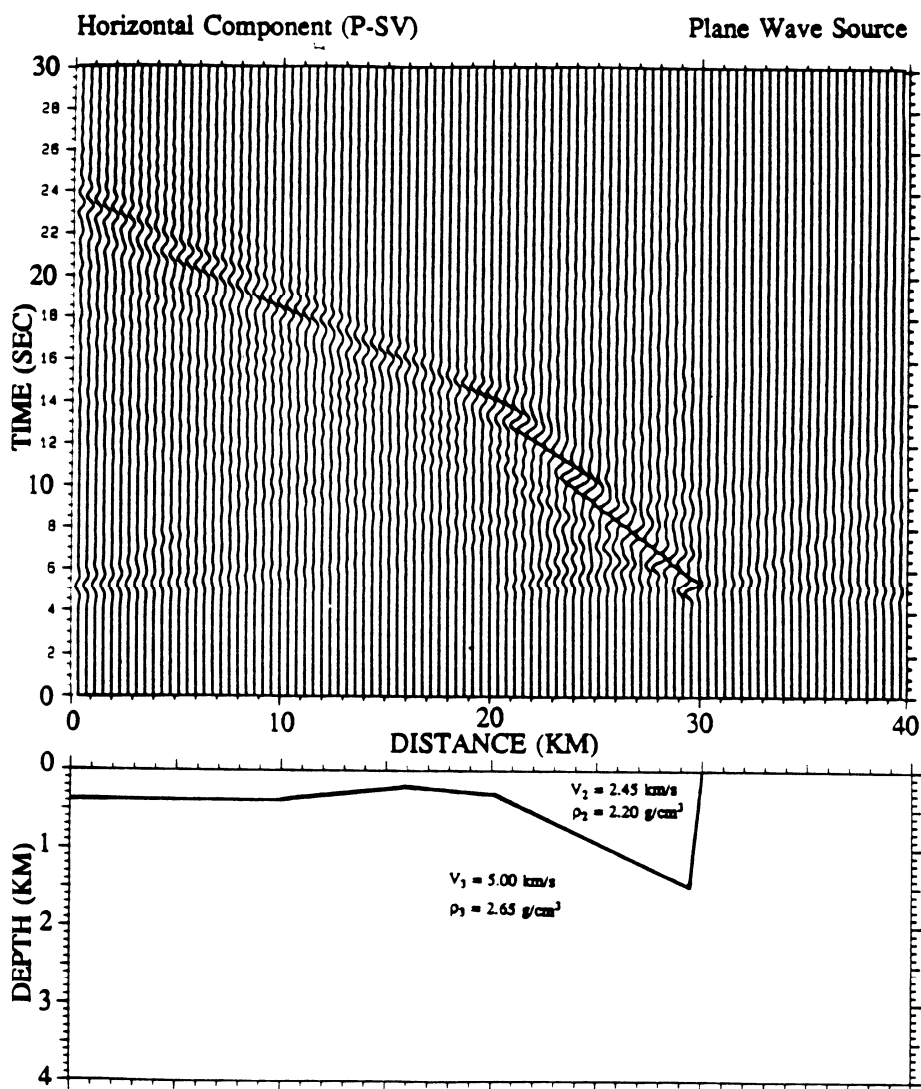


Figure 28. Horizontal component synthetic seismogram for model of R-11 consisting of only reflector 2. The source is a vertically incident plane wave with a peak frequency of 0.95 Hz.

Reflectors 1 & 2 Model

Unconsolidated - Semiconsolidated Sediment Contact

Semiconsolidated - Consolidated Sediment Contact

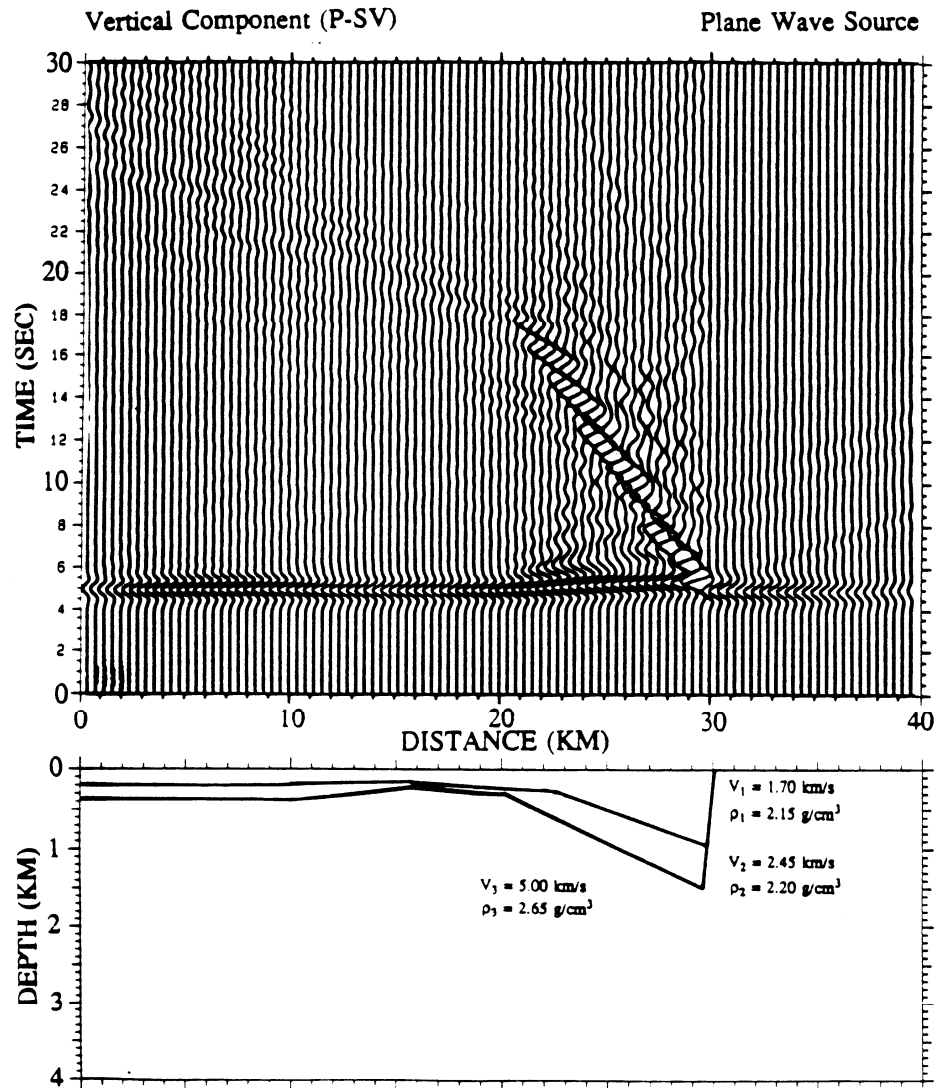


Figure 29. Vertical component synthetic seismogram for model of R-11 consisting of reflectors 1 & 2. The source is a vertically incident plane wave with a peak frequency of 0.95 Hz.

Reflectors 1 & 2 Model

Unconsolidated - Semiconsolidated Sediment Contact

Semiconsolidated - Consolidated Sediment Contact

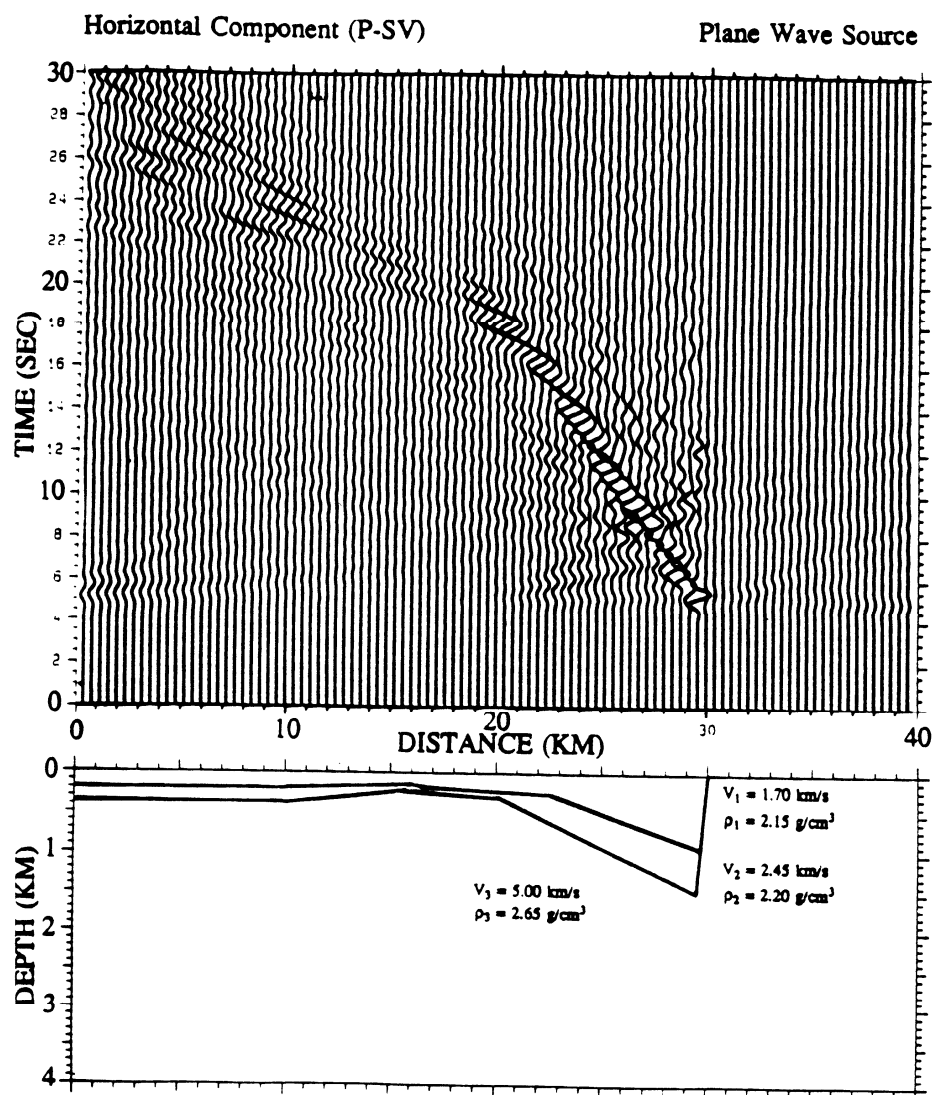


Figure 30. Horizontal component synthetic seismogram for model of R-11 consisting of reflectors 1 & 2. The source is a vertically incident plane wave with a peak frequency of 0.95 Hz.

R-11 Profile

Reflectors 1, 2 & 3 Model

Unconsolidated - Semiconsolidated Sediment Contact

Semiconsolidated - Consolidated Sediment Contact

Consolidated Sediment - Basement Contact

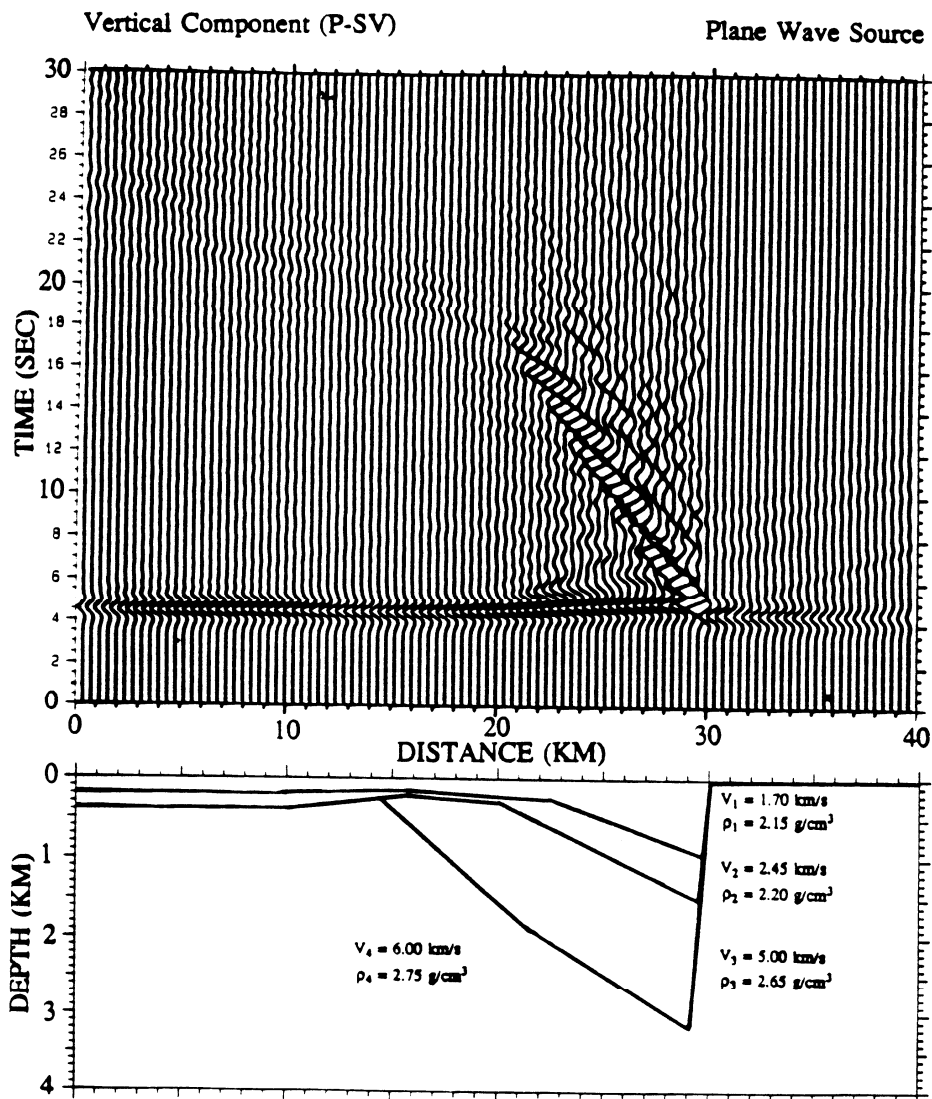


Figure 31. Vertical component synthetic seismogram for model of R-11 consisting of all three reflectors. The source is a vertically incident plane wave with a peak frequency of 0.95 Hz.

R-11 Profile

Reflectors 1, 2 & 3 Model

Unconsolidated - Semiconsolidated Sediment Contact

Semiconsolidated - Consolidated Sediment Contact

Consolidated Sediment - Basement Contact

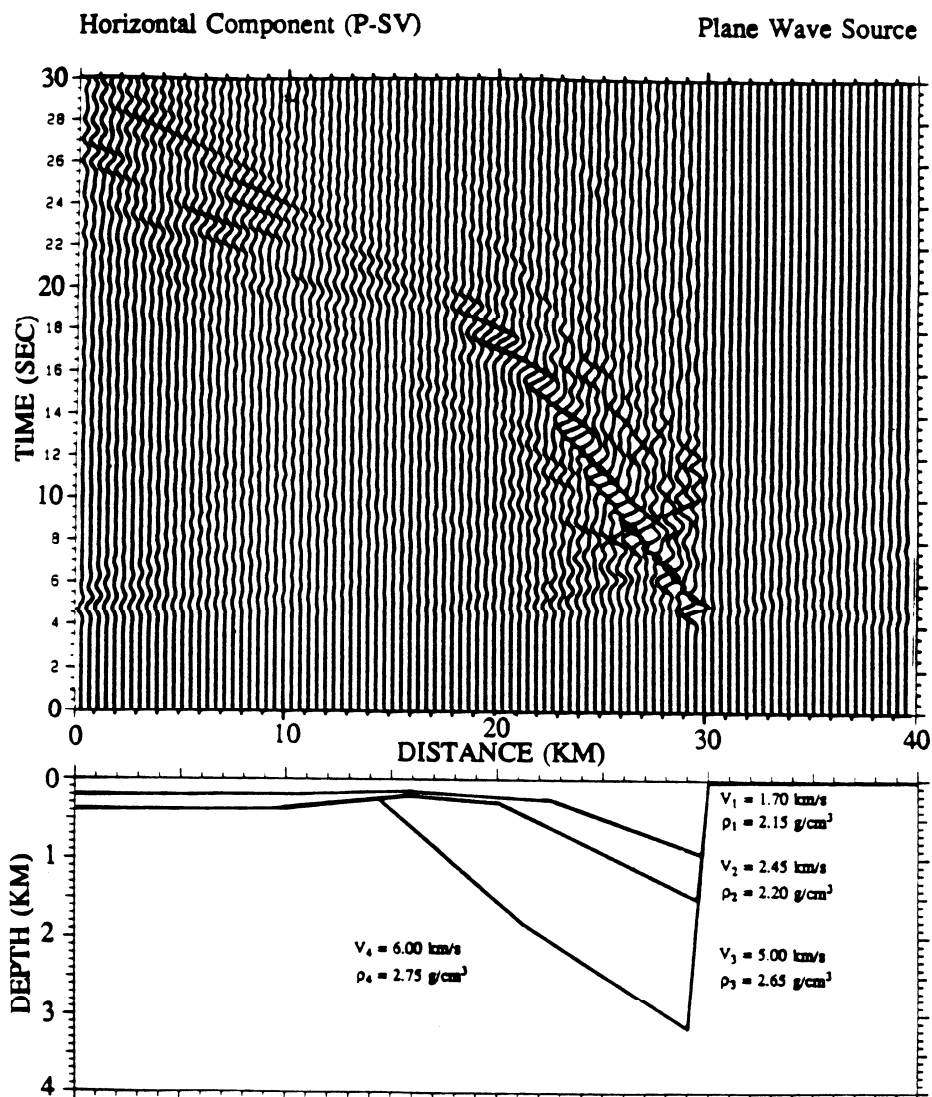


Figure 32. Horizontal component synthetic seismogram for model of R-11 consisting of all three reflectors. The source is a vertically incident plane wave with a peak frequency of 0.95 Hz.

earthquake along the Wasatch (Warm Springs) fault. Because most of the incident source energy from underneath the basin is still vertical, these seismograms (Figures 33, 34) are very similar to those for the plane wave source (Figure 31, 32). The main features are the direct wave on the vertical component and the eastward traveling Rayleigh waves generated off the fault.

The seismograms with the line source located under the western part of the basin, at 5 km east and 10 km depth illustrate how source location can affect shaking in the basin. On all previous seismograms, the incident source energy in the basin had been nearly entirely vertical, and most of the horizontal energy resulted from wave conversions. In Figures 35 and 36, a good portion of the incident wave energy is horizontal, and this, in addition to the strong amplitude surface waves which are generated from the western part of the basin and are reflected off the Wasatch fault, increases the duration of shaking above the basin. Also note that with the source in the west, very little energy is transmitted to the hardrock sites in the east (> 35 km).

Although the R-11 profile is not located near King's USGS spectral ratio stations, synthetic spectral ratios, calculated at locations estimated to be similar in underlying structure to those at King's stations 3 and 8, were compared for the three different types of sources. A spectral ratio is a relative measure of amplification of a sedimentary location with respect to a hardrock location; it is calculated by dividing the Fourier response of a sedimentary site seismogram by the Fourier response of a hardrock site seismogram. The synthetic spectral ratios for the R-11 profile are calculated by dividing the Fourier response of the basin trace at 28 km by that of the hardrock trace at 35 km. All the spectral ratios were calculated using sedimentary and hardrock traces from the same component, with the exception of those from plane wave source. Because the plane wave source is vertically incident, the horizontal component does not record a

R-11 Profile

Reflectors 1, 2 & 3 Model

Unconsolidated - Semiconsolidated Sediment Contact

Semiconsolidated - Consolidated Sediment Contact

Consolidated Sediment - Basement Contact

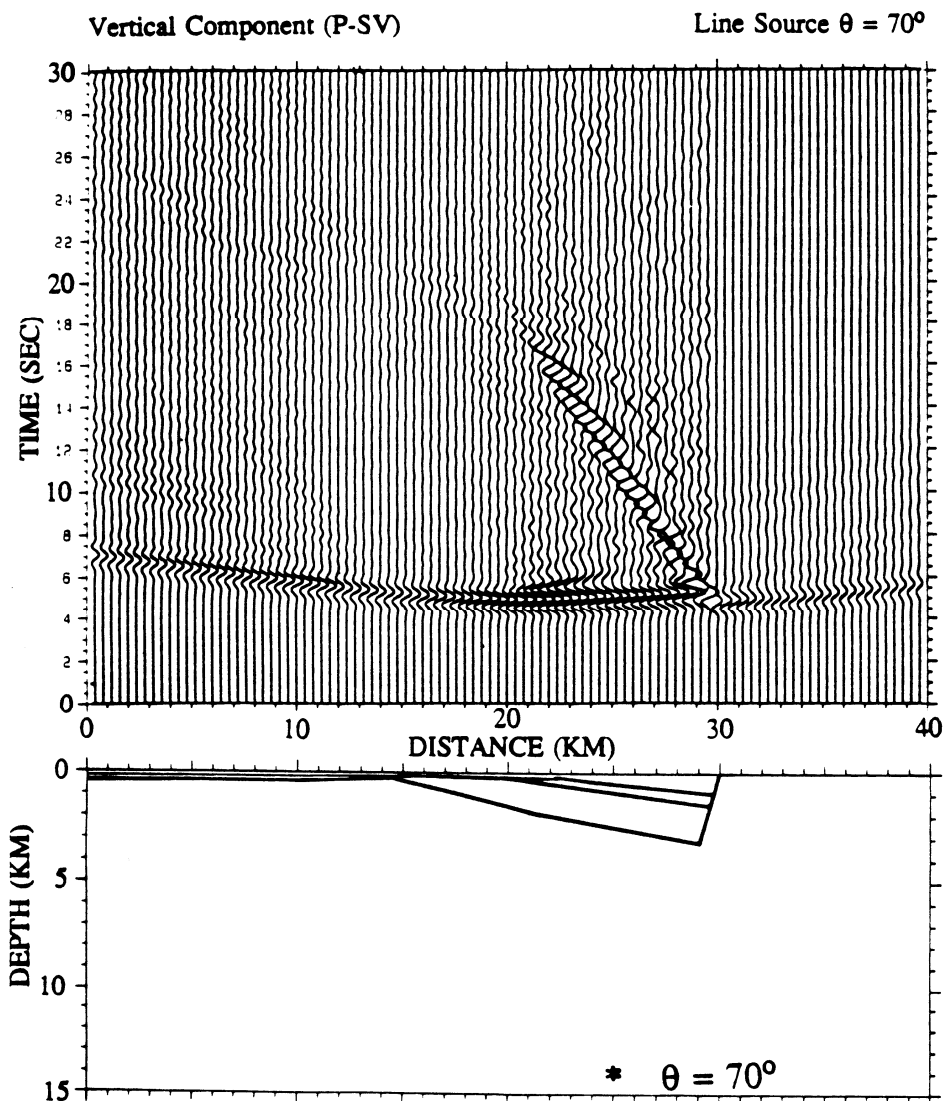


Figure 33. Vertical component synthetic seismogram for model of R-11 consisting of all three reflectors. The source is a line source located at 25 km east and 14.8 km depth. The source propagates with radial displacements about the line, and the wavelet has a peak frequency of 0.95 Hz.

R-11 Profile

Reflectors 1, 2 & 3 Model

Unconsolidated - Semiconsolidated Sediment Contact

Semiconsolidated - Consolidated Sediment Contact

Consolidated Sediment - Basement Contact

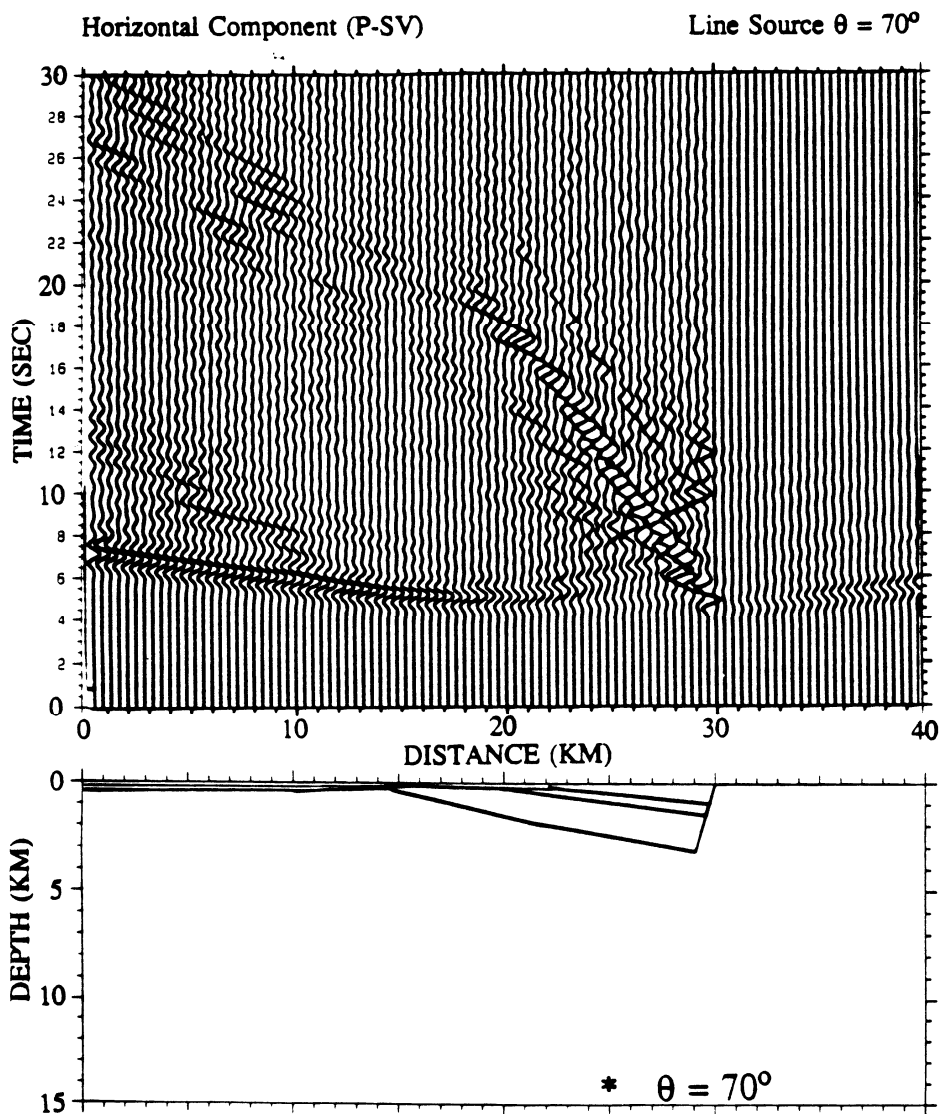


Figure 34. Horizontal component synthetic seismogram for model of R-11 consisting of all three reflectors. The source is a line source located at 25 km east and 14.8 km depth. The source propagates with radial displacements about the line, and the wavelet has a peak frequency of 0.95 Hz.

R-11 Profile

Reflectors 1, 2 & 3 Model

Unconsolidated - Semiconsolidated Sediment Contact

Semiconsolidated - Consolidated Sediment Contact

Consolidated Sediment - Basement Contact

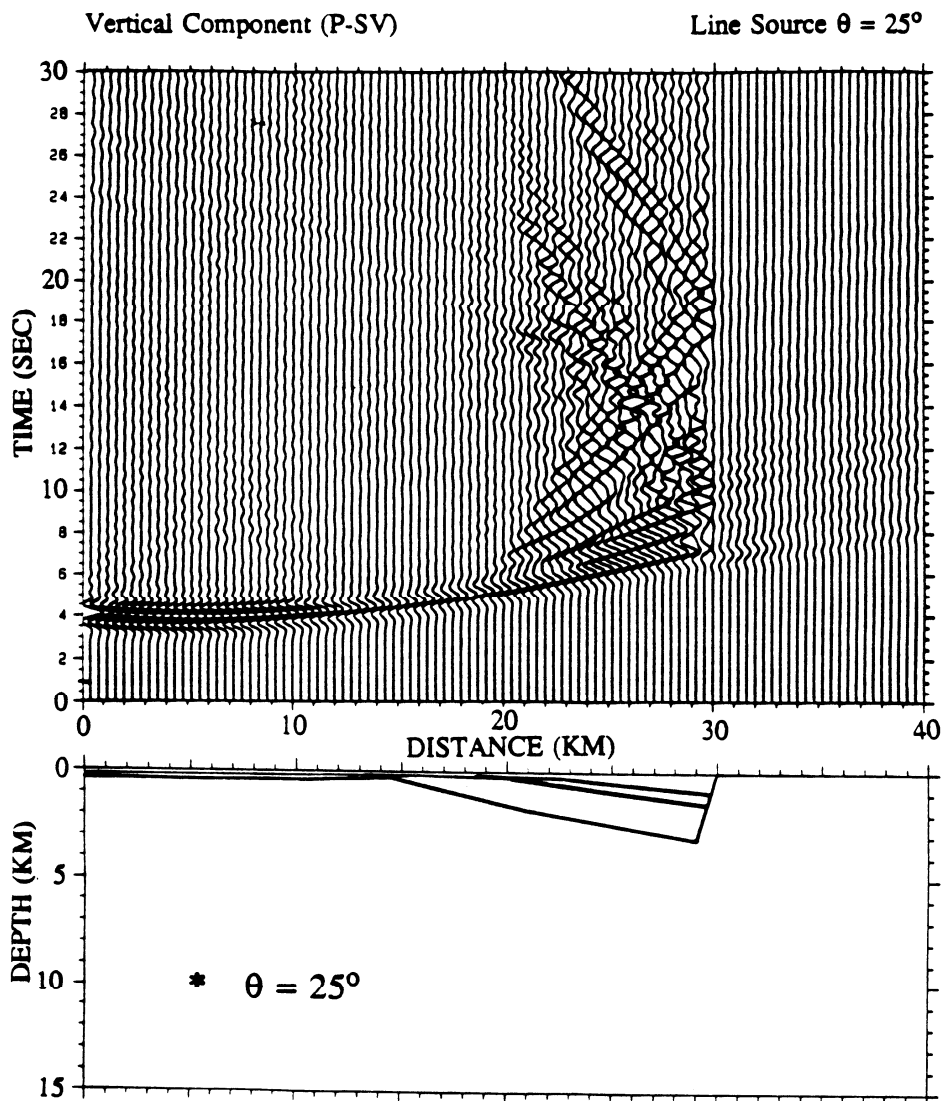


Figure 35. Vertical component synthetic seismogram for model of R-11 consisting of all three reflectors. The source is a line source located at 5 km east and 10 km depth. The source propagates with radial displacements about the line, and the wavelet has a peak frequency of 0.95 Hz.

R-11 Profile

Reflectors 1, 2 & 3 Model

Unconsolidated - Semiconsolidated Sediment Contact

Semiconsolidated - Consolidated Sediment Contact

Consolidated Sediment - Basement Contact

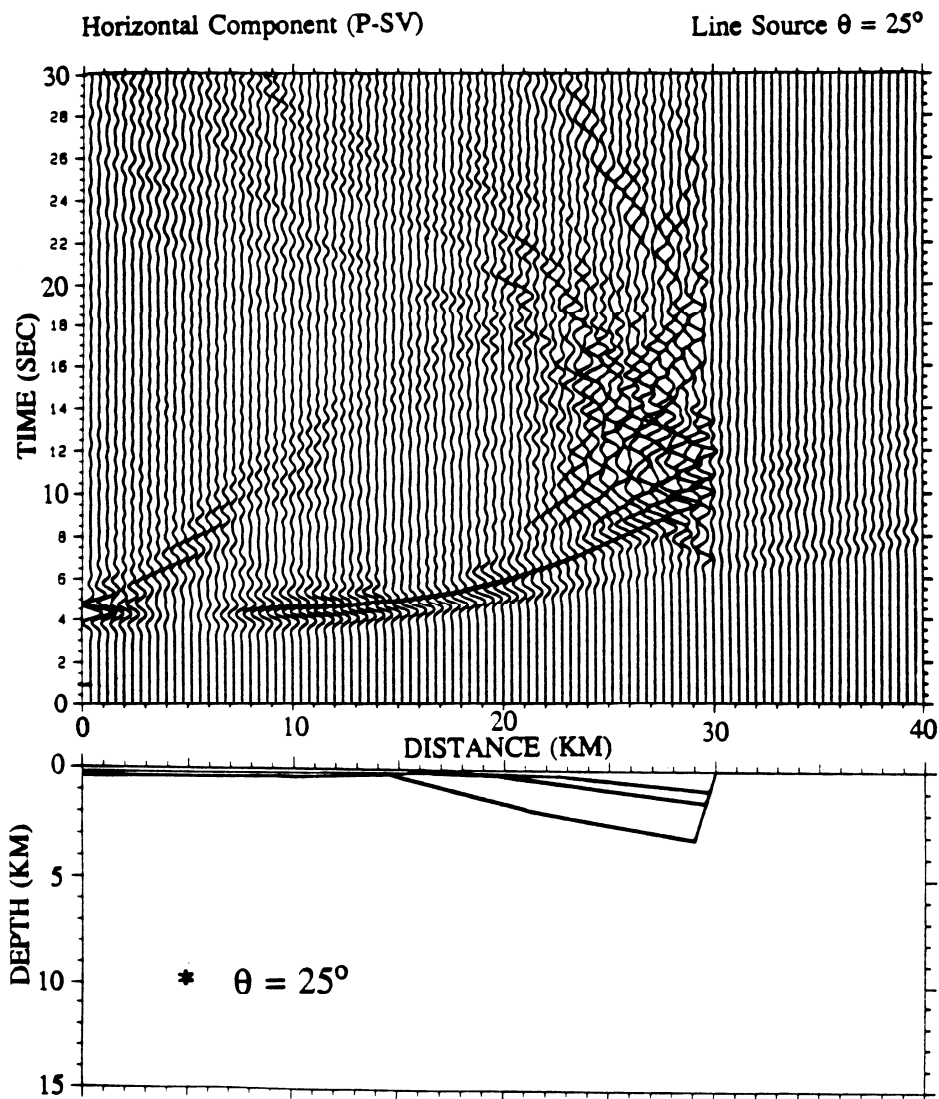


Figure 36. Horizontal component synthetic seismogram for model of R-11 consisting of all three reflectors. The source is a line source located at 5 km east and 10 km depth. The source propagates with radial displacements about the line, and the wavelet has a peak frequency of 0.95 Hz.

direct arrival and contains very little energy. Therefore for all the horizontal spectral ratios with a plane wave source, a vertical component trace was used to calculate the hardrock Fourier response.

In addition, because of the narrow bandwidth of the source, the synthetic spectral ratios are calculated from 0.3 to 1.7 Hz, while the USGS spectral ratios are calculated from 0.3 to 5.0 Hz. For comparison of the synthetic and measured mean amplification, the bandwidth from 0.3 to 1.7 Hz was used to calculate both synthetic and USGS means.

The synthetic spectral ratios for the plane wave source (Figure 37) show good correlation with the USGS spectral ratios for sites 3 and 8. The synthetic horizontal mean amplifications are within 42% of the measured USGS mean amplifications of stations 3 and 8. The synthetic vertical mean amplifications are within 60% and 83% of the measured means at stations 3 and 8, respectively. The synthetic spectral ratio means for the line source at $\theta = 70^\circ$ (Figure 38) improve to an average of 68% of the USGS measured mean amplifications for the horizontal component and 85% for the vertical component.

The synthetic spectral ratios increase dramatically for the line source $\theta = 25^\circ$ (Figure 39). The synthetic mean amplifications are approximately 158% of measured mean amplification for the horizontal component, and 360% of the measured mean amplification for the vertical component. The amplification increase occurs because when the line source is located in the west, very little energy is transmitted to the hardrock sites in the east. The seismograms (Figures 35, 36) show that most energy traveling from west to east is reflected back into the basin. This reduces the energy transmitted to the hardrock site, which inflates the spectral ratio.

The last sequence of synthetic seismograms are generated for cross-sectional

R-11 Profile - Plane Wave Source

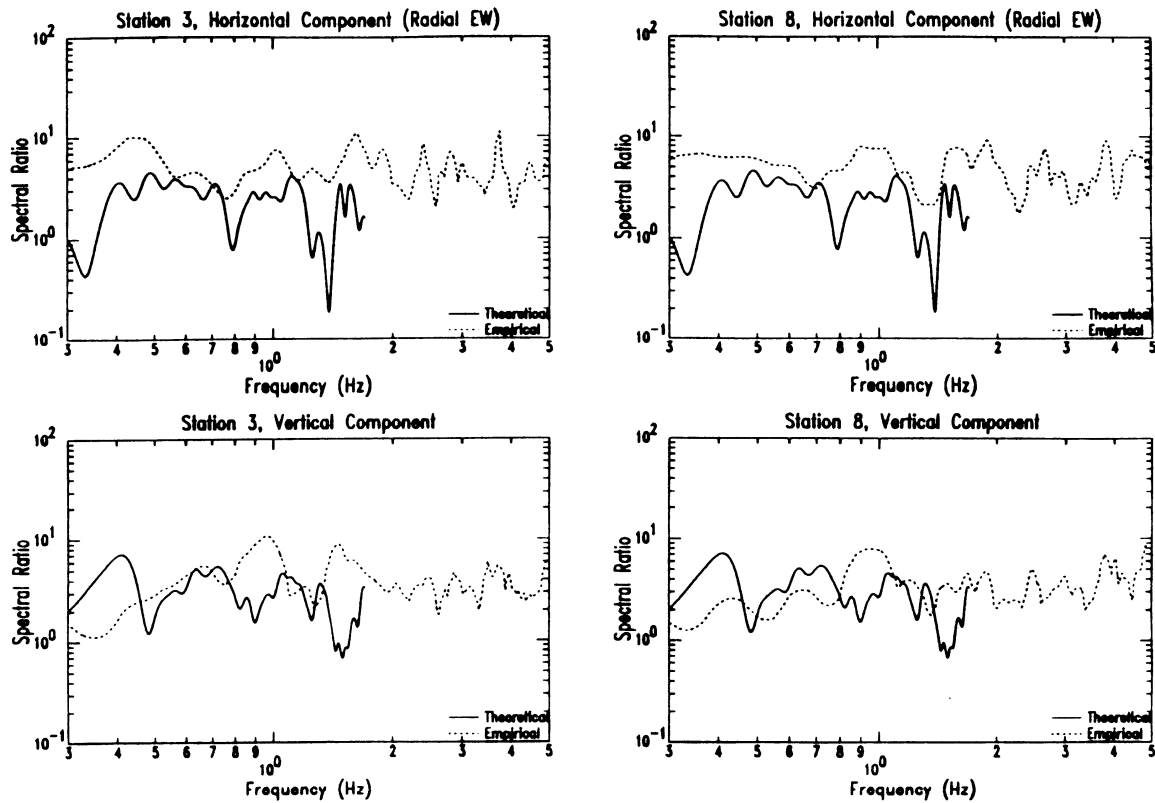


Figure 37. Empirical and synthetic spectral ratios for the R-11 model consisting of all three reflectors. The source for the synthetics is a plane wave source with a peak frequency of 0.95 Hz (Figures 31, 32) The synthetic spectral ratios for the horizontal and vertical components are plotted against empirical measurements from USGS stations 3 and 8.

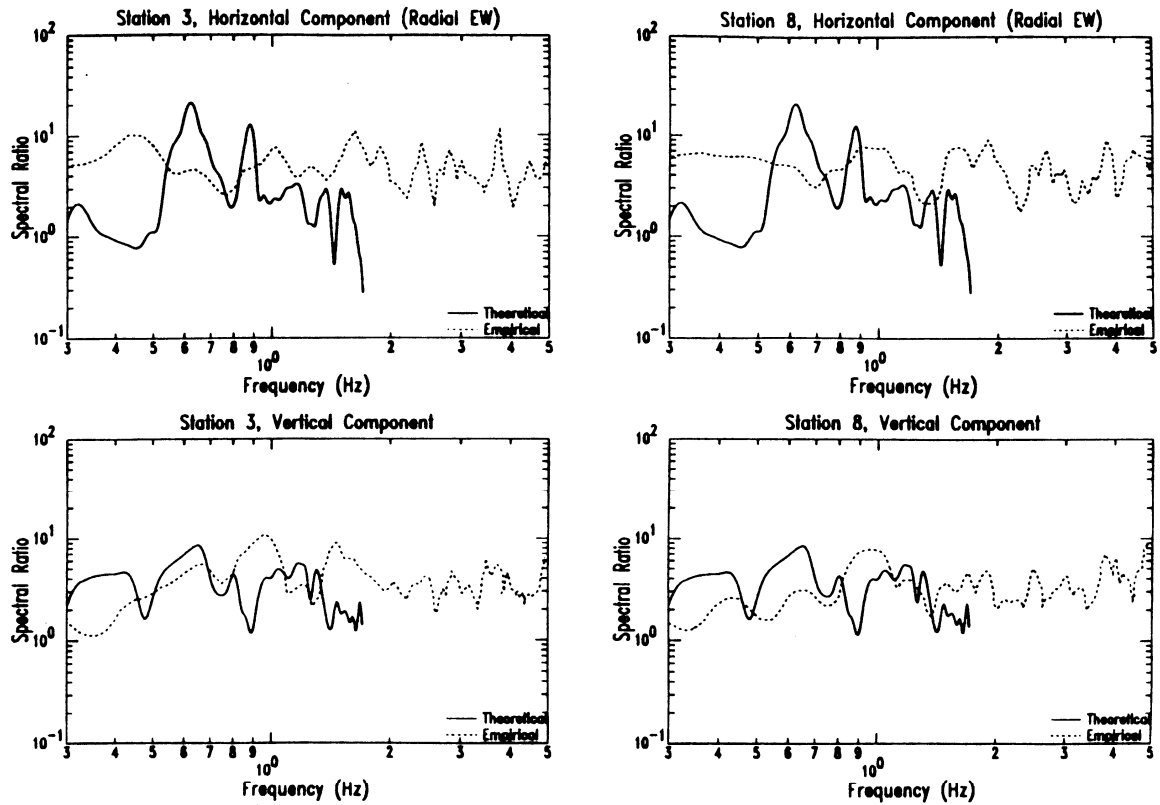
R-11 Profile - Line Source $\theta = 70^\circ$ 

Figure 38. Empirical and synthetic spectral ratios for the R-11 model consisting of all three reflectors. The source for the synthetics is a line source with a peak frequency of 0.95 Hz located at 25 km east and 14.8 km depth (Figures 33, 34). The synthetic spectral ratios for the horizontal and vertical components are plotted against empirical measurements from USGS stations 3 and 8.

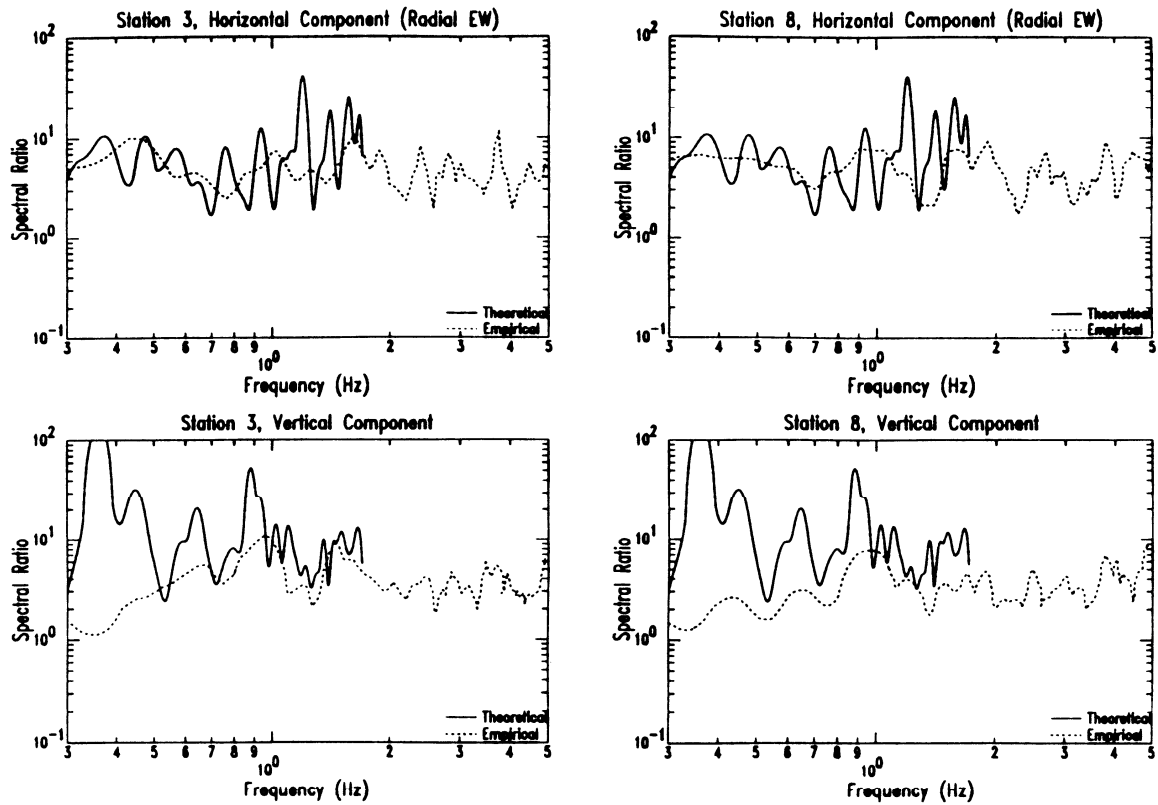
R-11 Profile - Line Source $\theta = 25^\circ$ 

Figure 39. Empirical and synthetic spectral ratios for the R-11 model consisting of all three reflectors. The source for the synthetics is a line source with a peak frequency of 0.95 Hz located at 5 km east and 10 km depth (Figures 35, 36). The synthetic spectral ratios for the horizontal and vertical components are plotted against empirical measurements from USGS stations 3 and 8.

models constructed from Fox's gravity inversion map and Arnow and Mattick's Quaternary sediment map. Fox constructed a 2-D cross-section C-C' by inverting gravity data with an assumed contrast of 0.45 g cm^{-3} , which is the density contrast across the R2 reflector in the R-11 profile. The Fox cross-section used for the Salt Lake City profile also runs through the area where King's spectral ratio stations are located (Figure 26). The geometry of Fox's 2-D cross-section C-C' is used as the Salt Lake City profile's R2 layer. The R1 layer was picked from contours from Arnow's Quaternary sediment map. The two layers in the Salt Lake City profile are assumed to have the same impedance contrasts as those across the R1 and R2 reflectors in the R-11 profile.

The attenuation is assumed to be zero and Poisson's ratio is assumed to be 0.25 throughout the model. The peak frequency is 1.95 Hz for the plane wave model, and 1.3 Hz for the line source model. Because of the increase in frequency, the seismogram lengths have been reduced to 20 seconds. The cross-section model A-A' shown on Figure 10 is located on the synthetic model from 12.1 km to 35 km, with the padding from 0.0 km to 12.1 km and 35 km to 50 km added to minimize edge and corner effects on the interior traces.

Figures 40 and 41 show the synthetic seismograms for the Salt Lake City profile. The largest amplitude waveform is the direct arrival at 3 km on the vertical component. The first multiple on the vertical component is the next largest, with the slow Rayleigh waves having displacements less than 50% of those of the direct arrivals. The Rayleigh waves have smaller amplitudes with respect to the direct arrivals for the Salt Lake City profile than for the R-11 profile for two reasons: (1) the geometry of the R2 reflector between 22 and 30 km is flat, which prevents wave conversion to the horizontal direction from vertically incident sources, and (2) the basin-hardrock contact at 35 km dips shallowly, rather than at 70° , which apparently suppresses the formation of Rayleigh waves.

Salt Lake City Profile

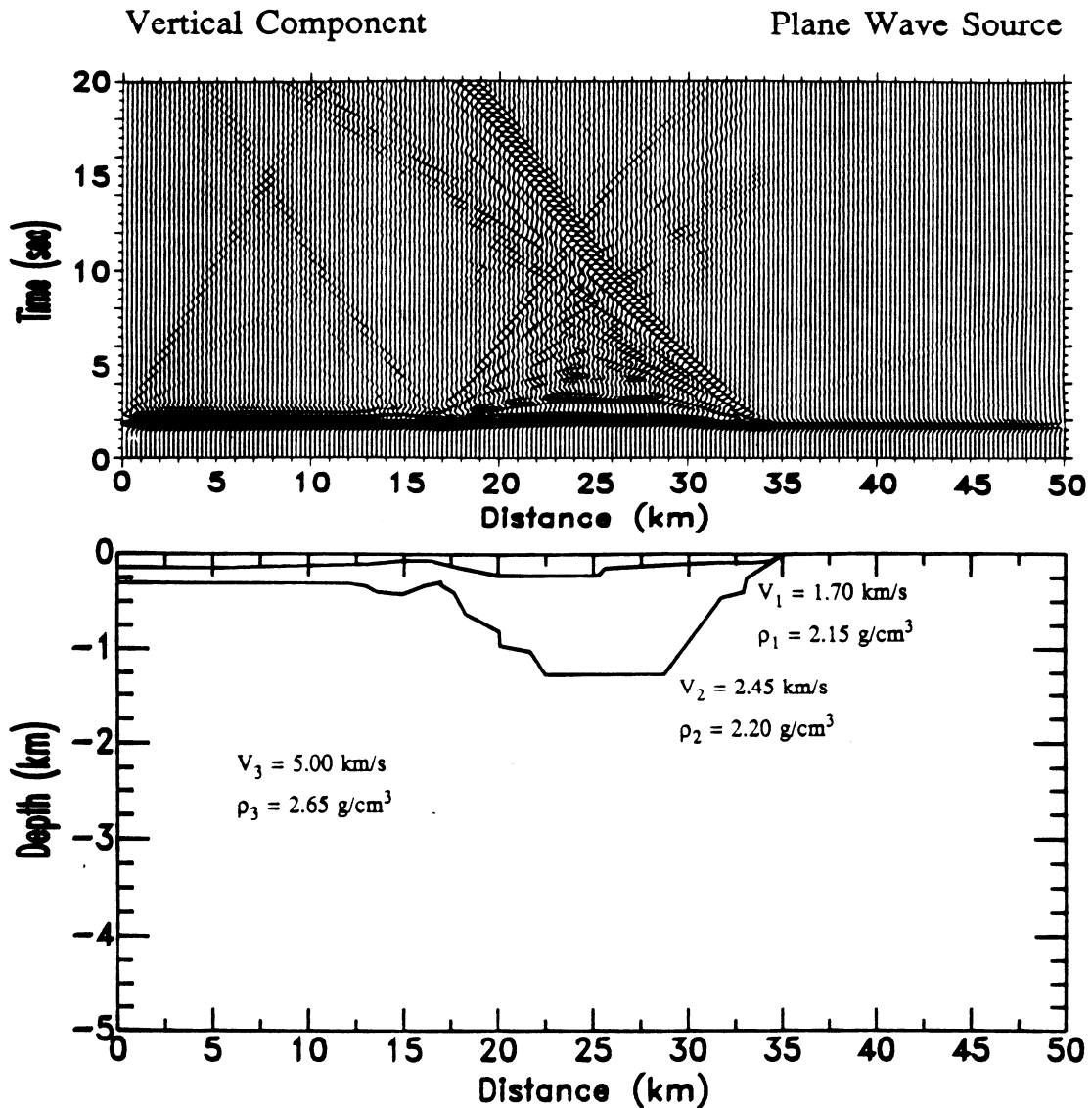


Figure 40. Vertical component synthetic seismogram for Salt Lake City profile A-A'. The velocities and densities are identical to those above the R1, R2, and R3 layers. The source is a plane wave with vertical particle displacement, and the source wavelet has a peak frequency of 1.95 Hz.

Salt Lake City Profile

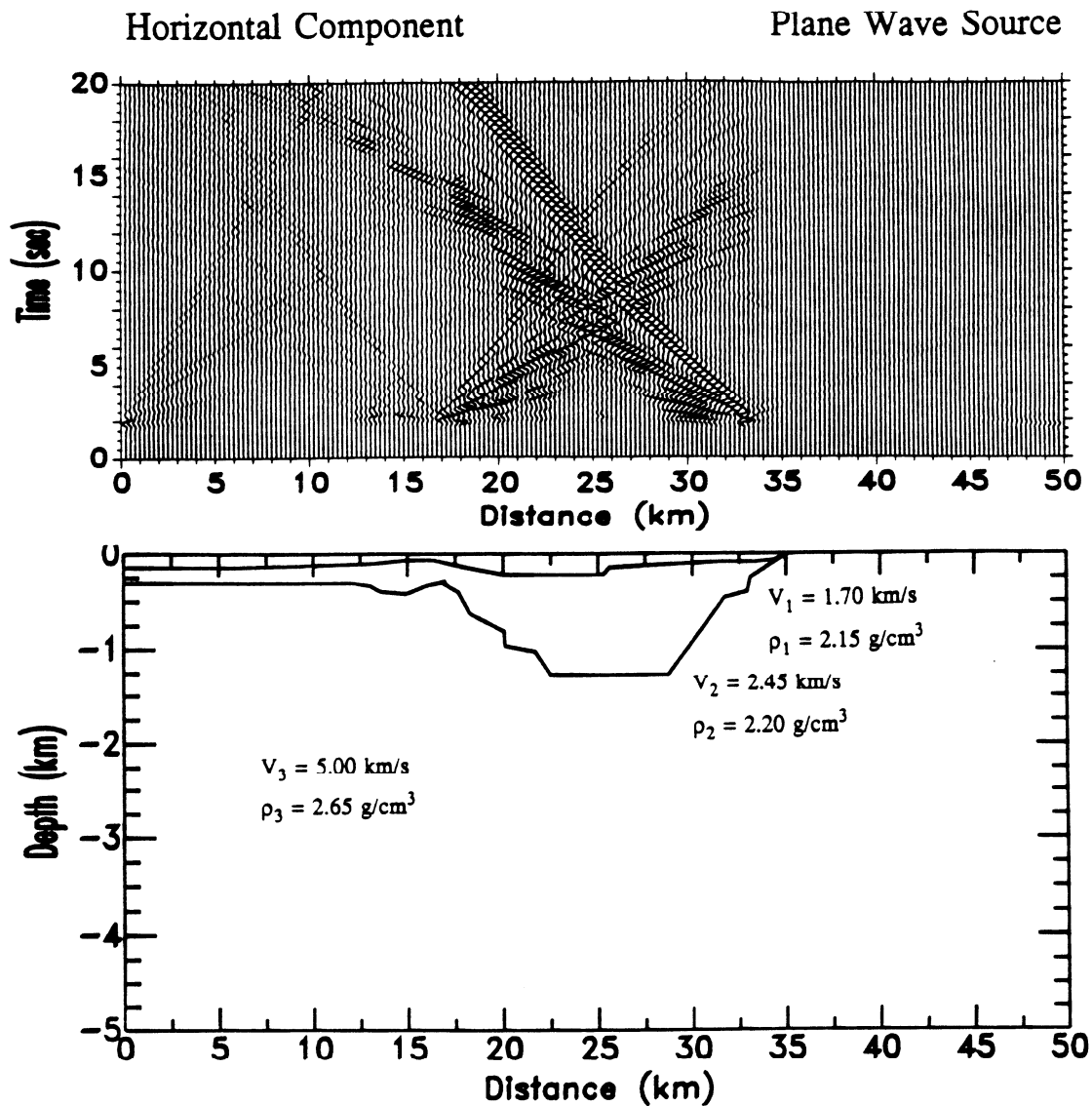


Figure 41. Horizontal component synthetic seismogram for Salt Lake City profile A-A'. The velocities and densities are identical to those above the R1, R2, and R3 layers. The source is a plane wave with vertical particle displacement, and the source wavelet has a peak frequency of 1.95 Hz.

The last synthetic seismogram model illustrates the basin response to a line source located at 5 km east and 10 km depth (Figures 42, 43). The largest amplitude is again the direct arrival on the vertical component, but the maximum displacement on the horizontal component is now 60% of the vertical maximum, and is located at 21 km. The Rayleigh waves on this model travel from west to east, and very little Rayleigh waves get reflected back into the basin because of the shallow dipping basin-hardrock contact at 35 km.

The synthetic spectral ratios of appropriate traces on the Salt Lake City profile are compared (Figure 44, 45) to King's measured spectral ratios at stations 3 and 8 (Figure 26). Because of the higher frequency sources, the synthetic spectral ratios are calculated from 0.3 to 3.3 Hz. The horizontal spectral ratios correlate poorly for the plane wave source (Figure 44). This poor correlation occurs because the basin model is relatively flat on the bottom with shallow sloping edges, which suppresses the conversion of vertical energy to horizontal energy; therefore the horizontal traces have a lower energy content than the vertical traces. Using the hardrock trace on the vertical component to calculate this synthetic horizontal spectral ratio emphasizes this energy contrast. The horizontal synthetic spectral ratios only predict about 10% of the measured mean amplification, while the vertical component only predicts about 30%.

The comparison of spectral ratios for the line source in the west for the Salt Lake City profile would be expected to correlate the best, since the stations are located very near the cross-sectional profile and the source from the Nevada Test Site nuclear explosions is incident from the southwest. This synthetic simulation results in the best correlation. The synthetic horizontal spectral amplification means (Figure 45) are within 57% and 64% of the mean amplification measured at stations 3 and 8, respectively. The vertical synthetic spectral ratio means are 99% and 119% of the measured USGS spectral amplification means.

Salt Lake City Profile

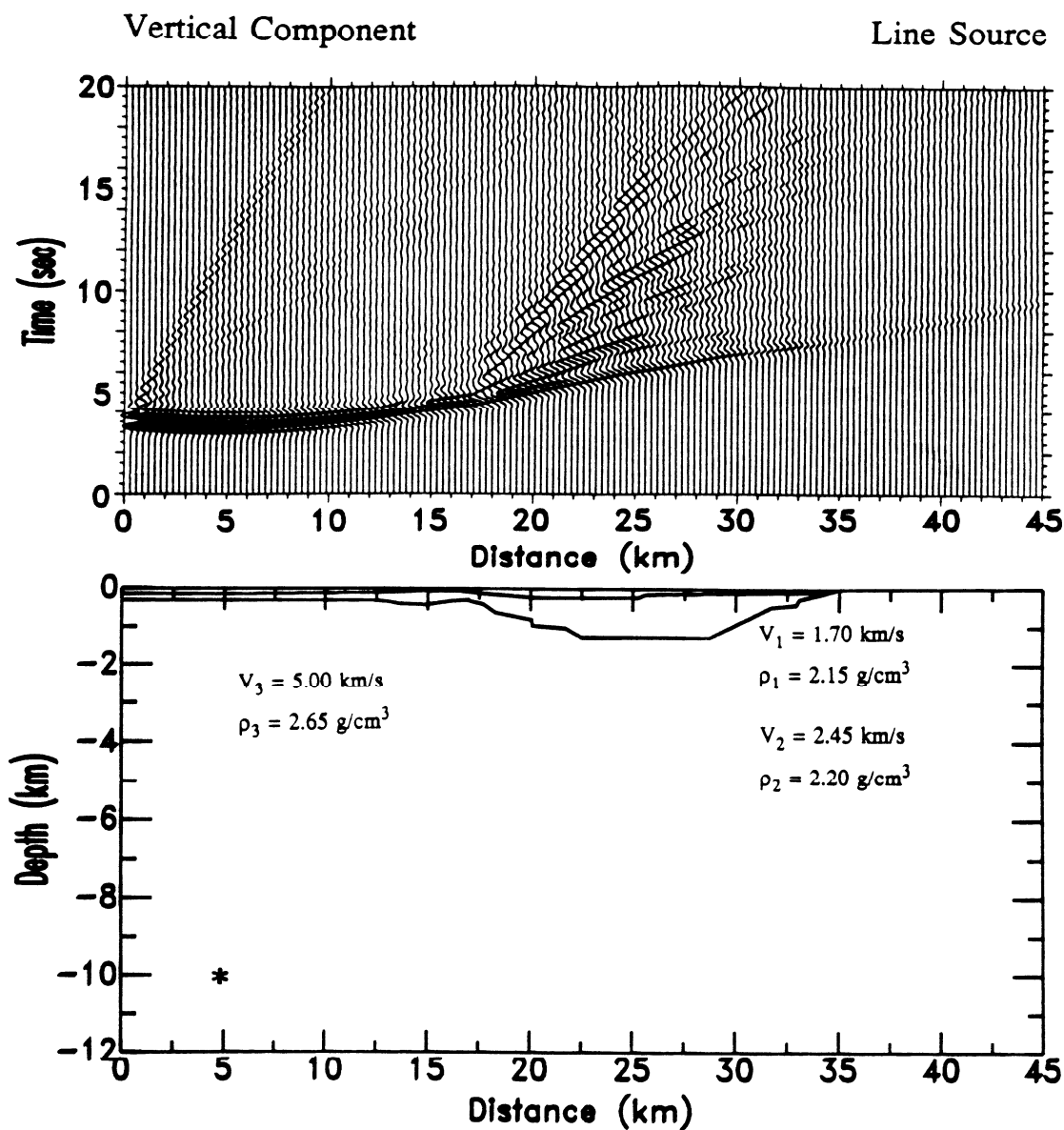


Figure 42. Vertical component synthetic seismogram for Salt Lake City profile A-A'. The velocities and densities are identical to those above the R1, R2, and R3 layers. The source is a line source with radial particle displacement at 5 km east and 10 km depth, and the source wavelet has a peak frequency of 1.3 Hz.

Salt Lake City Profile

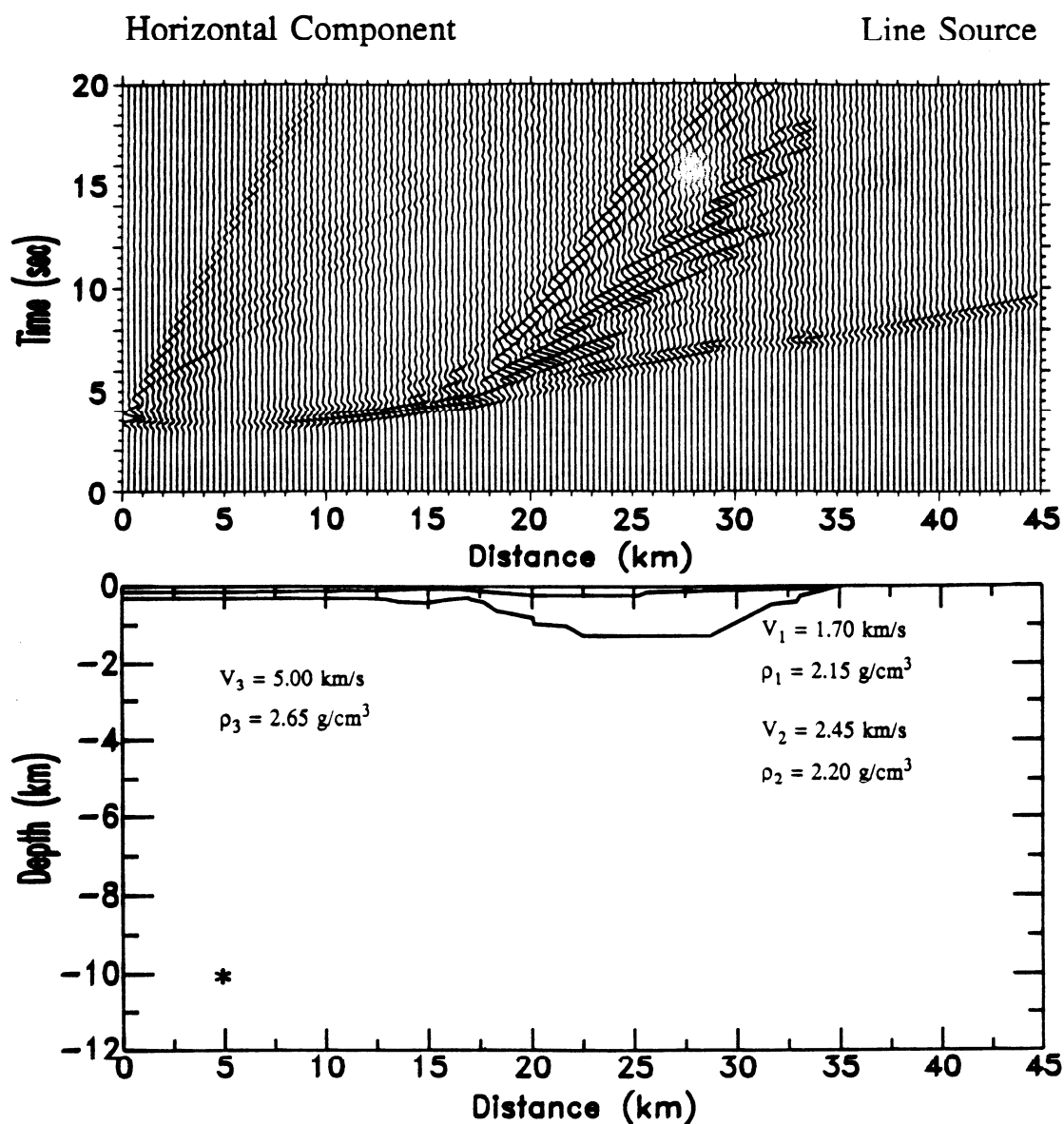


Figure 43. Horizontal component synthetic seismogram for Salt Lake City profile A-A'. The velocities and densities are identical to those above the R1, R2, and R3 layers. The source is a line source with radial particle displacement at 5 km east and 10 km depth, and the source wavelet has a peak frequency of 1.3 Hz.

Salt Lake City Profile - Plane Wave Source

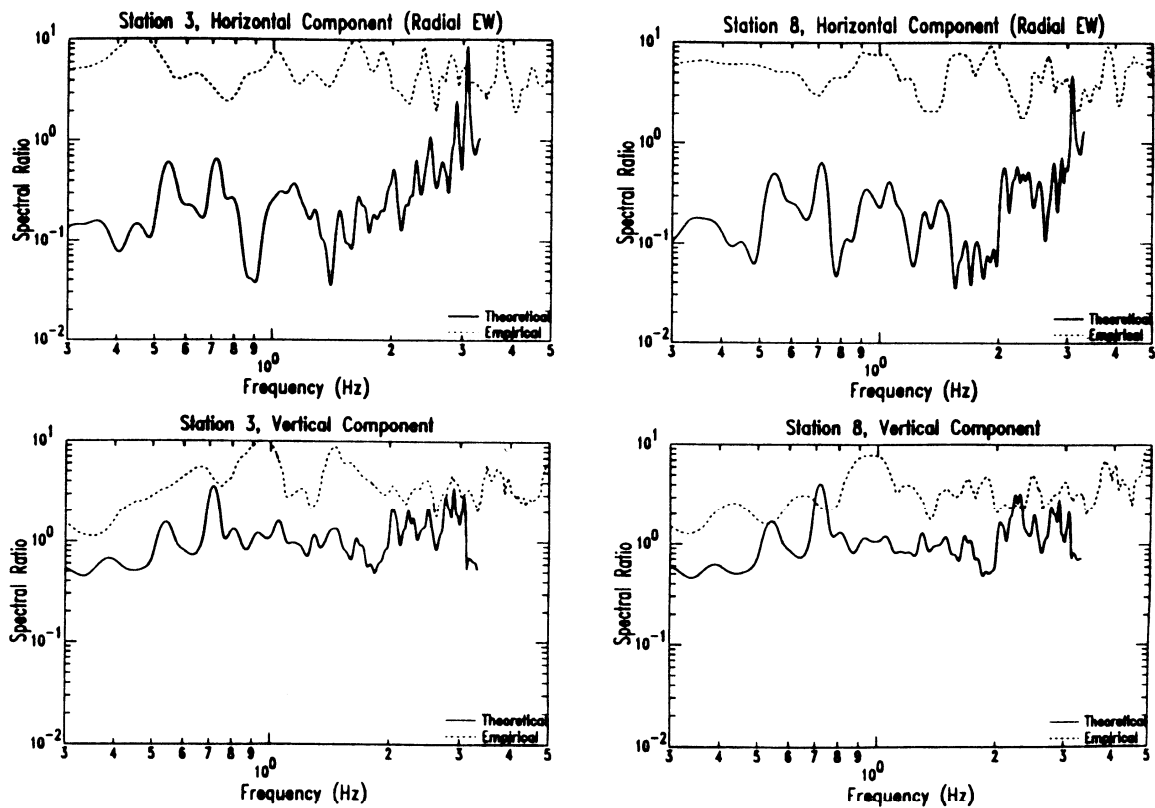


Figure 44. Empirical and synthetic spectral ratios for the Salt Lake City profile A-A'. The source for the synthetics is a plane wave source with a peak frequency of 1.95 Hz (Figures 37, 38) The synthetic spectral ratios for the horizontal and vertical components are plotted against empirical measurements from USGS stations 3 and 8. Please note change of spectral ratio scale.

Salt Lake City Profile - Line Source

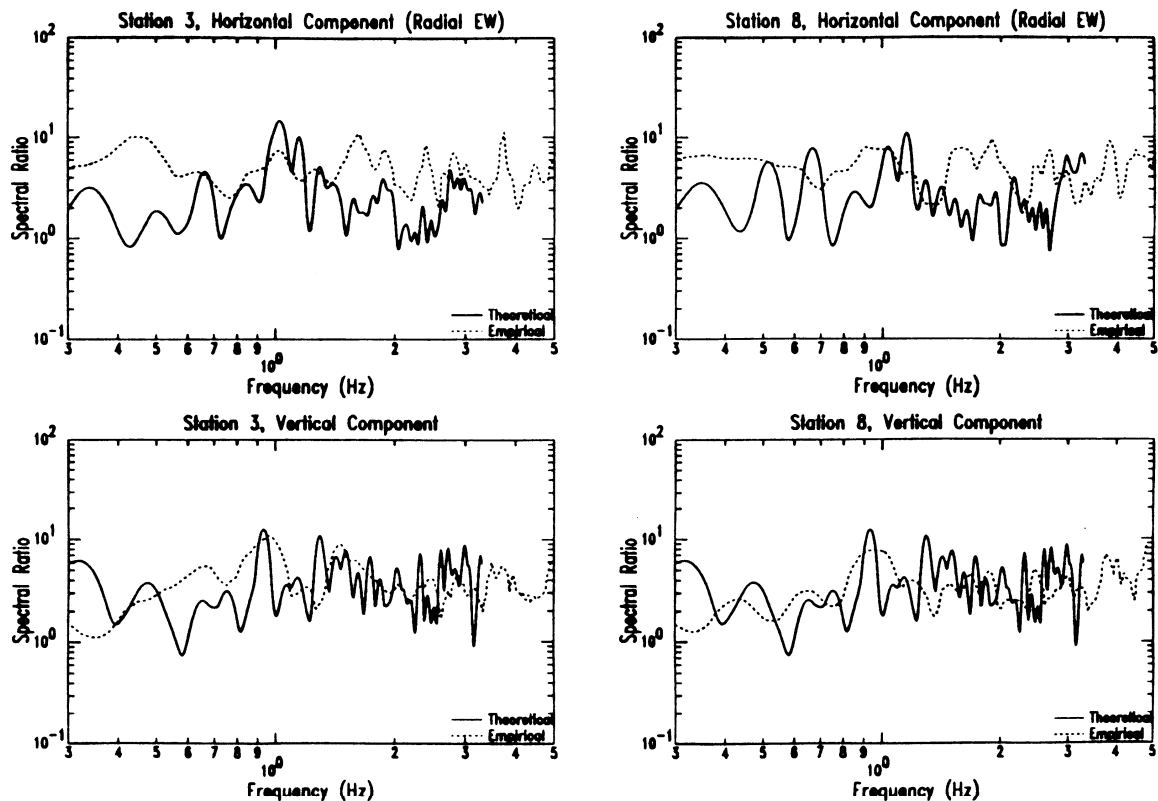


Figure 45. Empirical and synthetic spectral ratios for the Salt Lake City profile A-A'. The source for the synthetics is a line source with a peak frequency of 1.3 Hz located at 5 km east and 10 km depth (Figures 39, 40). The synthetic spectral ratios for the horizontal and vertical components are plotted against empirical measurements from USGS stations 3 and 8.

These results clearly illustrate that site amplification is dependent upon source incidence angle, and that the deep basin structure is responsible for a significant amount of low frequency amplification. Basins bounded by steeply dipping contacts convert more waveforms into the horizontal direction than do basins with shallow-dipping contacts. These steep boundaries also produce larger amplitude Rayleigh waves.

Three-dimensional Elastic Wave Simulation.

A staggered grid finite difference scheme, fourth-order in space and second-order in time, is used to model the three-dimensional elastic response of the Salt Lake Basin. This method solves for both velocity and stress (Levander, 1988; and Virieux, 1986) at each grid point using two coupled first-order equations. This is to be compared to the previous second-order differencing scheme which solved for displacement at each grid point using the second-order wave equation. The main advantages of the staggered grid method are that it is stable over a wide range of Poisson's ratios and fault sources are easily implemented; the disadvantage is that it requires about 1.5 times more physical memory than an equivalent displacement scheme.

The objective of this three-dimensional modeling exercise is to assess the three-dimensional nature of resonance and focusing in the basin. This is important because the previous two-dimensional studies assumed that these effects would not influence their conclusions, namely, low frequency seismic energy tended to collect in the deeper part of the basin for sources west of the basin. In order to verify this conclusion, three-dimensional elastic simulations are performed for a point double-couple source located in the southwestern part of the basin. The basin model is correct in depth but is about 1/3 the areal extent of the actual Salt Lake Basin. This scaled down basin model should tend to overesti-

mate resonance effects due to surface waves propagating in the north-south directions.

The basin model, depicted in Figure 46, is gridded into a 110 x 110 x 40 point model, i.e., a model 17 km x 17 km in areal extent and 6 km in depth. Since a fourth-order differencing scheme is used then the model is discretized at five nodes/wavelength, where the minimum shear velocity (1.1 km/s) and maximum source frequency (1.1 Hz) is used to compute the node spacing of 0.15 km. The source is a Ricker wavelet with a center frequency of 0.7 Hz, the compressional wave velocities are approximately those given in Figure 31, and the V_s/V_p ratio is taken to be 0.6. Although the actual basin model is about 40 km x 35 km x 3 km in dimension, this scaled down basin can serve as a initial model to understand some of the important basin features which control seismic amplification.

As an example, Figures 47 to 49 depict the results from simulating a dip-slip fault (represented by a double couple point source) rupturing in the southwest part of the basin model at a depth of 3 km. These simulations are an attempt to model earthquakes which are observed to occur along the western part of the basin; such events have the potential for inducing strong ground shaking within the valley.

For the experiment described above, the cumulative seismic energy for the horizontal and vertical particle velocity along the valley floor is given in Figures 47 and 48, respectively. The total seismic energy at the elapsed time of 1.5 seconds and 30 seconds is given, respectively, in Figures 47a, 48a and 47b, 48b. These figures indicate that the low frequency seismic energy accumulates in the deeper part of the basin; this is consistent with the results from the two-dimensional simulations. Figure 49 depicts snapshots of the wave propagation for

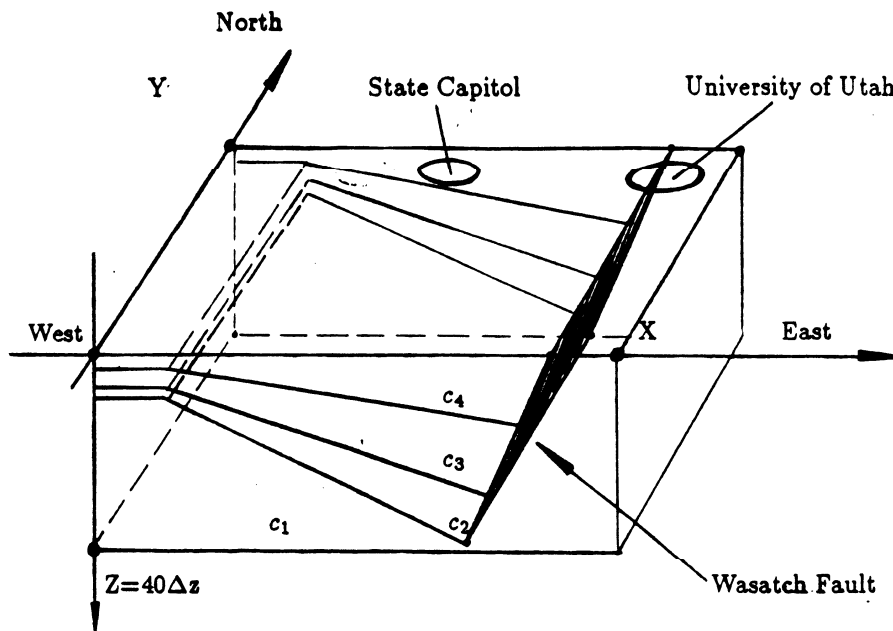


Figure 46. Salt Lake Basin model, approximately 6 km deep and 17 km in N-S and E-W directions. This basin model is about 1/2 the size of the actual basin model.

Figure 47. The cumulative horizontal seismic energy on the valley floor of the Figure 46 Model for a double couple point source located in the southwest portion of the basin at a depth of 2.25 km. The left portion depicts the energy distribution at the time of 1.5 seconds and the right depicts energy distribution at 30 seconds. The top (bottom) of each figure is west (east); red (green) color indicates greatest (least) seismic energy.

Figure 47

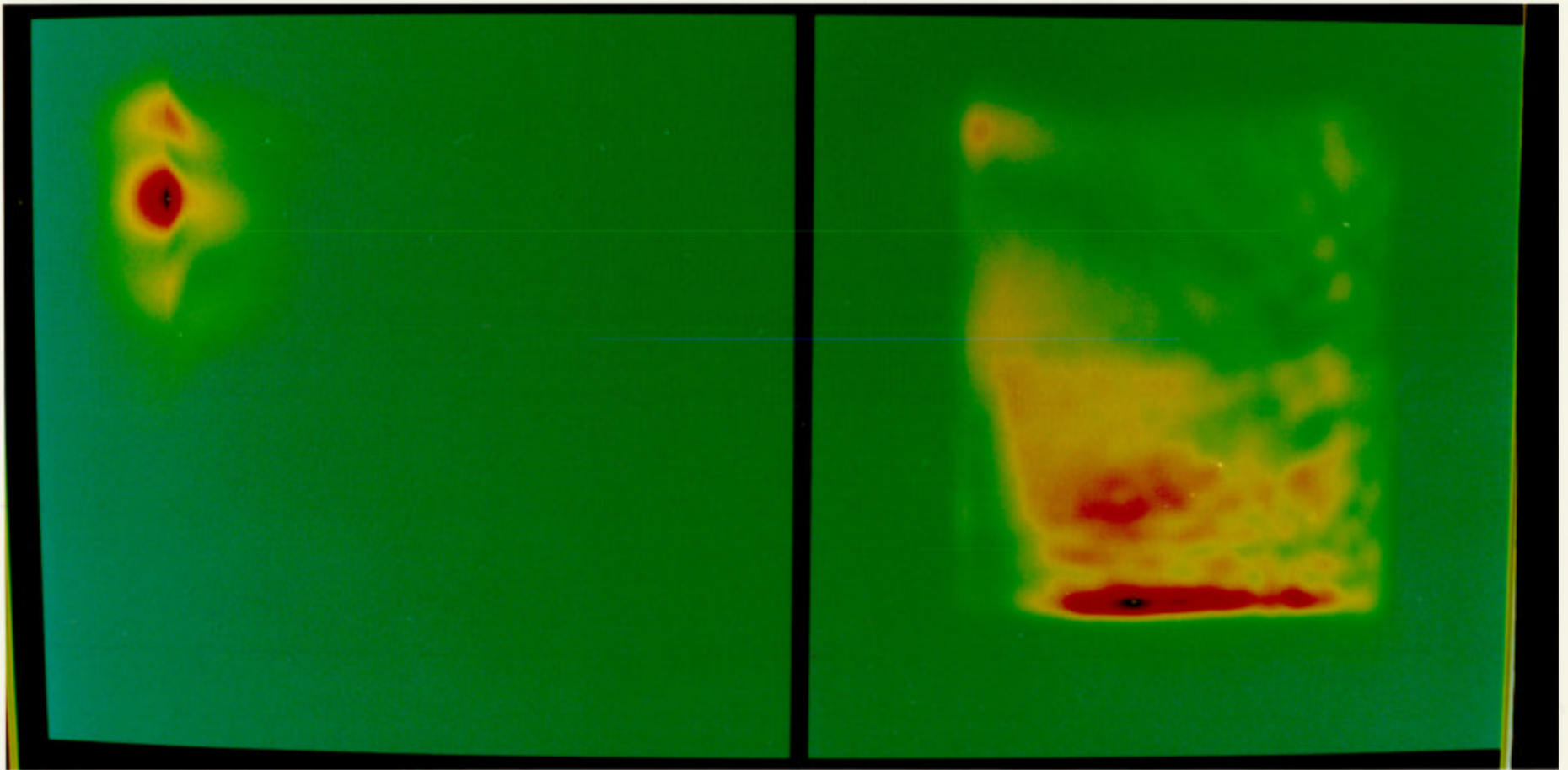


Figure 48. Same as Figure 47, except that the seismic energy is for the vertical component of displacement.

Figure 48

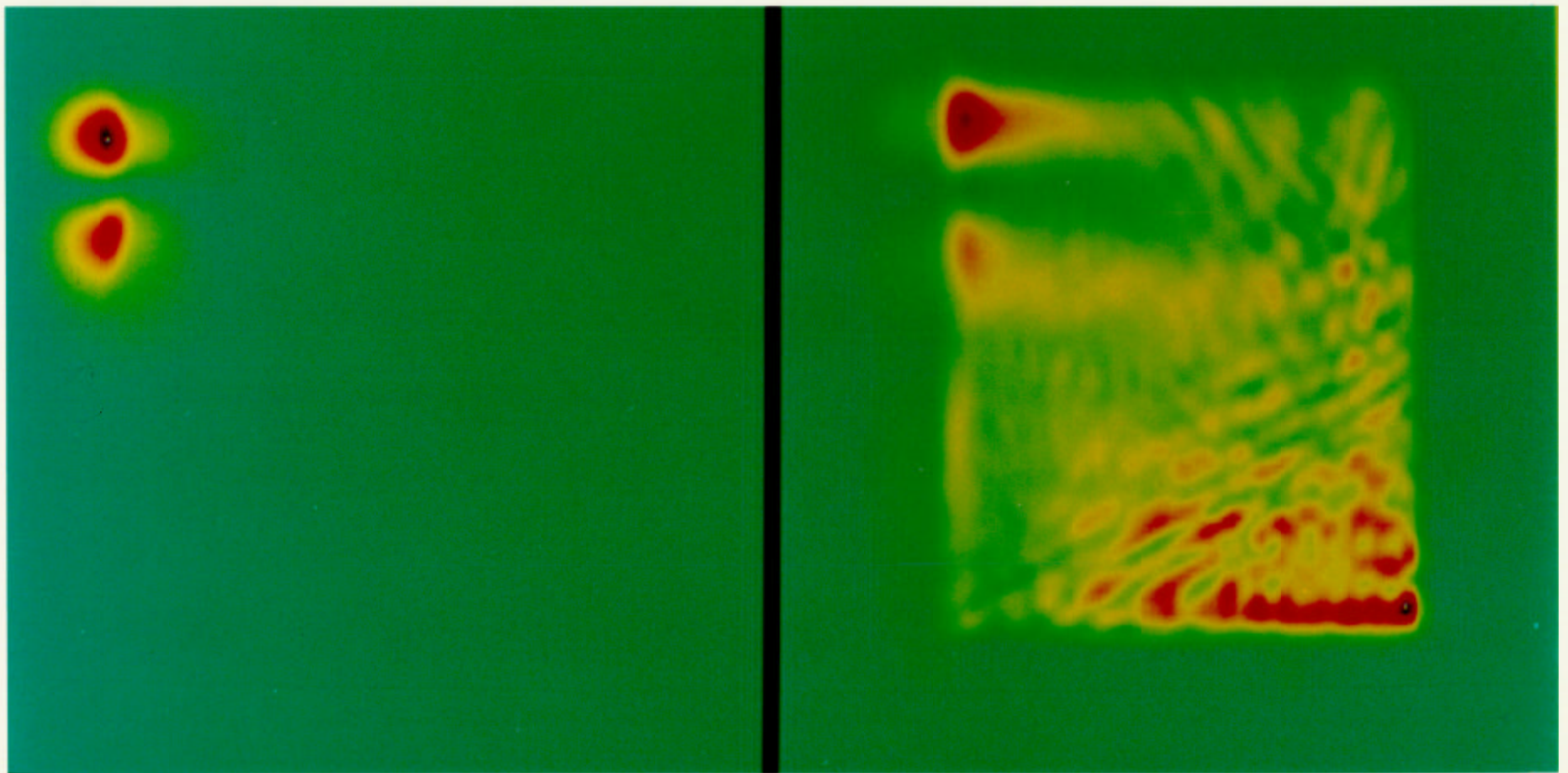
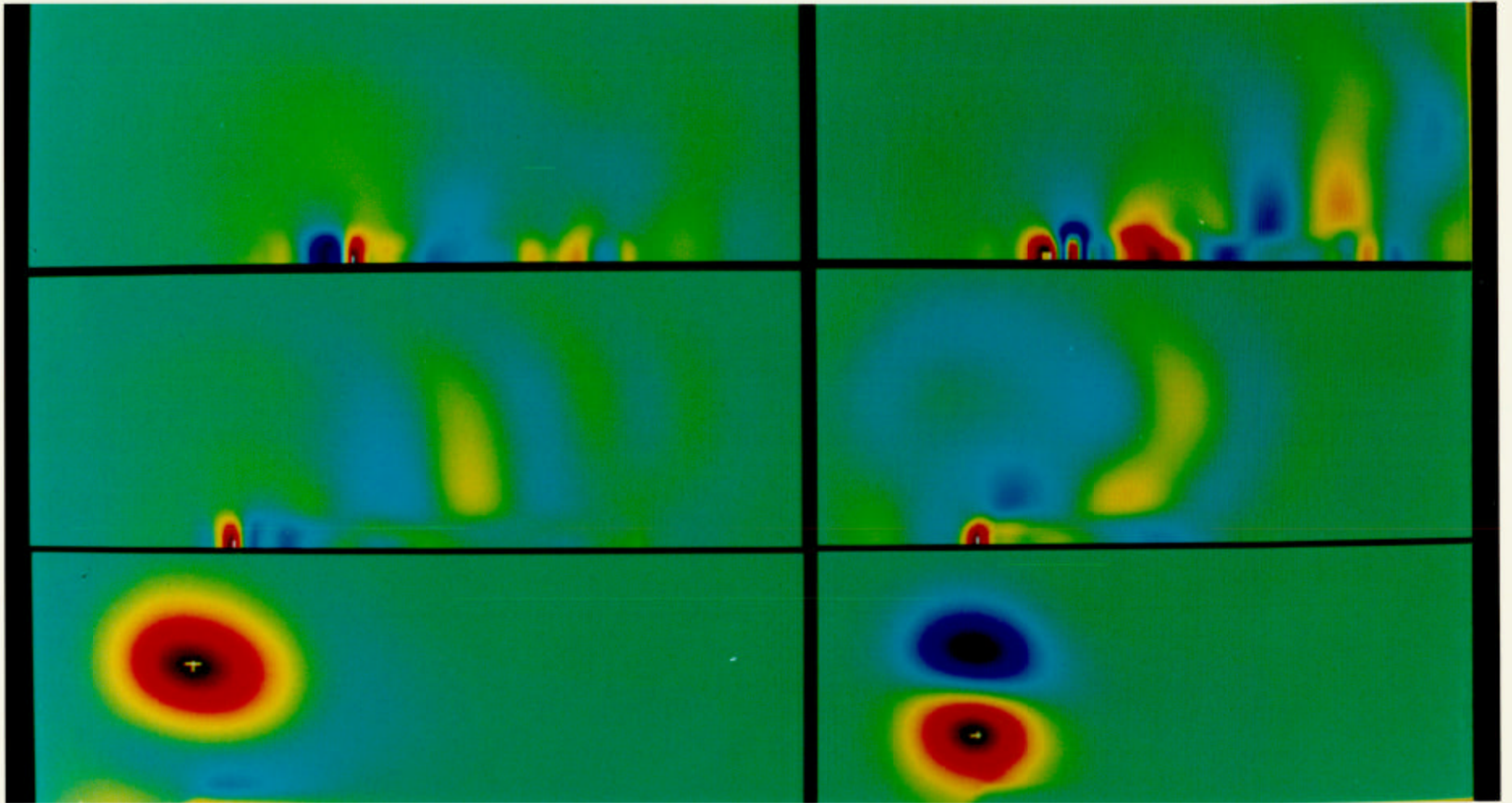


Figure 49. Vertical component snapshots for E-W cross-sections centered in the middle of the basin model. Time increases from left to right and from top to bottom, with about 1.5 seconds of time between snapshots. The upper leftmost snapshot is at the time of 1.5 seconds from the initiation of the earthquake.

Figure 49



an E-W cross-section in the middle of the basin which, when viewed in a rapid movie like manner, illuminates the important physics of the wave propagation. Figure 50 depicts the z-component seismograms for a line of surface receivers trending E-W and centered in the middle of the basin. Similar to Figure 33 for the 2-D simulations, a dominant phase reflects from the fault surface and travels from east to west. It is interesting to note that simulations for a source located just south of the basin (Provo earthquake) produced a cumulative energy pattern (not shown) quite different than that depicted in Figure 47. In this case, most of the energy accumulated in the northern, not the eastern, part of the basin.

The results from these 2-D and 3-D simulations can only provide rough estimates of what causes low frequency resonance in Salt Lake Basin. They cannot, at this stage, be used to precisely predict areas of greatest ground motion amplification. Current and near future modeling studies, however, are on the verge of making much more precise predictions.

Current research involves examining the relationships between seismic amplification and source radiation pattern, source location and source depth. In these simulations the basin models are the same size as the actual Salt Lake basin. In addition, the topography of the Wasatch mountains will be incorporated as they are almost as high as the basin is deep.

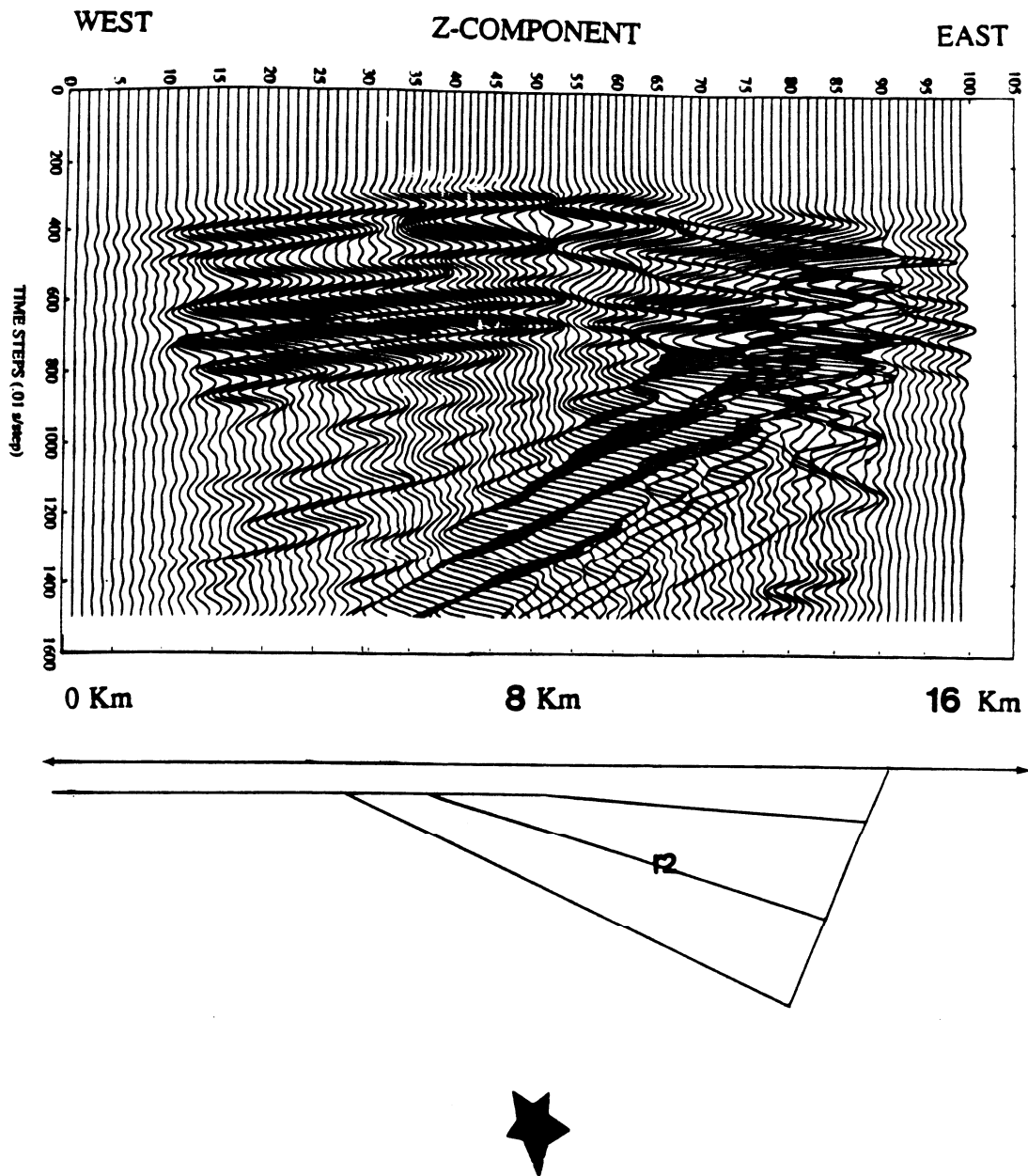


Figure 50. Vertical component seismograms measured on the free-surface for a W-E seismic line centered in the middle of the Figure 46 basin model. The source is the same as that in Figure 47

SUMMARY

This report presents the geophysical data of the Salt Lake Valley and numerical simulations of P-SV wave propagation in 2-D and 3-D models of Salt Lake Basin.

Fox's depth to basement interpretation is considered to be the best single source for the whole Salt Lake Basin. For the northern portion of the basin Fox's model along with the deep seismic data provide the most credible model. Fox did not use the available seismic data for control which could have changed the interpretation; so, for more detailed studies away from these seismic lines even the Fox interpretation must be used with caution. Since the Arnov et al. model departs from Fox's model and the seismic interpretation in the deeper portions of the northern basin, it is believed to be only somewhat reliable and should be used for control with much caution in developing a basin model especially where basement is thought to be deep.

Fox's model for the southern part of the basin shows fair to good correlation with the Kennecott model and shows some similarities with Bashore's model. However, due to the nature of these data and interpretations, the southern portion of the basin model is deemed to be of only fair reliability. In the central portion of the basin a comparison of gravity interpretations by Fox and Wong show only fair correlation. Therefore, since there is no deep seismic control, the subsurface features of the middle part of the basin are to be considered essentially unknown.

The shallow seismic studies are important to site amplification but the layers resolved are of little importance in the focusing of incident low frequency seismic energy in the valley. Since the location of R2 is critical to the seismic focusing studies, its location should be determined by either forward gravity

modeling or gravity inversion throughout the valley using all available seismic data and well data for control.

2-D P-SV synthetic modeling has shown that low frequency seismic energy accumulates in the deeper part of the basin, and that deep basin structure is responsible for a good portion of low frequency wave amplification. Good correlation exists between synthetic spectral ratios and measured USGS spectral ratios, particularly for the Salt Lake City profile with the line source incident from the west. Comparison of the R-11 and Salt Lake City profile seismograms shows that basins with steeply dipping walls increase the conversion of vertical energy into horizontal energy, and enhance the formation of surface waves.

Preliminary 3-D modeling results suggest that N-S propagating waves will induce a significantly different resonance pattern on the surface than an E-W propagating wave. These results also confirm the conclusions from the 2-D study which suggest that strong amplification of ground motion occurs over the deeper part of the basin.

ACKNOWLEDGEMENTS

Thanks are extended to Richard C. Fox for supplying his report, maps, and time to the Geology and Geophysics Department. James C. Pechmann is thanked for his insights, and Kevin Snider and Joel Scoville of Celsius Energy Co. are acknowledged for supplying the reflection lines. Jay Hammett's searching through Kennecott's records is appreciated. Jay supplied the total magnetic intensity map as well as the Kennecott gravity models. And, Rick Hulse is very appreciated for tracking down the gravity data set and spending much time generating the color contour map of the gravity data set.

APPENDIX

Gravity data for the Salt Lake Valley were made available by Bob Klauk of the Utah Geologic and Mineral Survey (U.G.M.S) and Richard Fox, formerly of Meiji Resource Consultants. These data consist of some 2300 station locations and includes the original gravity survey data collected done by Cook with additional data that was taken by Meiji. The two data sets were merged so as to insure continuity at the boundaries. The data was processed as complete bouguer anomaly and stored on magnetic tape. Hand contoured maps of the data were made available through the U.G.M.S report file number 38. Because of some question to the interpretation and contouring of the data, further effort was made to analyze the gravity survey data.

The magnetic data tape format was incompatible with any computer equipment available at the University of Utah and the data was not retrievable. Through the efforts of Cheryl Skillern, of Arco Oil and Gas, the data was retrieved and reformatted in a usable form. Also through the facilities of Arco, the data was mapped by the use of a computerized mapping system (Zygor 87-06).

The data set was projected onto a spheroid (Clarke 1886) by using the Universal Transverse Mercator (UTM) projection. The data was then gridded on 500 foot intervals, which gave a 90 % confidence level that the data was evenly distributed through the gridding base. Use of a lesser or greater grid range would have resulted in wide spread or clustered data sets, serious errors would have developed in the contouring procedure with a confidence level of less than 65 %.

After the data set was gridded it was contoured. Data contouring was done by a moving Least Squares operator with a search radius of 5000 feet (ten times

the grid interval), this was to insure that the data set was represented properly. If a larger radius were used, extreme smoothing of the data may have resulted. A smaller search radius would have produced irregular shaped anomaly patterns. The contouring was done to include extrapolation into those areas where no data were taken, but where gridding of the data set was included. These contours were then placed on a geopolitical base map of Salt Lake County and surrounding area.

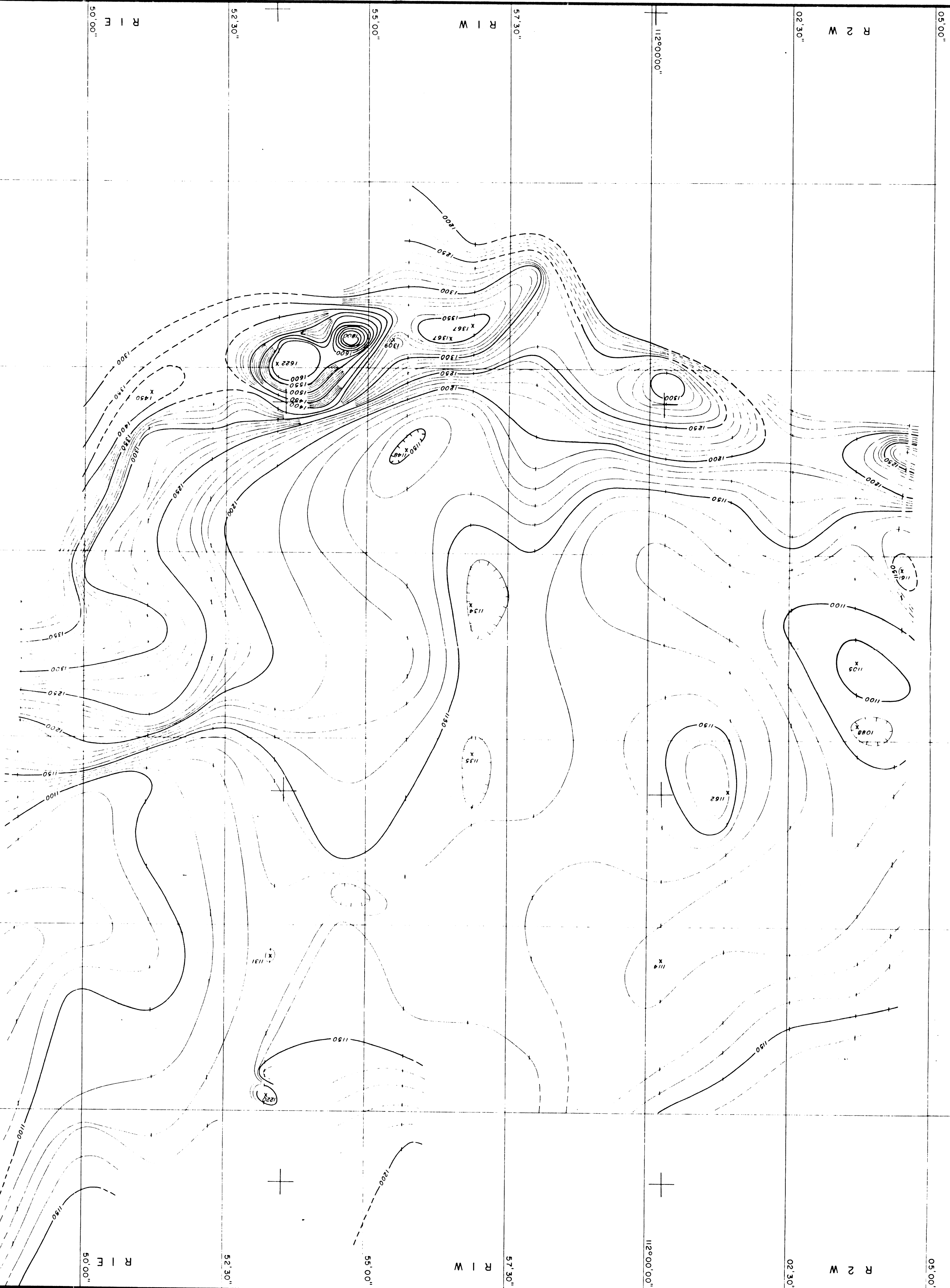
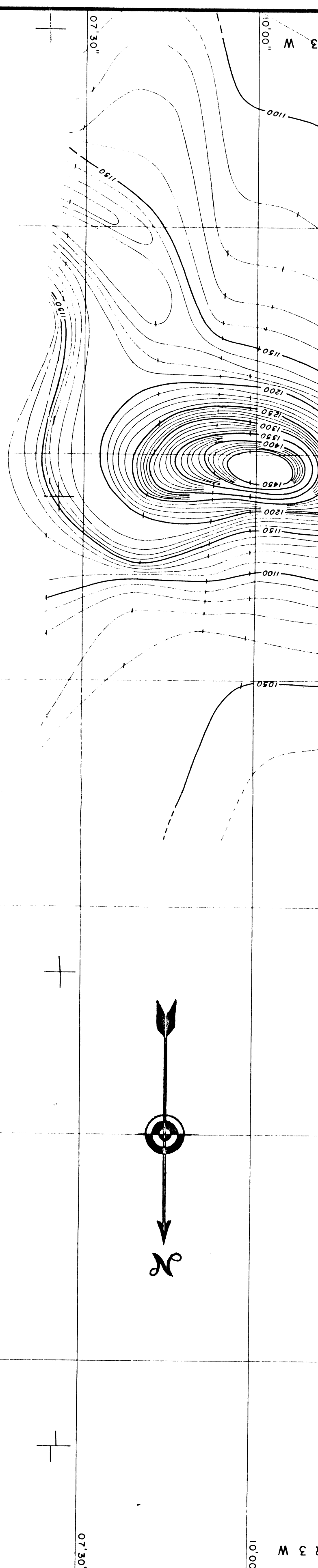
The base map is color coded and contoured on 5 milligal intervals with red representing the smallest negative anomaly and blue the largest negative values. Also it is based on the UTM projection with the area of interest being number 12. This color map produced by the Zycor program was photographed and reduced to a normal page size. This reproduction accompanies this appendix.

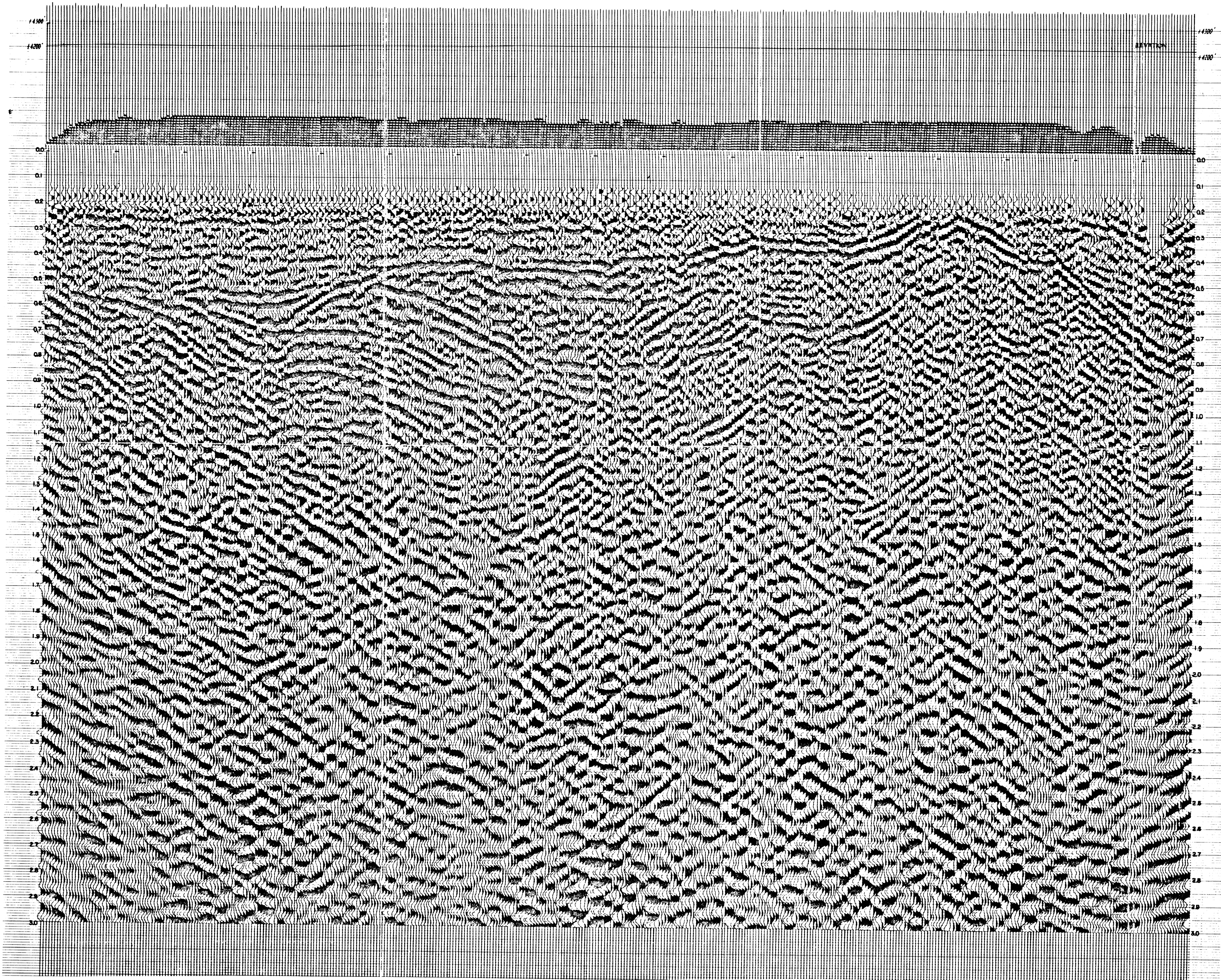
In the process of sorting, a statistical operation of the data was performed. The data set was checked to insure that no errors were made when the reformatting process was complete. No extreme values were found in the data set, this step was done before any gridding or contouring was begun. Because the contouring is performed as a numerical operation, hand contouring of the same data may produce different results. These should be minor changes from the computer results.

REFERENCES

- Arnow, T., and Mattick, R. E., 1968, Thickness of valley fill in the Jordan Valley east of the Great Salt Lake, Utah: U.S.G.S. Prof. Paper 600-B, B79-B82.
- Arnow, T., Van Horn, R., and La Pray, R., 1970, The pre-Quaternary surface in the Jordan Valley, Utah: U.S.G.S. Prof. Paper 700-D, D257-D261.
- Bashore, W., 1982, Upper crustal structure of the Salt Lake Valley and the Wasatch Fault from seismic modeling: M. S. thesis, Univ. of Utah.
- Benz, H., and Smith, R., 1988, Elastic-Wave propagation and site amplification in the Salt Lake Valley, UTah, from simulated normal faulting earthquakes: Bull., Seis. Soc. Am., **78**, 1851-1874.
- Fox, R. C., 1983, Gravity based interpretive bedrock geology of the Jordan Valley, Salt Lake City, Utah: Copy received directly from R. C. Fox.
- Hill, J. A., 1988, A finite difference simulation of seismic wave propagation and resonance in Salt Lake Valley, Utah: M. S. thesis, University of Utah.
- King, K. W., Williams, R. A., and Carver, D. L., 1987, Relative ground response in Salt Lake City and areas of Springville-Spanish Fork, Utah: U.S.G.S. Open-File Report, 87-585, V II.
- Levander, A., 1988, Fourth-order finite difference P-SV seismograms: Geophysics, **53**, 1425-1436.
- Machette, M., Personius, S., and Nelson, A., 1987, Quaternary geology along the Wasatch Fault Zone: segmentation, recent investigations and preliminary conclusions: U.S.G.S. Open-File Report, 87-585, V II.
- Mattick, R. E. 1970, Thickness of unconsolidated sediments in Jordan Valley, Utah: U.S.G.S. Prof. Paper 700-C, C119-124.
- Virieux, J., 1986, P-SV wave propagation in heterogeneous media: velocity-stress finite difference method: Geophysics, **51**, 889-901.
- Wong, I. G., 1979, Site amplification of seismic shear waves in Salt Lake Valley, Utah: Earthquake Studies in Utah, 1850 to 1978, W. J. Arabasz, Smith, R. B., and Richins, W. D., Editors, University of Utah Seismograph Stations, Salt Lake City, Utah, 321-337.

Youngs, R. R., Swan, F. H., Power, M. S., Schwartz, D. P., and Green, R. K., 1987, Probabilistic analysis of earthquake ground shaking hazard along the Wasatch Front, Utah, U.S.G.S. Open-File Report, 87-585, V II.





LINE R-10
AREA SALT AIR SALT LAKE COUNTY, UTAH
FOR MOUNTAIN FUEL SUPPLY COMPANY
BY **Sci-mograph Service Corporation**
A SUBSIDIARY OF RAYTHEON COMPANY
P.O. BOX 1590 • TULSA, OKLAHOMA 74102 • (918) 627-3330
Job Number 745064
Date 5/30/74
PROCESSED WITH **the PHOENIX** ON SITE DIGITAL DATA SYSTEM

PROCESSING SEQUENCE

- 1 Demultiplex - Edit - Sum
- 4 VIBROSEIS® Correlation
- 5 Velocity Analysis
- 2 Normal Moveout
- 6 Datum Statics
- 7 Automatic Statics
- 7 Stack 12 Fold
- 9 Deconvolution
- 3.10 Filter
- 8.12 Trace Equalization
- Additional Processing
- * 11 Time Migration

PROCESSING PARAMETERS

CORRECTIONS
Datum 4100 Ft.
V₀ 6.000 Ft/sec. V_w
Automatic Statics Window 200 to 1200 sec.
Additional

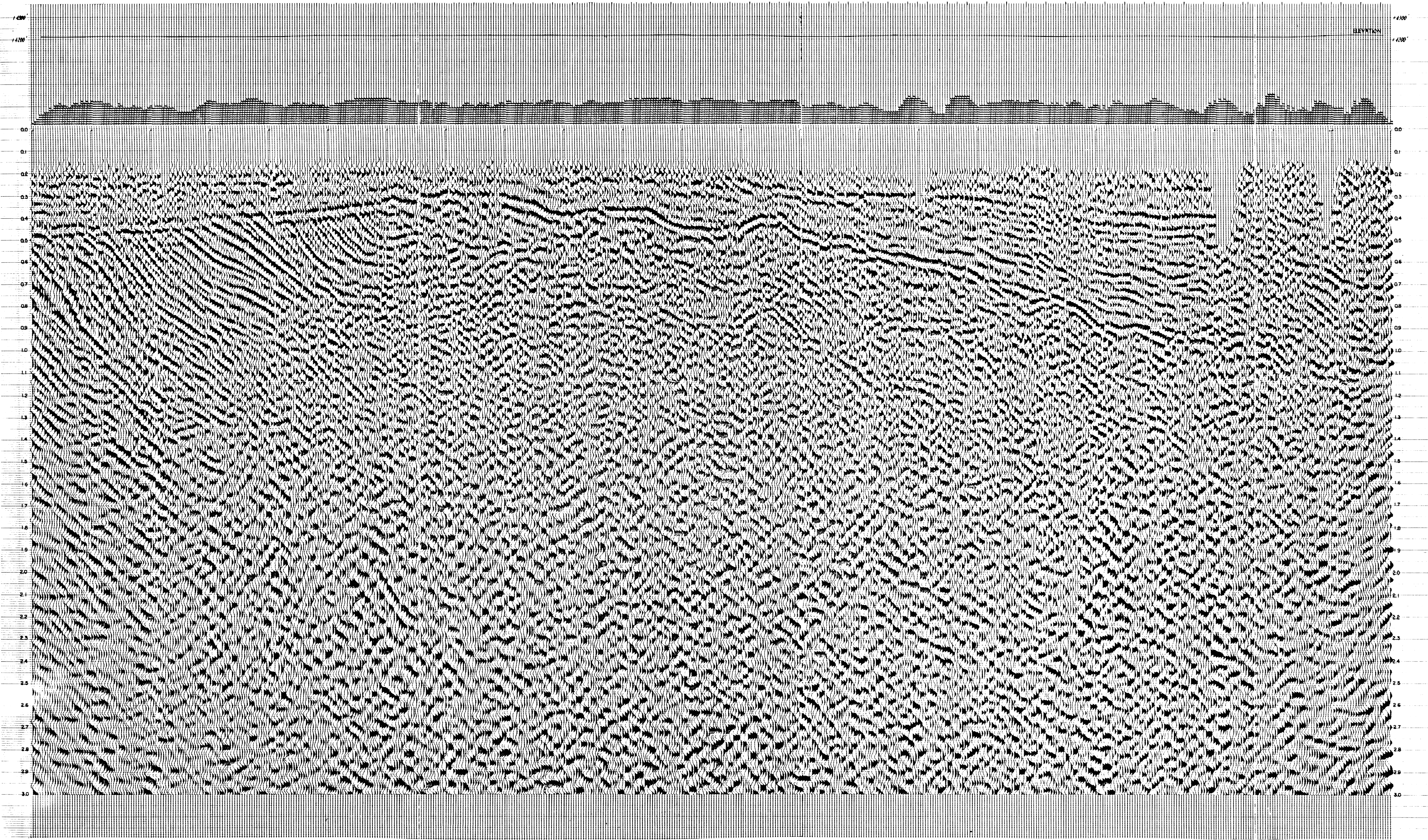
	Operator Length (ms)	Design Window (sec)	Prediction Time (ms)
DECONVOLUTION BEFORE STACK			
DECONVOLUTION AFTER STACK	400	200 - 2300	

	Band Pass (Hz)	Application Time (sec)	Overlap Time (sec)
BAND PASS FILTERS	(3) 16.20 - 56.60	0.000 - 1.500	
	12.16 - 56.60	1.500 - 2.200	
	10.16 - 56.60	2.200 - 5.000	
(10)	14.16 - 32.36	0.000 - 1.000	
	12.14 - 28.32	1.000 - 5.000	

Sample Rate 4 ms
Traces Per Inch 12
One Second 7.5 inches
Playback Gain 4 dB

RECORDING PARAMETERS

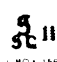
Contract 2475 Party B Date Recorded 2/2, 8, 11, 12/74
SP/VP Interval 220 Instrument Type OFS III ADD IT
Geophone Interval 220 Amplifiers Binary Gain
Near Offset 440 Recording Filter 12.62 HZ
Far Offset 2860 Sample Rate 2 ms
Number Traces 24 Record Length 5 sec
Configuration Split Straddle Sweep Length Pushover
Progression W to E Sweep Frequency
Geophones/Trace 27 Number Sweeps



LINE R-II

AREA SALTAR SALT LAKE COUNTY, UTAH

FOR MOUNTAIN FUEL SUPPLY COMPANY

BY  Seismograph Service Corporation
4000 S. 1000 E. SUITE 100, SALT LAKE CITY, UTAH 84119
Job Number 740664 Date 5/28/74

PROCESSED WITH **the PHOENIX** ON SITE DIGITAL DATA SYSTEM

PROCESSING SEQUENCE

1 Demultiplex Edit Sum

2 Vibroseis Correlation

3 Velocity Analyst

4 Normal Moment

5 Datum Statics

6 Automatic Statics

7 Stack 12 Fold

8 Deconvolution

9 Filter

10 Trace Equalization

11

12 Additional Processing

Time Migration

PROCESSING PARAMETERS

CORRECTIONS

Datum -4200 Ft

Vs 6000 Ft/Sec Vs

Automatic Statics Window 200 to 1400 ms

Additional

DECONVOLUTION BEFORE STACK

Operator Length (ms) Design Window (sec) Prediction Time (ms)

DECONVOLUTION AFTER STACK

200 200 2300

BAND PASS FILTERS

	Start Freq (Hz)	Stop Freq (Hz)	Application Time (sec)	Overlap Time (sec)
(1)	16.32	56.60	8	1.5
(2)	17.74	56.60	1.8	2.2
(3)	10.14	56.60	2.2	5.0
(4)	16.16	32.36	0	1.0
(5)	12.14	26.32	1.0	5.0

Sample Rate .4 ms

Traces Per Inch 12

One Second 7.5 inches

Playback Gain .6 dB

RECORDING PARAMETERS

Contract 2475 Party B

SP VP Interval 220 Ft

Geophone Interval 220 Ft

Near Offset 660 Ft (440 Ft SP 101 125)

Far Offset 3080 Ft (2860 Ft SP 101 125)

Number Traces 24

Configuration Split Straddle

Progression E to W

Geophones Trace 27 (SP 101 185)

18 (SP 186 178)

Date Recorded Feb. 12, 16, 18, 25, 1974

Instrument Type DFS III Add it

Amplifiers

Recording Rate 14.62 Hz

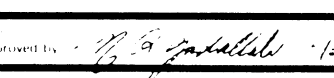
Sample Rate 2 ms

Record Length 5 ms

Survey Length

Survey Frequency

Recorder Swings

Approved By  5/31/74

